2019-06

FILLING THE GAP: ROCKET DELIVERED SHORT-TERM EXPEDITIONARY BEYOND LINE-OF-SIGHT NARROWBAND COMMUNICATIONS RELAY

Pross, John W.

Monterey, CA; Naval Postgraduate School

NAVAL POSTGRADUATE SCHOOL

MONTEREY, CALIFORNIA

THESIS

FILLING THE GAP: ROCKET DELIVERED SHORT-TERM EXPEDITIONARY BEYOND LINE-OF-SIGHT NARROWBAND COMMUNICATIONS RELAY

by

John W. Pross

June 2019

Thesis Advisor:	Wenschel D. Lan
Co-Advisor:	James H. Newman
Second Reader:	Nicholas R. Koeppen (USMC)

THIS PAGE INTENTIONALLY LEFT BLANK

REPORT DOCUMENTATION PAGE			*Form Approved OMB No. 0704-0188*

1. AGENCY USE ONLY *(Leave blank)*	**2. REPORT DATE** June 2019	**3. REPORT TYPE AND DATES COVERED** Master's thesis

4. TITLE AND SUBTITLE
FILLING THE GAP: ROCKET DELIVERED SHORT-TERM EXPEDITIONARY BEYOND LINE-OF-SIGHT NARROWBAND COMMUNICATIONS RELAY

5. FUNDING NUMBERS

6. AUTHOR(S) John W. Pross

7. PERFORMING ORGANIZATION NAME(S) AND ADDRESS(ES)
Naval Postgraduate School
Monterey, CA 93943-5000

8. PERFORMING ORGANIZATION REPORT NUMBER

9. SPONSORING / MONITORING AGENCY NAME(S) AND ADDRESS(ES)
N/A

10. SPONSORING / MONITORING AGENCY REPORT NUMBER

11. SUPPLEMENTARY NOTES The views expressed in this thesis are those of the author and do not reflect the official policy or position of the Department of Defense or the U.S. Government.

12a. DISTRIBUTION / AVAILABILITY STATEMENT
Approved for public release. Distribution is unlimited.

12b. DISTRIBUTION CODE
A

13. ABSTRACT (maximum 200 words)

The current Department of Defense (DoD) satellite communications (SATCOM) network consists of large, exquisite, and expensive constellations providing service across the radio frequency spectrum. However, the current SATCOM architecture is vulnerable to adversary actions including interference, jamming, directed energy, and antisatellite weapons. Despite the rise in adversary threats, the DoD continues to grow more reliant on SATCOM services in execution of all seven joint warfighting functions. The Marine Corps Operating Concept acknowledges that traditional beyond line-of-sight (BLOS) communications capabilities will be severely degraded or non-existent in the future fight. This research demonstrates a near-term solution that increases resiliency in BLOS communications consisting of a rocket-delivered expeditionary narrowband radio relay with an applicable use case. The payload of the relay consists of a software-defined radio controlled by a single-board computer and demonstrates resiliency by cross-banding signals between very high frequency and ultra high frequency transmit and receive frequencies, respectively. After a rigorous design and test process, this research culminated with an actual demonstration over the air and an attempted delivery by an actual rocket to a target altitude of 30,000 feet.

14. SUBJECT TERMS
expeditionary, rocket, payload, satellite communications, software defined radio, raspberry pi, narrowband communications, Marine Corps Operating Concept, resiliency

15. NUMBER OF PAGES
251

16. PRICE CODE

17. SECURITY CLASSIFICATION OF REPORT	**18. SECURITY CLASSIFICATION OF THIS PAGE**	**19. SECURITY CLASSIFICATION OF ABSTRACT**	**20. LIMITATION OF ABSTRACT**
Unclassified	Unclassified	Unclassified	UU

NSN 7540-01-280-5500

Standard Form 298 (Rev. 2-89)
Prescribed by ANSI Std. 239-18

THIS PAGE INTENTIONALLY LEFT BLANK

Approved for public release. Distribution is unlimited.

FILLING THE GAP: ROCKET DELIVERED SHORT-TERM EXPEDITIONARY BEYOND LINE-OF-SIGHT NARROWBAND COMMUNICATIONS RELAY

John W. Pross
Major, United States Marine Corps
BS, U.S. Naval Academy, 2006
MA, Marshall University, 2015

Submitted in partial fulfillment of the
requirements for the degree of

MASTER OF SCIENCE IN SPACE SYSTEMS OPERATIONS

from the

NAVAL POSTGRADUATE SCHOOL
June 2019

Approved by: Wenschel D. Lan
Advisor

James H. Newman
Co-Advisor

Nicholas R. Koeppen
Second Reader

James H. Newman
Chair, Department of Space Systems Academic Group

THIS PAGE INTENTIONALLY LEFT BLANK

ABSTRACT

The current Department of Defense (DoD) satellite communications (SATCOM) network consists of large, exquisite, and expensive constellations providing service across the radio frequency spectrum. However, the current SATCOM architecture is vulnerable to adversary actions including interference, jamming, directed energy, and antisatellite weapons. Despite the rise in adversary threats, the DoD continues to grow more reliant on SATCOM services in execution of all seven joint warfighting functions. The Marine Corps Operating Concept acknowledges that traditional beyond line-of-sight (BLOS) communications capabilities will be severely degraded or non-existent in the future fight. This research demonstrates a near-term solution that increases resiliency in BLOS communications consisting of a rocket-delivered expeditionary narrowband radio relay with an applicable use case. The payload of the relay consists of a software-defined radio controlled by a single-board computer and demonstrates resiliency by cross-banding signals between very high frequency and ultra high frequency transmit and receive frequencies, respectively. After a rigorous design and test process, this research culminated with an actual demonstration over the air and an attempted delivery by an actual rocket to a target altitude of 30,000 feet.

THIS PAGE INTENTIONALLY LEFT BLANK

TABLE OF CONTENTS

THIS PAGE INTENTIONALLY LEFT BLANK

LIST OF FIGURES

LIST OF TABLES

LIST OF ACRONYMS AND ABBREVIATIONS

A	ampere
AEHF	Advanced Extremely High Frequency
AGC	automatic gain control
APL	Johns Hopkins University Applied Physics Laboratory
ARG	Amphibious Ready Group
ARRL	Amateur Radio Relay League
ASD	acceleration spectral density
ASAT	antisatellite
atm	atmosphere
ATP	Army Techniques Publication
BLOS	beyond line-of-sight
°C	degrees Celsius
C2	command and control
CB	Citizen's Band Radio Service
CFR	Code of Federal Regulations
CO2	carbon dioxide
cm	centimeter
cm^3	cubic centimeter
CONOPS	concept of operations
COTS	commercial off-the-shelf
CSIS	Center for Strategic International Studies
DARPA	Defense Advanced Research Projects Agency
dB	decibel
dBi	decibels-isotropic
dBm	decibel-milliwatt
DoD	Department of Defense
DSB	Defense Science Board
EDU	engineering design unit
EHF	extremely high frequency
EM	electromagnetic

f	frequency
FAA	Federal Aviation Administration
FLTSATCOM	Fleet SATCOM
FM	frequency modulation
fps	feet per second
fps	frames per second
ft	feet
FY	fiscal year
g	gram
GAO	Government Accountability Office
Gbps	gigabits per second
GB	gigabyte
GEO	geosynchronous orbit
GHz	gigahertz
GPS	Global Positioning System
G_{rms}	G-force root-mean-square
GUI	graphical user interface
HAB	high-altitude balloon
IEEE	Institute of Electrical and Electronic Engineers
ITU	International Telecommunications Union
JP	joint publication
K	Kelvin
kbps	kilobits per second
kg	kilogram
km	kilometer
lbf	pound-force
lbs	pounds
LED	light-emitting diode
LEO	low earth orbit
LOS	line-of-sight
LPF	low pass filter
LNA	low-noise amplifier

m	meter
m/s	meters per second
mA	milliamp
mm	millimeter
MATLAB	Matrix Laboratory
MEO	medium earth orbit
MEU	Marine Expeditionary Unit
MHz	megahertz
MOC	Marine Operating Concept
MOS	military occupational specialty
MPE	maximum predicted environment
mph	miles per hour
MUOS	Mobile User Objective System
NASA	National Aeronautics and Space Administration
NPS	Naval Postgraduate School
OAT	outside air temperature
OV-1	operational view-1
PNT	positioning, navigation, and timing
RAM	random access memory
RF	radio frequency
rPi	Raspberry Pi
RDCS	Rocket-Delivered Communications System
SATCOM	satellite communication
SDR	software-defined radio
SHF	super high frequency
SNR	signal-to-noise ratio
SPDT	single-pole double throw
SSAG	Space Systems Academic Group
TTP	tactic, technique, and procedure
UART	universal asynchronous receiver/transmitter
UAV	unmanned aerial vehicle
UHF	ultra high frequency

UFO	UHF Follow-on
USB	universal serial bus
USMC	United States Marine Corps
V	volt
VHF	very high frequency
W	Watt
WGS	Wideband Global SATCOM
Z	Zulu

EXECUTIVE SUMMARY

Modern methods of warfare rely heavily on space-based capabilities—in particular, SATCOM—for beyond line-of-sight (BLOS) communications. However, adversaries are increasing their capability to interfere with this service, which presents a risk to leaders, particularly in executing command and control (C2) functions. Potential solutions to this challenge span the orbital, near-space, and terrestrial regimes, and all must be operated within the current SATCOM architecture to be effective near-term solutions. A near-space solution that is expeditionary and responsive is the rocket-delivered communications system (RDCS). A concept of operations (CONOPS) was developed which includes a realistic scenario based in the South China Sea in which a shipboard battalion commander utilizes RDCS to communicate nearly 375 miles away, despite adversary SATCOM jamming efforts.

Based on this scenario presented in the CONOPS, the RDCS design was completed through a detailed mission and trade analysis, resulting in an integrated system of hardware and software between the bus and payload. The bus design leverages existing experience at the Naval Postgraduate School but also includes modifications to facilitate rocket integration and protect against expected thermal conditions at altitude. RDCS was demonstrated after a thorough trade analysis, design, and testing regime. Testing of RDCS incorporated sub-system and full-system testing, which validated the hardware and software design, the culmination of which was an over-the-air test at a range of 3.2 km. Additionally, rocket integration and vibration testing validated the RDCS design in preparation for the demonstration flight.

The demonstration flight was the opportunity for RDCS to exhibit its capabilities in an operationally relevant environment from a target altitude of 30,000 feet. However, RDCS experienced a premature deployment as the rocket suffered an anomaly at approximately Mach 1.5, which resulted in fragmentation of RDCS. However, the rigorous design, construction, and testing process demonstrated RDCS is viable as an expeditionary near-term solution to assuring C2 through resilient BLOS narrowband communications for battlefield leaders in an uncertain future operating environment.

THIS PAGE INTENTIONALLY LEFT BLANK

ACKNOWLEDGMENTS

This project was not an individual effort but a product of faithful support from a number of individuals. First and foremost, I am thankful for the person and work of Jesus Christ in my life, as He has given me the skills, desire, and opportunity to pursue my graduate degree. Secondly, although you will not see the names of my wife and three children anywhere on the degree, this thesis and degree are just as much theirs as mine, only made possible by their faithful encouragement and devotion. To my wife, Meredith, and children, John, Katherine, and William, thank you for loving me despite the late nights and occasional working weekend.

To my thesis advisors, Dr. Lan and Dr. Newman, thank you for always being patient and willing to answer my questions; RDCS wouldn't be anything more than a drawing on a napkin without your guidance. Capt Nick Koeppen, my second reader, your operational experience was critical to making RDCS applicable to the USMC tactical commander. Dr. Matthews, your knowledge of SDRs is unsurpassed, and RDCS would have failed without your long-suffering and timely troubleshooting. To the Small Sat Lab team—David Rigmaiden, Alex Savattone, Ron Phelps, Dan Sakoda, Jim Horning, Levi Owen, Dr. Minelli, and Noah Weitz—your tireless daily efforts and experience were indispensable to building a functioning prototype. Capt Pierce, your epic ambition, unvarnished creativity, and relentless drive propelled RDCS upward to its end, for which you had but one job.

No matter how effective, applicable, or useful the concept of RDCS is, I do not intrinsically possess the skills to compose prose in a manner that is clear, intelligible, and accessible. I relied heavily on the enduring forbearance and unmatched expertise of Mr. Matt Norton, my Graduate Writing Center Coach, for whom I am most grateful. Finally, I owe a debt of gratitude to Col Lyons, the Senior Marine of NPS, for his masterful coaching and mentorship in the art of public speaking in the effort to transition RDCS from a prototype to being adopted as a new practice for a community of interest. True innovation.

The hands-on experience with these consummate professionals was humbling and reinforced; how much I really don't know. To Him be the glory.

I. INTRODUCTION AND BACKGROUND

The National Aeronautics and Space Administration (NASA) dates the dawn of the Space Age to October 4, 1957 [1], when the Soviet Union launched Sputnik 1, the first artificial object to orbit the Earth. NASA describes Sputnik 1 as "an aluminum 22-inch sphere…[that] weighed only 183 pounds…It carried a small radio beacon that beeped at regular intervals and could by means of telemetry verify exact locations on the Earth's surface" [1]. Over the past 60 years, space-based capabilities have evolved to support government, military, and civilian organizations in a myriad of missions ranging from positioning, navigation, and timing (PNT) to remote sensing.

The level of incorporation of space-based capabilities into the modern battlefield by the United States military was first demonstrated in 1991, when the U.S. Air Force Chief of Staff Merrill A. McPeak recognized the Persian Gulf War as "the first space war" [2]. Since then, space-based capabilities have become imbedded in all seven joint functions listed in Joint Publication (JP) 3-0 [3]: command and control (C2), protection, sustainment, movement and maneuver, intelligence, information, and fires. C2 relies heavily on space-based assets to provide satellite communications (SATCOM) and friendly-force tracking. Protection and sustainment functions rely on space-based communications links to coordinate logistical and defensive requirements for the commander across the battlespace. Movement and maneuver are aided through coordinated navigation provided by space-based assets; intelligence functions rely on products, like imagery, derived from space-based capabilities; information on the modern battlefield spans across all domains, to include space, and fires are accurate due to precise targeting and position data provided by the Global Positioning System (GPS).

As space-based capabilities have become more available and dependable, the U.S. military has increasingly relied on these unique resources—a reliance most evident in the capability of SATCOM. The Joint Force has access to exquisite SATCOM constellations that cost billions of dollars with the capability to transmit gigabits per second (Gbps) of data around the world. These constellations will continue to form the backbone of networks

used to execute C2 functions in future warfare, in which the battlefield extends beyond line-of-sight (BLOS).

The U.S. military's increasing reliance on SATCOM has spurred our adversaries to develop capabilities to interrupt these critical services. Recent conflicts in Iraq, Afghanistan, and Syria have been characterized by a technologically inferior adversary, which has allowed the Joint Force to use space-based capabilities relatively unimpeded. However, the SATCOM architecture is vulnerable to adversary actions including interference, jamming, directed energy, and antisatellite (ASAT) weapons, and the future fight with an adversary of similar technological aptitude will almost certainly result in SATCOM service interruptions.

An increasing reliance on the current SATCOM architecture could thus impose a significant disadvantage on the Marine Corps in a future conflict. As a member of the Joint Force, the United States Marine Corps (USMC) is no different from the rest of the Department of Defense (DoD) in its use of and reliance on BLOS communications almost entirely enabled by SATCOM. In recognition of the likely capabilities of a potential future adversary, the Marine Corps Operating Concept (MOC) [4] acknowledges that space-based capabilities will be less available and reliable in the operations of an expeditionary force in the 21st century. The future operating environment, the MOC says, will therefore require tactical units, maybe even as small as a platoon, "to operate in a distributed posture in a complex, non-permissive environment"—one in which freedom of movement or action in one or all domains is not guaranteed due to adversary influence. These adversary effects could markedly impact the battlefield, including C2 networks like SATCOM. The Marine Corps Strategy for Assured Command and Control [5] further echoes this concern, saying that as "Marines operate in C2-contested environments, we must not become overly reliant on any single method or technology (e.g., SATCOM)." A C2-contested environment that specifically impacts SATCOM services is known as a SATCOM-degraded environment. Non-permissive environments are expected to particularly challenge the current paradigm's reliance on space-based C2 for tactical units, which typically do not have access to bulky, static ground terminals or large power sources and rely on relatively

lightweight, low-power, and man-portable equipment for their SATCOM C2 network, increasing their susceptibility to interference.

Given that Marine Corps operations focus on the tactical level of war in expeditionary locations, it is imperative that the Marine Corps, and the DoD at large, develop solutions, space-based or otherwise, to ensure that tactical users have assured BLOS C2 in the non-permissive environment of the future fight. Any such solution must provide resiliency to the C2 network of a tactical unit without overburdening the user and while still being cost effective. Due to terrain and distribution, BLOS communications are crucial. In permissive environments, these BLOS needs are supported by SATCOM, but in non-permissive environments, short-term BLOS solutions may be sufficient for continued operations; five or ten minutes of connectivity should be sufficient for conducting basic C2 actions like situation or intelligence reporting. At the same time, while increasing network resiliency is paramount, a solution does not need to completely replace SATCOM but must augment its capabilities.

There are several potential solutions to ensuring such a resilient communications architecture will exist to support the 21st-century Marine Corps fight, some more mature than others; moreover, some may be more expeditionary than others. Given advances in miniaturization and the relatively inexpensive price of computing power, one particularly promising solution is a rocket-delivered, expeditionary, and narrowband communications payload that can be used as a near-term solution to increase resiliency in short-duration BLOS narrowband communications. This system could exploit the versatility of a software-defined radio (SDR) controlled by a single-board computer to provide a communications relay between users employing a man-portable radio and operating BLOS from other units. The flexibility and programmability of an SDR allow for that communication to be cross-banded on different frequencies or even dynamically changing between different receiving and transmitting frequencies, which increases network resiliency. This communications payload would be delivered by a rocket to an altitude above traditional air-breathing platforms but below traditional satellites, known as a near-space altitude. A communications relay payload in this altitude regime can extend communication BLOS to support a user on the distributed battlefield.

Despite how useful such a solution could be, little work in the area of using rockets to deliver communications payloads to near-space altitudes has been conducted. Historically, such equipment has been expensive, making a disposable system that provides a limited-connectivity window cost prohibitive. However, advances in enabling technologies like single-board computers, SDRs, and additive manufacturing have facilitated access to otherwise untapped solutions. A rocket-delivered communications relay could harness these emerging technologies to assure USMC BLOS command and control in a non-permissive environment.

Therefore, the purpose of this research is to develop the use case and demonstrate the utility and feasibility of a rocket-delivered communications relay system to a tactical user. The research will use widely available commercial off-the-shelf (COTS) hardware, ultimately resulting in an asset that supports the warfighter on the ground, in the air, or at sea. This capability is applicable to all military services in which BLOS communications via traditional SATCOM assets are not achievable due to the operating environment, terrain, or adversary actions. This research will also be useful to academia and the private sector as a demonstration of the utility of rockets for near-space payload research on a scale supportable at the collegiate level, expanding near-space research options.

A. RESEARCH QUESTIONS

How can a rocket-delivered communications relay system be used to augment the current SATCOM architecture to provide an alternative communication path for a tactical user, thereby increasing resiliency and ultimately lethality against adversaries capable of exploiting U.S. SATCOM dependencies?

B. LITERATURE REVIEW

The modern U.S. communications architecture is reliant on fragile and expensive constellations of exquisite, state-of-the-art satellites. Understanding the current SATCOM architecture is essential to characterizing the problems posed by an increasing reliance on SATCOM services, as is the literature related to the U.S. military's critical dependence on SATCOM. Next, potential sources of SATCOM service interruption are assessed to reveal

the challenges of the future fight. Finally, an evaluation of currently proposed or fielded systems across the orbital, near-space, and terrestrial regimes identifies the realm of possible solutions.

1. Increasing Reliance on SATCOM in U.S. Military Operations

In 2010, the Air Force Space Command estimated that bandwidth requirements grew from 2 kilobits per second (kbps) per person in 1991 during the Desert Storm conflict to over 20 kbps in 2007 during Operation Enduring Freedom and Operation Iraqi Freedom, much of which was delivered using SATCOM [6]. They further estimated that by 2011 that number would increase to approximately 30 kbps, a fifteen-fold increase in bandwidth requirements since 1991. Supporting [6], The Air University Space Primer [7] reported that "SATCOM bandwidth grew 30 times within the 13 years" from 1991 to 2004. Although these estimates differ, they clearly indicate a large increase in SATCOM demand during this period. A significant contributor to the rise in DoD SATCOM demand is the emergence of unmanned aerial vehicles (UAVs), which, according to the Government Accountability Office (GAO), increased the SATCOM bandwidth requirement by 300% between 2007 and 2011 [8]. Since the demand for more data exceeds the military's SATCOM capability, commercial SATCOM is contracted to provide additional throughput capability; the GAO reported that, from 2000 to 2011, the DoD's "reliance on commercial SATCOM rose by over 800 percent" [8]. This inflation of bandwidth requirements extends to the USMC, which has adopted modern communications and UAVs as part of its current warfighting capabilities.

Given this substantial increase in bandwidth requirements, it is clear that SATCOM has become fully integrated into the modern DoD C2 structure. In 2015, the GAO declared that the "DoD has become increasingly reliant on commercial SATCOM to support ongoing U.S. military operations" [9]. The increasing reliance on SATCOM, both military and commercial, presents a critical vulnerability to USMC command and control networks.

2. Sources of SATCOM Service Interruption

The growth of the U.S. military's use of SATCOM has led to a rise in interruptions of these critical communication services, ranging from hostile adversarial action in the

form of kinetic ASAT weapons to unintentional jamming by a friendly force. The increase in SATCOM interruption capabilities, whether intentional or not, presents a significant concern for users on the battlefield.

The People's Republic of China and the Russian Federation have proved to be the most advanced emerging threats. The Center for Strategic International Studies (CSIS) reported that "China has made rapid progress in developing both its space and counterspace capabilities. The country has tested direct-ascent ASAT weapons, on-orbit robotics, and remote proximity operations. Reports indicate that China is also developing and testing directed-energy and jamming technologies" [10]. This report also claimed that "Russia's space and counterspace capabilities suffered after the fall of the Soviet Union, but it has since made significant progress rebuilding both programs" [10]. These emerging counterspace capabilities present a growing threat to U.S. SATCOM services.

However, SATCOM jamming is not limited to adversary nation-states like China or Russia; it can also be a result of unintentional friendly interference. General John Hyten, leader of Air Force Space Command, remarked at the 2015 Association of Old Crows Electronic Warfare Conference that, "In 2015, thus far, we have had 261 cases where we have been jammed from getting information from our satellites down to the ground segment. How many were caused by an adversary? I really don't know. My guess is zero" [11]. With the increase in SATCOM demand, users, and terminals, it is reasonable to expect friendly interference jamming to increase as well. SATCOM jamming, whether adversarial or friendly, can significantly degrade mission effectiveness and presents a substantial concern to assured communications for tactical users.

3. Satellite Constellations: Expensive and Operationally Unresponsive

The increase in reliance on SATCOM coupled with the rise in sources of interruption presents a significant challenge to assured communications in a future conflict. However, this challenge is not easily solved with satellites because space-based systems have historically been expensive and operationally unresponsive. The costs associated with these large and exquisite satellite constellations, coupled with long acquisition timelines and inflexible launch schedules, make traditional SATCOM constellations challenging to

rapidly reconstitute. In 2015, Program Executive Office (Space Systems) reported a $5.8B cost for the five-satellite constellation, the Mobile User Objective System (MUOS), which includes four operational satellites with one on-orbit spare [12]. Other military SATCOM systems like Wideband Global SATCOM (WGS) and Advanced Extremely High Frequency (AEHF) constellations are no different, with their respective 2016 Selected Acquisition Reports (SARs) totaling $3.8B for WGS [13] and AEHF estimated at an astounding $9.1B [14]. Should one of the satellites in a constellation cease to operate, whether by intentional or unintentional means, replenishing the constellation would be very costly. The projected price for a single sixth MUOS satellite as a constellation replenishment is estimated at $1.4B [12].

In addition to such costs, the significant reduction in capability resulting from a nonfunctional satellite may last for a substantial amount of time if there are no available on-orbit spares due to prolonged launch schedules. As of October 27, 2018, the Space Exploration Technology Corporation (SpaceX), one of the leading launch providers in the United States, had a launch manifest of 35 future missions on their website [15]; at the pace of 1 launch every 13 days, the soonest a replacement satellite could be launched is approximately 455 days, or 1 year and 3 months. However, this assumes a replacement satellite could be funded, built, tested, and ready for launch in such a timeline.

Another challenge related to the current SATCOM architecture is responsiveness. Funding for the MUOS program was appropriated in fiscal year (FY) 2000; it received approval to be built only in February of 2008, and the first satellite was ready for delivery in 2012—12 years from initial funding to delivery [12]. MUOS is just one example of the long acquisition timelines that contribute to making SATCOM constellations incredibly expensive, costly to replenish, and relatively operationally unresponsive to the tactical warfighter.

In response, the DoD established up the Operationally Responsive Space (ORS) office in 2007 to specifically address the responsiveness issue. The National Security Space Office described the plan for ORS as "[to] improve the responsiveness of existing space capabilities…and to develop complementary, more affordable, small satellite/launch vehicle combinations and associated ground systems that can be deployed in operationally

relevant timeframes" [16]. The eighth ORS project in 12 years, ORS-8 is a mission-critical weather satellite, the contract for which was awarded in September 2018 [17]. Previous ORS projects included communications and intelligence, surveillance, and reconnaissance payloads. Nevertheless, while this office has successfully demonstrated a certain level of responsiveness, it has not fundamentally changed the acquisition or operational framework of modern satellites.

4. Current SATCOM Architecture

A potential solution to the problem of assured BLOS communications in a contested environment may exist outside the current SATCOM architecture, but an effective and near-term solution should be designed to operate with the same terrestrial-based user equipment. This equipment is specialized to operate with one or more of the four unique frequency bands associated with radio frequency (RF) communications. The primary frequency bands for tactical level RF communications are very high frequency (VHF) and ultra high frequency (UHF), with UHF being the primary SATCOM frequency band. Two other SATCOM frequency bands exist, super high frequency (SHF) and extremely high frequency (EHF), but USMC company-sized elements and below typically do not have access to these architectures. While SHF and EHF may not specifically apply to a relatively small foot-mobile unit, these bands are critical to battlefield C2 above the company level for the USMC. Each band has unique characteristics, common applications, and associated users within the modern SATCOM architecture.

a. VHF

While not normally used for BLOS communications, company-sized elements typically use the VHF band for line-of-sight C2, as VHF is ideally suited for dismounted and highly mobile units. The International Telecommunications Union (ITU) defines VHF frequencies from 30–300 megahertz (MHz), which includes commercial frequency modulation (FM) radio stations familiar to a majority of users in the United States [18]. VHF frequencies are normally used at the company level because terminals tend to be small, lightweight, inexpensive, and man-portable. The limited bandwidth associated with VHF frequencies also make them better suited to the company's lesser need for large data

transmissions as compared to a higher level of command. VHF transmissions can be analog or digital, can use a variety of modulation techniques, and are highly capable of penetrating foliage. However, VHF transmissions produce large beam patterns, making these signals more susceptible to detection and interference. VHF is therefore ideal for relatively short-distance, line-of-sight (LOS) communications; as such, they are not normally used as part of a SATCOM architecture. However, because company-sized units will still most likely be operating man-portable VHF systems to communicate internally and with higher echelons of command in a future conflict, the VHF band is fitting for incorporation in a rocket-delivered communications relay system.

b. UHF

The most common SATCOM band for a disadvantaged user is UHF. The ITU defines UHF frequencies as those falling between 300 MHz and 3 gigahertz (GHz) [18]. The Army Techniques Publication (ATP) 6–02.54 [19] describes these communications as narrowband SATCOM services, which are provided to the U.S. military by Fleet SATCOM satellites (FLTSATCOM), UHF Follow-on (UFO) satellites, and the most recent MUOS satellites. These satellites are operated in geosynchronous orbit (GEO), which provides the largest access to the Earth while keeping the satellite in essentially the same relative spot over the ground, simplifying network technology and management requirements. Traditionally, a narrowband satellite operates by simply receiving a UHF signal from within its antenna footprint and retransmitting it on a different frequency within the same band and within the same antenna beam pattern through the use of a transponder. This simultaneous sending and receiving capability is known as full-duplex—a characteristic of many narrowband satellites. From GEO, an Earth-coverage antenna has access to nearly one-third of the Earth's surface, allowing users to communicate a very long but limited distance. Advanced technologies in MUOS allow a tactical user to communicate with any other MUOS terminal in the world, significantly enhancing the traditional range of narrowband SATCOM.

As narrowband SATCOM range is improving, UHF frequencies are in high demand. This demand results in apportioning a number of channels with relatively small

bandwidths to individual users to support the significant demand. Due to this limited bandwidth, UHF is typically used by company-sized units for voice communications or relatively low-data transmissions. ATP-6-02.54 further describes that "narrowband SATCOM radios connect tactical operations centers across echelons and support long-range surveillance units…separated from the main forces." Similar to VHF, these transmissions can be analog or digital, may use a variety of modulation techniques, and readily transmit through foliage. UHF frequencies, similar to VHF, produce a relatively large beam pattern, which is relatively easily to jam or interfere. It is likely that a command post or headquarters, whether on shore or afloat, will be operating both UHF and VHF frequencies to communicate with distributed disadvantaged users.

c. SHF

Although extremely useful for the U.S. military, SHF services are not normally required by a company-sized Marine unit. The 3–30 GHz frequency band is defined as SHF [18]. This region of the electromagnetic (EM) spectrum has significantly more bandwidth available, allowing for large volumes of data transmission. SHF is the typical frequency range for satellite television or similar high-capacity data services. As explained in [19], the U.S. military receives SHF service, also referred to as wideband, from military systems like WGS, as well as from commercial systems. Transmissions are nearly exclusively digital, encrypted, and range from large-file transmission services to video teleconferencing. While SHF is a critical link within today's SATCOM architecture and the overall C2 of the modern U.S. military, it is not a suitable option for the C2 bands associated with a foot-mobile unit.

d. EHF

As with SHF, EHF bands are typically reserved for military echelons above the company-level user. However, EHF, defined as the 30–300 GHz frequency band [18], is fundamental to U.S. strategic military C2. SATCOM services in this range are known as protected SATCOM [19]; AEHF is an example of a protected SATCOM system. As the Lockheed Martin Corporation explains [20], this frequency band has a large amount of available bandwidth that can be used to transmit considerable amounts of data or to

implement various techniques that make this waveform very jam-resistant, with a low probability of interception. However, the hardware and software that enable protected communications are exceptionally complicated and expensive, so their distribution is limited to only the highest-priority assets. As the Army states [19], "these unique capabilities make the use of [the] protected SATCOM frequency band ideal for the most critical strategic forces, and mission command systems" but make EHF less than ideal as a choice for a tactical C2 radio relay.

5. Potential Solutions

Given the U.S. military's increasing reliance on BLOS communications and the rise of adversary capabilities, finding solutions to narrowband BLOS communications is imperative to the future warfighting capability of the USMC and DoD at large. The DoD Defense Science Board (DSB) Task Force on Military Satellite Communication and Tactical Networking, which concluded in March 2017, acknowledged the vulnerability of SATCOM in its concluding report [21]. In this report, the Federal Advisory Committee examined satellite communications, tactical networking, and commercial capabilities to determine gaps and propose solutions. The DSB recommends investment in new jam-resilient waveforms, increased investment in science and technology "toward alternative, protected, and BLOS architectures," and advice for Combatant Commands to "develop and exercise with tactics, techniques, and procedures (TTP) for operations with degraded MILSATCOM services" [21]. This report demonstrates the clear need for a solution to the vulnerability presented by the current SATCOM architecture but offers few, if any, feasible near-term solutions. Yet, numerous potential near-term solutions do exist to increase the resiliency of the current SATCOM architecture. These solutions include the orbital, terrestrial, and near-space regimes, discussed in detail in the following sections.

a. Orbital Regime

Orbital-regime solutions consist of increasing the number of satellites within currently existing constellations or populating new constellations in non-traditional orbital regimes. A Johns Hopkins Applied Physics Laboratory (APL) article [22] proposed two answers, one being a proliferation of traditional large-sized satellites in either medium earth

orbit (MEO) or low earth orbit (LEO) and the other an entirely new constellation of nanosatellites in LEO. The proliferation of large satellites in MEO or LEO is simply a variation of the current architecture, consisting primarily of exquisite and expensive satellites at GEO. The LEO constellation-of-nanosatellites design mirrors a current project of the Defense Advanced Research Projects Agency (DARPA) known as Blackjack. Blackjack is a LEO constellation program with proposed key parameters from DARPA's Broad Agency Announcement [23] that include a 0.5 m cube payload weighing less than 50 kilograms (kg) and a cost of no more than $1.5M. These figures do not include the bus to control such a payload, but $1.5M is significantly less than a single traditional GEO communications satellite. Additionally, a 2018 Naval Postgraduate School (NPS) thesis by Phillip Swintek [24] also proposed a constellation of nanosatellites to address the critical vulnerability of satellite-based narrowband communications.

The proposed orbital solutions are capable of increasing resiliency to a tactical unit's C2 network; each idea uses narrowband communications to extend C2 BLOS, well in excess of the 25–300 mile operational distance associated with a tactical unit, regardless of the orbital regime. With the proper architecture design, these orbital solutions could potentially provide persistent connectivity to the tactical user, allowing for near-continuous C2. However, these ideas have four limitations: cost, response time, sustainment, and predictability. The cost constraint of traditional communications satellites limits the number of spacecraft on-orbit and restricts the ability to develop a resilient constellation through simply proliferating GEO-based assets. Even if a satellite were launch-ready to support an existing constellation, the inflexible launch schedule of current space-lift capabilities significantly increases the time needed for the asset to achieve operational capability on orbit.

Thus, the creation of entirely new nanosatellite constellations would likely be expensive and take years to develop. It would also generate a significant sustainment support requirement in terms of personnel and training. The Marine Corps does not currently man, train, or equip personnel to operate or maintain a constellation of spacecraft. Creating such a program would also require additional manpower in new military occupational specialties (MOSs) with unique training to be successful. Although a LEO

nanosatellite constellation may be a potential future solution the SATCOM resiliency issue, a fully-operational solution could likely not be realized by the USMC in less than a decade.

Finally, orbital solutions to SATCOM are predictable. Adversary jamming capabilities, normally applied to assets in GEO, could be modified for use against satellites in any orbital regime, making orbital solutions equally susceptible. Additionally, the nature of orbital mechanics allows satellite locations to be relatively easy to obtain and propagate, further adding to the jamming susceptibility of orbital solutions. While proposed orbital solutions will likely significantly increase SATCOM resiliency in the future, the USMC requires a solution that can be rapidly developed and proliferated in the near term.

b. Terrestrial Regime

Terrestrial solutions to increasing resiliency in BLOS communications in support of future Marine Corps warfighting needs center primarily on airborne relays for either manned or unmanned platforms. While not a satellite, terrestrial systems—i.e., aircraft—are capable of extending communications networks, much like satellites. This mission is known as airborne radio relay and is a capability that has been incorporated into U.S. military aircraft for decades. The Harris FALCON III® RF-7850A-MR is a multi-channel airborne networking radio certified for aircraft and specifically designed for networking signals of various forms on the battlefield, demonstrating that the technology currently exists to execute this type of communications [25]. Unmanned or remotely piloted platforms provide similar capabilities to manned aerial platforms with reduced risk to the pilot.

However, like orbital solutions, terrestrial solutions also have significant limitations. One is vulnerability: to effectively relay a UHF or VHF signal from a disadvantaged user BLOS, an aerial platform, whether manned or unmanned, needs to be positioned to maintain LOS between both users in the SATCOM link. Under certain conditions, this requirement could place the relay vehicle in a location vulnerable to adversary actions, increasing the risk to vital and expensive assets that are likely capable of mission sets that extend beyond communications relay. Unmanned platforms reduce the risk to human life; however, the risk to the expensive and limited asset still remains.

Another limitation to the use of air-breathing aircraft to augment current BLOS communication capabilities is the service ceiling. The higher a relay platform, the further the LOS and, consequently, the longer the relay range capability. This is one reason satellites are placed in GEO—to maximize their range capability. Air-breathing engines are limited in their maximum altitude due to the reduction in air density as altitude increases. Traditional air-breathing platforms organic to the USMC, like the F/A-18 Hornet, have a published service ceiling of 50,000+ feet (ft) [26]. Although useful for extending communications BLOS, the range performance at this altitude is not commensurate with that needed to augment SATCOM capabilities for a disadvantaged user in excess of 300 miles.

c. Near-Space Regime

The near-space environment, beyond the reach of typical air-breathing engines but at altitudes prohibitive to sustained orbital velocities, presents an opportunity for potential solutions. Space Data Corporation is an American company producing a helium balloon that delivers a 225–375 MHz UHF relay to altitudes ranging from 85,000–100,000 ft [27]. This SkySat™ can be tethered or untethered and can carry a payload of 12 pounds (lbs) or less. As was reported in *15th MEU News* [28], the USMC 15th Marine Expeditionary Unit (MEU) has demonstrated a tethered Combat SkySat reaching an altitude of 85,000 ft with a radio relay range of 600 nautical miles. Combat SkySat has also been used in Libya, Afghanistan, and Pakistan.

While the Combat SkySat presents a near-term solution to BLOS communications, it does have its limitations in expeditionary utility and operational responsiveness. A tethered balloon lacks expeditionary utility as it cannot be anchored to a ship underway, effectively narrowing the USMC use case for a balloon to the untethered option. NASA launches untethered balloons in support of meteorology and scientific research; however, the typical ascent rate of these balloons is 1,000 feet per minute, meaning that a balloon could take nearly 100 minutes to reach an altitude of 100,000 ft [29]. Such a timeframe presents an issue of responsiveness, as this delay between launch and operating altitude could have a significant impact on the battlefield.

d. Proposed Solution

In light of the inadequacies of these existing solutions, this research proposes a near-space solution to relay VHF to UHF voice transmissions, much like a traditional narrowband transponder, in the form of the Rocket-Delivered Communications System (RDCS). Unlike orbital solutions, a rocket-delivered payload would be considerably faster to develop, launch, and deploy. Sustainment of a rocket-delivered solution would require minimal change to the current Marine Corps training and manpower construct: while the Marine Corps does not have personnel who operate satellites, it does have an abundance of qualified explosives handlers and operators who can launch a rocket. Moreover, the response time of a rocket, on the order of a few minutes, is much faster than the approximately 1.5 hours associated with a balloon. Rockets are capable of achieving or exceeding the operating altitudes of balloon-based systems like Combat SkySat, resulting in comparable communication ranges on the order of 600 miles. Moreover, although near-space altitudes do not provide the communications range capability across a third of the earth like an earth-coverage antenna from GEO, a 600-mile communication relay has significant utility to the Marine Corps for the future operating environment. Also, the use of a rocket virtually eliminates the commander's risk to critical assets like an aircraft or UAV, presenting minimal risk to human life. Enabling technologies are highly capable and exist as COTS hardware, making them widely available, which allows a payload to be rapidly developed into a near-term solution. Information security is also of minimal risk as no onboard encryption is required to simply receive and retransmit a signal. The combination of COTS hardware with no encryption allows RDCS to be expendable, which reduces the burden to the operational unit. Finally, the expeditionary nature of rockets allows them to be transported and fired from the deck of virtually any ship or potentially even a pickup truck. RDCS could thus be highly proliferated and dispersed throughout the battlespace to increase C2 network resiliency.

C. METHODOLOGY AND APPROACH

To research and develop the near-space solution of RDCS, Chapter II presents a thorough concept of operations (CONOPS), developing a use case that demonstrates utility

to the Marine Corps. Next, Chapter III conducts a detailed analysis of COTS hardware and software in the trade space and determines the most effective approach to designing the RDCS. Chapter IV discusses the testing of the RDCS from the component to integrated-system level to ensure proper functionality and suitability for the rocket environment. The culmination of this research, an attempted delivery by a rocket to a target altitude of 30,000 ft, is discussed in Chapter V. Using an iterative design, build, and test process, RDCS was systematically engineered and successfully demonstrated the ability to augment current SATCOM capabilities, enhancing resiliency in our communications architecture for a future USMC conflict.

D. CONCLUSION

The MOC and the DoD at large recognize the vulnerability associated with overreliance on SATCOM. The rise in adversaries' capabilities to interrupt SATCOM services furthers the imperative to find new and innovative solutions for ensuring SATCOM resiliency in the future. Numerous solutions exist in the space, terrestrial, and near-space environment, but some solutions require fixed-base operations, while others are unresponsive, impose significant risk of loss of life, or are too complex to be realized in the near term. RDCS is a near-space solution that is expeditionary, presents minimal risk to the commander, and can be developed relatively quickly, increasing BLOS communications resiliency for the United States Marine Corps in the future operating environment.

II. RDCS CONOPS

Understanding the intended application of RDCS is paramount to ensuring its design is operationally effective. This chapter explains how RDCS might be employed, the capability it provides to unit leaders in a contested operating environment, and the potential impact such a system could have on the battlefield. A CONOPS and operational view-1 (OV-1) give a graphical representation of RDCS operations. Next, a scenario provides an example, based on the MOC, in which RDCS could be effective. Finally, a discussion of the potential coverage capability of RDCS based on nominal near-space altitudes of a rocket demonstrates the utility of RDCS to the tactical warfighter and the Marine Corps.

A. CONCEPT OF OPERATIONS

RDCS is designed to increase tactical user network resiliency by providing an alternative to SATCOM for BLOS, narrowband communications in a contested environment. It is not designed to replace the technologically advanced SATCOM constellations that currently provide service to the U.S. military, especially in a permissive environment. Therefore, the RDCS CONOPS is essentially only applicable to a SATCOM-denied or -degraded environment.

There are three components to the employment of RDCS: users, rocket, and RDCS. The user segment consists of two or more users employing narrowband communications equipment to communicate. The next segment is the rocket that will deliver RDCS to near-space altitudes. This rocket could be fired by any party, but for the best range performance, it should be fired close to middle of the group of users. The final segment is RDCS itself, which is contained inside the rocket and performs the full-duplex relay.

To employ RDCS, the rocket is fired to a near-space altitude. At the rocket's highest point, or apogee, it deploys RDCS. After deployment, RDCS starts descending back to Earth under a parachute and immediately begins receiving VHF transmissions from one user. The VHF path from the transmitting user to RDCS is known as the uplink. Functioning much like a traditional transponder, the system simultaneously retransmits that signal over a UHF frequency to the receiving user; this path is known as the downlink and

completes the communications path between the users. By functioning like a transponder, the system never de-modulates the signal; therefore, no onboard encryption is required. The design of the system, coupled with the unclassified nature of its payload, allows it to be disposable. RDCS is a full-duplex system that is able to connect users in a SATCOM-degraded environment and increase network resiliency by providing an augmentation to SATCOM.

B. SCENARIO

A fictional scenario illustrates how RDCS could be employed by USMC units in the field. As described in Chapter I, the MOC will require tactical units, potentially as small as a platoon, to operate in excess of 300 miles away from a higher-level unit. This large ground distance typically requires the commander to rely heavily on SATCOM as a means of executing the seven joint functions. The following scenario demonstrates the vulnerability of SATCOM, its specific implications to the C2 and intelligence functions, and how RDCS could be used to provide an alternative communications path for tactical users. Following the vignette, Figure 1 depicts an operational view-1 for RDCS in this particular case.

> It is currently 2025. In response to recent provocations by the People's Republic of China (PRC), the 15th MEU, as part of Joint Task Force-50 (JTF-50), has been deployed to Southeast Asia to counter aggression by the People's Liberation Army Navy (PLAN) against the Philippines. JTF-50 is actively engaged in combat operations but has yet to establish air superiority. As a multi-domain competitor, the PRC has also been conducting actions in the cyber and space domains. Reports of naval mines across the various straits and inlets that connect the South China Sea to the Philippine Sea are forcing the Amphibious Ready Group (ARG), led by USS America (LHA-6), to remain in safe waters in the Celebes Sea, beyond the range of the PLAN's anti-ship missiles. The 3rd Battalion, 1st Marine Regiment (3/1) is the ground combat element (GCE) currently headquartered on USS America. Intelligence suggests that PLAN mining vessels are operating from San Antonio Bay near the town of Bataraza on the Philippine Island of Palawan.
>
> Yesterday, 3/1 successfully inserted 1st Platoon into a remote section of the island 375 miles from USS America. That platoon is now moving on foot to the target area. Their mission is to provide observation of the area, report any enemy activity in and around San Antonio Bay, and be prepared to

conduct follow-on operations in support of JTF-50. The movement for 1st Platoon from the landing zone to the target area is expected to take two days. They are relying on multi-band (VHF- and UHF-capable) Harris PRC-117G radios for SATCOM over UHF frequencies as their primary means of communication with battalion headquarters (HQ), embarked on LHA-6, 375 miles away. They have also been allocated a single VHF frequency for communication internal to the platoon. Intelligence and situation reports will primarily be passed using FM voice transmissions, minimizing data requirements.

After two days of movement and 12 hours of observation, it is 1430 Zulu Time (Z), and 1st Platoon is prepared to give its first position and intelligence reports. However, when the radio call is made, HQ does not respond. From the radio operator's perspective, and according to all of his troubleshooting procedures, the transmission should have been received. However, HQ never answers.

Meanwhile, on the USS America, the 3/1 Commanding Officer (CO) has not received a single transmission from 1st Platoon for nearly 50 hours—just static. The CO does not know their status or disposition. They were expected to be in position and make their first report between 1400–1500Z. To complicate the situation, JTF-50 is demanding an update regarding San Antonio Bay from the MEU in order to neutralize the mining vessels and clear a path for ARG through the Sulu Sea. Ships have been unable to circumnavigate the mine fields, and time is of utmost importance.

In response to U.S. military actions, and unbeknownst to JTF-50, the PLA has been actively jamming the MUOS satellite serving the western Pacific for the past two days. This satellite is the primary provider of narrowband SATCOM communications in support of JTF-50. Without an alternative means of communication, 3/1 may not be able to provide the critical intelligence gained by 1st Platoon.

However, the battalion expected such contingencies and has trained for them extensively. In the event 1st Platoon is unable to establish positive, two-way communication with HQ by 1500Z two days after landing, communications will switch to the alternative plan. This plan uses a new system known as RDCS to augment the communications network in lieu of a satellite. At a pre-designated time, 2nd Platoon, operating on the remote island of Mapun in the Sulu Sea, launches RDCS. Each platoon commander was given a laminated card with communication windows based on time, which was synched prior to departing the ship. With the support of 2nd Platoon, 1st Platoon communicates the critical position and intelligence reports using VHF voice transmissions, which are uplinked to RDCS and relayed in UHF down to HQ, making use of the high-gain antenna onboard the ship. The nature of the payload make it disposable, so it harmlessly

descends into the Sulu Sea. Using only organic assets, 3/1 is able to provide JTF-50 with the 1st Platoon's intelligence and neutralize the PLAN's mining capability in the Sulu Sea, which enables the ARG/MEU to prepare for follow-on operations.

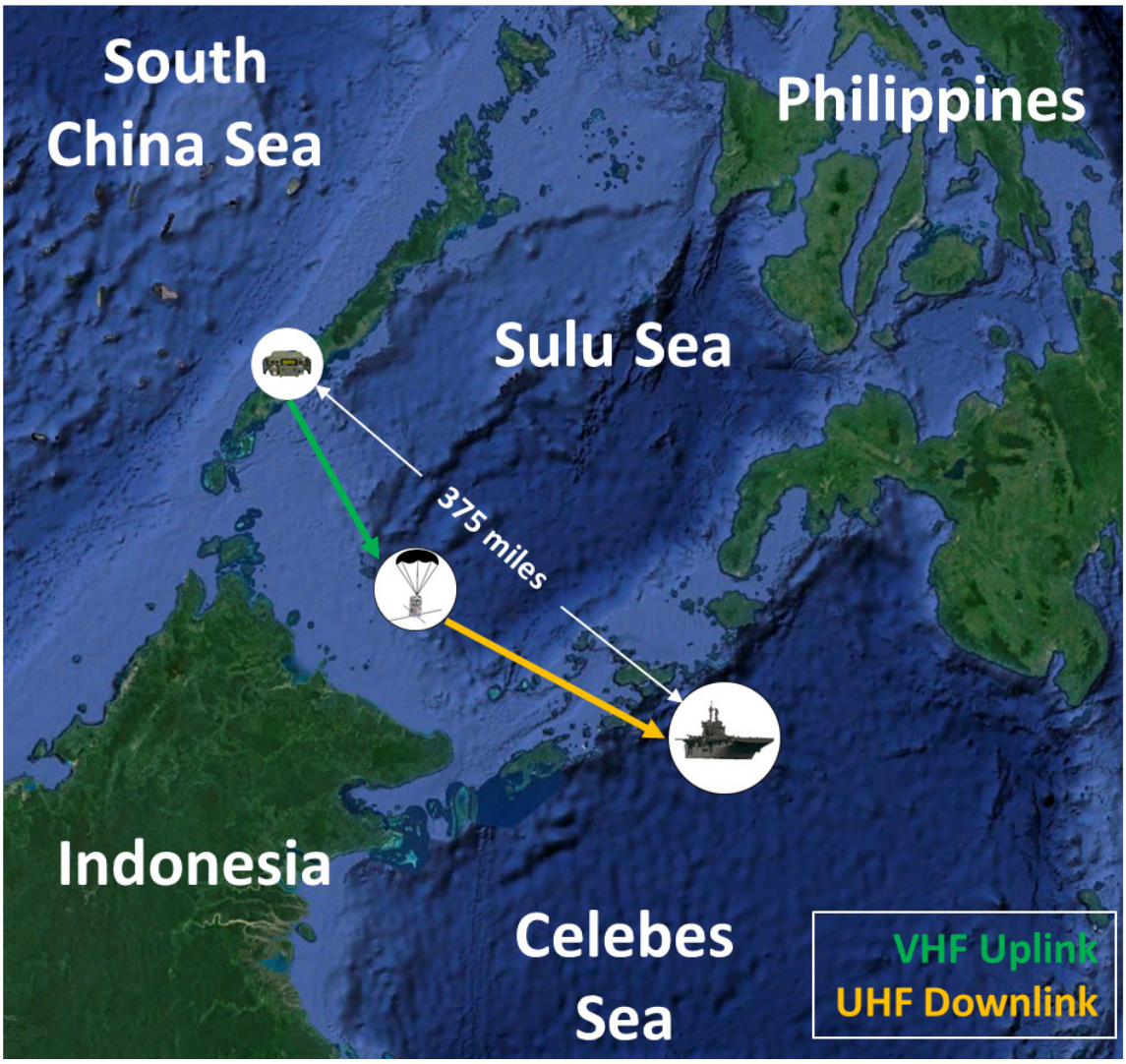

Figure 1. RDCS Operational View-1. Adapted from [30].

This scenario presents several potential implications of over-reliance on SATCOM to the Marine Corps and the greater Joint Force. If 1st Platoon had not had an alternative communications path, the operational effectiveness of the unit would have been severely degraded and would have impacted the JTF-50. However, RDCS provided that alternative

communications path, effectively negating the SATCOM jamming from the PLA. Because the Battalion was not over-reliant on SATCOM, had access to enabling technologies like RDCS, and was trained to properly employ the system, 3/1 successfully operated in a degraded environment using organic assets and continued to execute its mission.

C. RANGE AND TIME PERFORMANCE

RDCS is able to provide BLOS communications capability similar to that provided by a satellite, but from a lower altitude. In general, the higher the altitude, the larger the LOS distance to the horizon. Since RDCS uses VHF and UHF frequencies, which are limited to LOS, one of the limits to the maximum range capability of RDCS is altitude. The other limitation relates to signal processing characteristics that will be discussed in Chapter III. Upon deployment, at its highest altitude, RDCS obtains its maximum communications link range. As the system descends under a parachute, the maximum distance to the horizon decreases, reducing the link range. Thus, with all other variables constant, the longer the distance between users, the shorter the available connection time. While not ideal for persistent communications, the limited connection time could be enough in a SATCOM-degraded environment for the most basic mission tasks to allow continued operations.

Assuming an approximately 196,000-foot deployment altitude, the range and time performance of an RDCS is depicted in Figure 2. At the initial deployment altitude, the maximum operational range of RDCS is 638 miles as indicated by letter I in Figure 2. There are two components to this maximum operational range, the uplink ground range of 211 miles (letter H in Figure 2) and downlink ground range of 426 miles (letter G). RDCS range decrease as the system descends, limiting the connection time to the user. The colored portions of the diagram relate to and retain their color scheme from the scenario illustration in Figure 1. The uplink ground range is the distance over the ground between 1st Platoon's position in the vicinity of San Antonia Bay and the island of Mapun, where RDCS was launched—approximately 130 miles. The uplink slant range from 1st Platoon to RDCS is indicated by the green arrow and models the physical path the VHF transmission would follow. The downlink ground range, or distance between RDCS and

HQ onboard LHA-6, is approximately 275 miles. The downlink slant range from RDCS to HQ is depicted by the orange arrow and represents the path of the UHF downlink. Tracing these distances indicates that 1st Platoon has just over five minutes, as indicated by the red circle along the vertical axis, to complete their communication before RDCS is unable to complete the link. At this point, RDCS has descended through 133,000 ft and loses LOS between users. A complete diagram of RDCS range and time performance is contained in Appendix A.

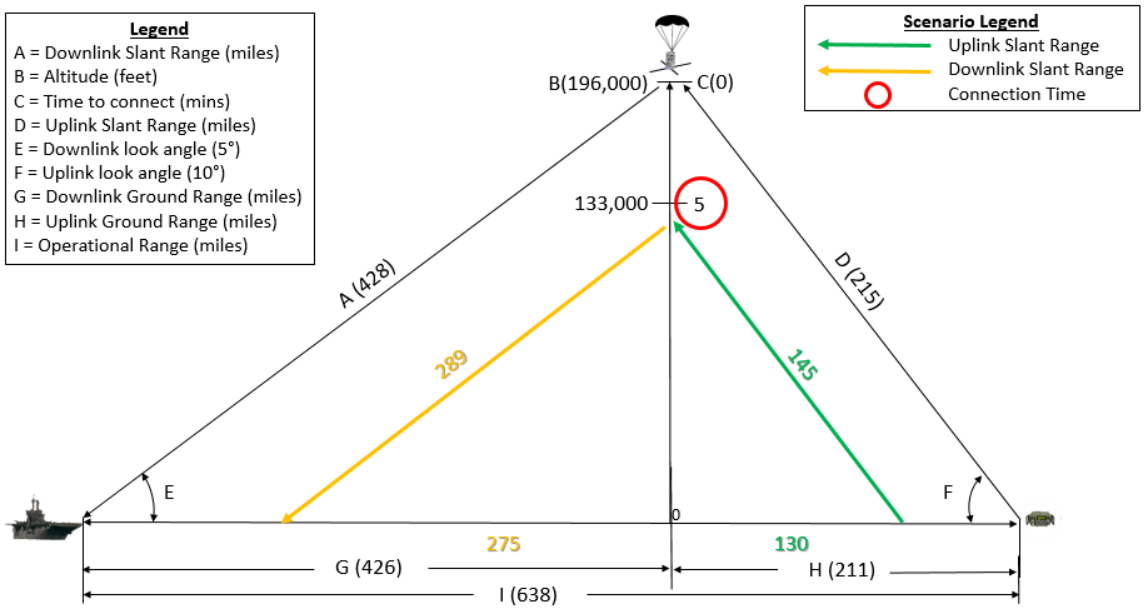

Figure 2. RDCS Range and Time Performance.

Although five minutes hardly compares to the persistent coverage of traditional SATCOM, it is enough time to pass the mission-critical information necessary for JTF-50 to continue combat operations. The deployment altitude of approximately 196,000 ft represents a nominal near-space altitude, and the time to descend is based on a predicted descent rate that gradually decreases throughout the descent. The derivation of Figure 2, including all equations, variables, and assumptions, is discussed in detail in Chapter III.

D. CONCLUSION

RDCS can provide an alternative to SATCOM in a contested environment. The scenario of this chapter highlights some of the challenges inherent to the MOC, one of which is command and control of distributed units in a contested environment. Presenting some of the possible dangers of SATCOM over-reliance, this scenario also demonstrates the potential capabilities a system like RDCS could provide to the USMC. Through proper training and planning, RDCS could be employed to provide short-term, surgical communication windows for units, thereby increasing the Marine Corps' flexibility, adaptability, and lethality on the battlefield.

THIS PAGE INTENTIONALLY LEFT BLANK

III. RDCS DESIGN

The communications capabilities demanded by the scenario described in Chapter II sets forth the considerations and process for the design of RDCS and are presented in this chapter. The system is a full-duplex radio relay that operates with existing communications equipment to provide BLOS communications. The discussion of the design process begins with the first design consideration, the operational frequencies, which have a significant impact on nearly every aspect of the design of any RF communication device. For the device to be effective and relevant as a near-term solution, it is imperative that these uplink and downlink frequencies be compatible with current radios and antennas, which allows users to seamlessly switch between traditional SATCOM and RDCS. The requirement for compatibility leads to an analysis of the user segment.

The results of these analyses directly informed the hardware and software of RDCS, which is divided into two major sections, the payload and the bus. Each has distinct functions related to the overall system, but both are critical to the success of RDCS. The payload portion has the required hardware and software to receive a VHF transmission containing an FM voice signal and relay that signal on UHF, identical to the scenario in Chapter II. The bus executes the administrative tasks like housing the payload, running startup scripts, regulating power, transmitting telemetry, and facilitating recovery.

However, before any specific design choices were made, a thorough understanding of the design constraints imposed by the operating environment, including both physical and administrative constraints, was paramount to the success of the RDCS.

A. DESIGN CONSTRAINTS

The Federal Aviation Administration (FAA) administratively imposes a weight restriction based on safety concerns, while the rocket imposes physical constraints on payloads it carries like length, width, and deployment altitude. Atmospheric air temperatures and pressures associated with the near-space regime also impact design considerations. While not part of the physical design, the external constraints and environmental effects have substantial influence on nearly all aspects of RDCS.

1. FAA Constraint

For compliance and demonstration purposes, RDCS has a weight constraint of 1.8 kg (4 lbs). While there are no specific regulations for unmanned items descending to earth under a parachute like RDCS, there is a portion of the Code of Regulations (CFR) that addresses unmanned free balloons, which can be applied to RDCS. Unmanned free balloons, like those launched by NASA and discussed in section I.B.5.c of this work, routinely carry payloads to near-space altitudes that then return to earth as an unmanned object under a parachute. These payload packages are limited by the CFR, Title 14, Volume 2, Subpart A of §101.1, which states that payload packages carried by unmanned free balloons must weigh less than 1.8 kg or be subject to additional constraints [31]. It is important to note that the recovery equipment associated with the payload package is not included in the 1.8 kg limitation. Although RDCS is not designed to require retrieval, recovery capabilities were included in the design to promote safety and facilitate academic research. While RDCS would not be required to abide by the CFR if operationalized, the system was designed to conform to these regulations for demonstration and safety purposes.

2. Rocket Constraints

Throughout the design process, launch vehicle integration was consistently a factor and had design implications for nearly every component of RDCS. The payload bay of the rocket, pictured in Figure 3 with a generic payload, physically constrains RDCS to a cylinder measuring approximately 15.42 centimeters (cm), or six inches, in diameter and 30 cm long [32]. For RDCS, the diameter of the rocket body is the limiting dimension.

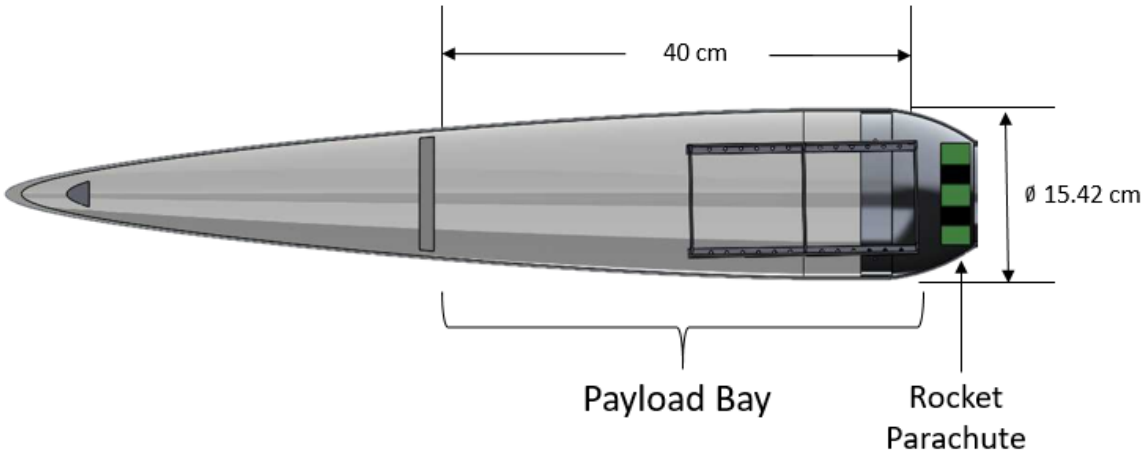

Figure 3. Payload Bay. Adapted from [32].

In order to avoid the use of mechanical deployment mechanisms, thereby reducing risk, payloads were not physically attached to the rocket inside the payload bay. Instead, payload movement inside the bay is constrained in the lateral direction by the inner surface of the rocket payload bay; the payload remains in place along the thrust (longitudinal) axis due to the vertical acceleration forces inherent to rocket flight.

At the highest point of ascent, or apogee, the rocket is designed to release compressed carbon dioxide (CO2) to expel the nose cone. The differential CO2 pressure inside the compartment separates the payload from the nose cone, deploying payloads for operation. The expected altitude of the rocket was 45.7 kilometers (km), or 150,000 ft, which imposed several environmental considerations and significantly impacted virtually every system of RDCS [32].

3. Environmental Effects

The planned deployment altitude of 150,000 ft presents temperature, pressure, and wind implications for RDCS. Figure 4 is a graphical representation of the atmospheric temperature and pressure profiles as a function of altitude, based on the 1976 Standard Atmosphere model [33]. These profiles are numerically summarized in Table 1. Based on these models, RDCS is subject to very cold temperatures and operates in a near-vacuum as

the outside air temperature (OAT) during the descent is rarely above freezing (0 degrees Celsius, or °C) and the pressures remain well below a standard atmosphere (1 atm).

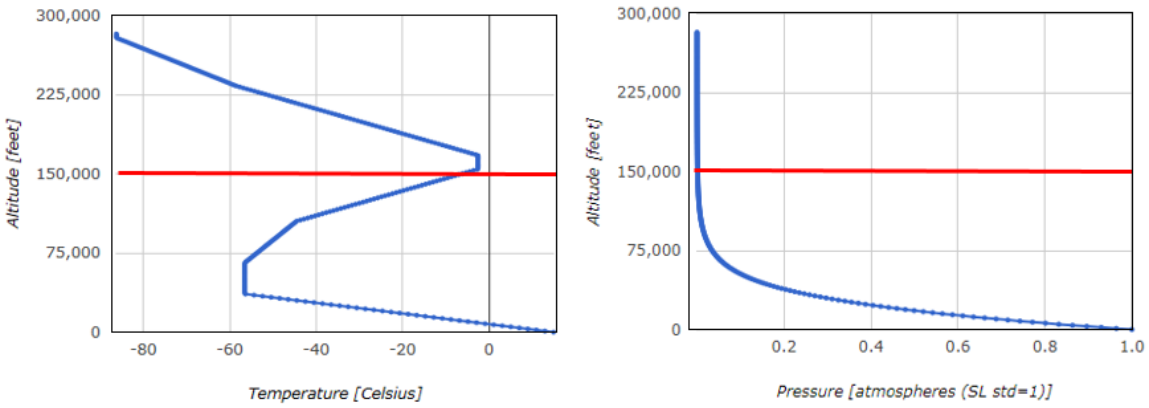

Temperature Profile (left) and Pressure Profile (right).

Figure 4. 1976 Standard Atmosphere Profiles. Adapted from [33].

Table 1. 1976 Standard Atmosphere Profiles Summary. Source: [33].

Altitude (ft)	**Temperature Range** (°C)	**Pressure Range** (°C)
150,000–75,000	-6.1 to -56.5	0.001–0.035
75,000–37,000	-56.5	0.035–0.214
37,000–surface	-56.5 to 20	0.214–1

The harshness of this operating environment is only exacerbated by the final weather effect, winds aloft, primarily in the form of the jet stream. The National Weather Service describes the jet stream as "relatively narrow bands of strong wind in the upper levels of the atmosphere" [34]. These strong winds range in altitude from approximately 6–13 km (20,000–43,000 ft) and can reach speeds of nearly 450 km per hour (275 miles per hour, or mph) [34]. The combination of cold temperatures and strong winds, coupled with the near-vacuum of much of the operating envelope, had substantial impact on the payload and bus design.

B. FREQUENCY TRADE ANALYSIS

Once the external constrains imposed on RDCS were understood, the uplink and downlink frequencies were next explored; these frequencies significantly impacted the design of RDCS. Ideally, the RDCS prototype created for this research would have been designed for the use of military frequency bands, as this would make for the most relevant demonstration. However, the lengthy authorization process, coupled with the limited number of COTS products to support these frequencies, made military bands prohibitive. To accelerate the development and test schedule, RDCS is instead designed to relay capabilities in the amateur bands. This limitation does not affect the overall concept of RDCS, only the hardware and software particular to these frequencies. The use of amateur bands significantly increases the COTS product availability and requires no external coordination beyond the Space Systems Academic Group (SSAG) Small Satellite Laboratory (subsequently be referred to as the Small Sat Lab) at NPS. Given the constraints of the amateur bands, the focus shifted to selecting the specific VHF and UHF frequencies for use on RDCS.

1. VHF Uplink

The VHF uplink frequency was chosen from within two potential ranges of the amateur frequency bands. According to the Amateur Radio Relay League (ARRL), the 50.0–54.0 MHz range (also known as the 6-meter band, referring to its characteristic wavelength) and 144.0–148.0 MHz range (also known as the 2-meter band) are designated for amateur use and conform to the ITU definitions of VHF [35]. Due to the size constraints the rocket payload bay imposes, the primary concern regarding frequency selection in these bands is antenna element length. Since antenna size is inversely proportional to frequency, a higher frequency requires smaller antenna elements; thus, the need for a smaller antenna narrowed the uplink frequency selection to the 144.0–148.0 MHz range.

Within to this 2-meter band, there are individual ranges designated for certain activities, ranging from repeater inputs to propagation beacons. The only frequency range specifically designated for FM repeater inputs, which correctly defines the uplink of

RDCS, is 144.60–144.90 MHz [35]. Based on the amateur band frequency designations, 144.60 MHz was chosen as the RDCS uplink frequency.

2. UHF Downlink

The UHF downlink frequency was also chosen from within two potential ranges of the amateur bands. The first option is in the range 222.0–225.0 MHz (1.25-meter band), and the second is 420.0–450.0 MHz (70-cm, band) [35]. There are two main concerns for downlink frequency selection: antenna size and proximity to uplink frequency. Here again, the higher the frequency, the shorter the antenna, which is more desirable for integration into the rocket. This parameter made the 70-cm band the preferred option.

The other factor, proximity of the downlink and uplink frequencies to each other, is a concern due to the potential for the onboard receive antenna to detect a high-power signal from the transmitting antenna, which poses the potential for interference. Since RDCS is a relatively small, full-duplex system, the antennas are positioned in close proximity to each other. Moreover, the uplink signal is always relatively weaker than the downlink transmission at RDCS because the uplink signal attenuates over the distance between the uplink user and the uplink antenna. The downlink signal from RDCS is transmitted at a high power level relative to the received uplink signal to communicate over the distance between RDCS and the receiving user. In this situation, there is potential for the uplink antenna to sense the radiated energy from the downlink transmission, which could distort the relatively weak uplink signal or, worse, damage uplink components.

This phenomenon is overcome by incorporating a filter in the uplink chain. However, the closer the frequencies are on the EM spectrum, the more complicated and potentially less effective the filter. It is better to have uplink and downlink frequencies that are separated from each other as much as possible, reducing the complexity and improving the effectiveness of the filter. Since the 420.0–450.0 MHz band was farther from the uplink frequency than the 222.0–225.0 MHz band, the 70-cm band was again the preferred option for the downlink frequency.

As with the 2-meter band, the 70-cm band has several smaller ranges specifically designated for various applications. The range from 435.00–438.00 MHz is designated for

satellite use only; given the potential altitudes for RDCS employment, its profile is more suited of a satellite than a traditional terrestrial-based repeater [35]. Furthermore, 433.00–435.00 MHz is specifically allocated for auxiliary or repeater links. Since RDCS operates at very high altitude for portions of its flight, the downlink frequency essentially functioned as a repeater link, and the frequency ranges associated with these two design parameters overlapped at 435.00 MHz. Therefore, 435.00 MHz was chosen as the downlink frequency for RDCS.

The trade analysis for the specific relay frequencies thus resulted in 144.60 MHz as the uplink frequency and 435.00 MHz as the downlink frequency. These frequencies align with the CONOPS, and the amateur band plans are sufficiently spaced on the EM spectrum to allow for an uplink filter.

C. USER SEGMENT

RDCS operates effectively by being compatible not only with the selected amateur bands but also with tactical users' pre-existing narrowband communication equipment. For a foot-mobile unit like 1st Platoon from the scenario in Chapter II, this equipment is in the form of man-portable tactical radios. These radios can be configured with different antennas that have varying performance at different frequencies. Since different radios have different capabilities, the user segment was analyzed to determine the most suitable radio and antenna combination.

1. User Radios

Two primary man-portable radios available to foot-mobile users like 1st Platoon are the Harris AN/PRC-117G and Harris AN/PRC-152A. These systems are well-known in the Marine Corps and can operate using FM voice communications across a range of frequencies, including the VHF and UHF amateur bands. However, each radio has distinct capabilities that could impact RDCS performance, particularly transmit power and sensitivity. Transmit power refers to the maximum signal energy the radio can transmit and is typically given in the units of decibel-milliwatt (dBm), which is a logarithmic scale referenced to one milliwatt. Transmission power is directly related to range performance of RDCS, so a higher transmit power was considered better. Sensitivity, normally

expressed as a radio's receive threshold, also in dBm, pertains to the lowest signal energy the radio can detect; a more sensitive receiver can detect weaker signals. A lower receive threshold value corresponds to a more sensitive receiver and therefore better range performance.

The characteristics of the two radios were compared and are presented below in Table 2. Based on the comparison, the higher transmit power and lower receive threshold capabilities of the AN/PRC-117G, pictured in Figure 5, made it the preferred radio to incorporate into the RDCS development.

Table 2. Man-Portable Radio Comparison. Sources: [36], [37].

Criteria (dBm)	**AN/PRC-117G**	**AN/PRC-152A**
Transmit Power	40.0	35.0
Receive Threshold	-118	-116

Figure 5. Harris AN/PRC-117G. Source: [36].

2. Antennas

The other primary component of the user segment is the antenna, which is used to radiate the RF signal generated by the radio. The user segment given in the scenario in Chapter II has two different types of users that operate different equipment—1st Platoon's antenna is man-portable, while the user onboard the ship is using more capable ship assets. Each user has unique antenna requirements for RDCS.

a. Foot-Mobile Antenna

The foot-mobile antenna of 1st Platoon is compact and optimized for narrowband communication frequencies. The two primary characteristics of any antenna are its gain and design frequency band. Gain is a dimensionless number related to antenna efficiency and is typically expressed in decibels-isotropic (dBi), which is a logarithmic scale referenced to a perfectly isotropic antenna. For RDCS, a more positive gain value is better, as a higher gain can increase range performance. Furthermore, a design frequency range that is closer to the selected amateur frequencies is also more desirable, as antenna gain decreases the further the frequency in use is from the design frequency. Two standard-issue Harris antennas familiar to USMC users and a COTS Citizen's Band (CB) antenna were considered and are summarized in Table 3.

Table 3. User Segment Antenna Trade Comparison. Sources: [38], [39], [40].

Criteria	**Nagoya NA-701**	**Harris RF-3150-AT152**	**Harris RF-3165-AT122**
Gain (dBi)	2.15	> 0	-15 to -5
Design Frequency Range	144/430 MHz	30-108 MHz	225-2,000 MHz

The NA-701 Nagoya Multiband antenna, depicted in Figure 6, is specifically engineered to operate within the two amateur bands that are already incorporated into the RDCS design. It is sized for hand-held radios, making it ideal for foot-mobile users. The higher gain, design frequency range, and size made the Nagoya Multiband antenna the preferred option for RDCS.

Nagoya Multiband Antenna (left) and Radio with Antenna Combination (right)

Figure 6. Foot-Mobile User Segment. Source: [38].

The combination of the Harris AN/PRC-117G man-portable radio and Nagoya NA-701 multiband antenna, presented in Figure 6, represents the equipment of the foot-mobile portion of the RDCS user segment. The performance graphic depicted in Figure 2 of Chapter II incorporates the capabilities of this equipment for 1st Platoon.

b. Shipboard Antenna

The scenario from Chapter II has a downlink from RDCS to LHA-6. This ship is equipped with a larger and more capable antenna than can be operated by a foot-mobile user. On December 15, 2017, Trivec-Avant Corporation was awarded the contract to produce a new UHF antenna, the AV2099-4, for all surface ships in the U.S. Navy, including those like LHA-6 [41] and is the shipboard antenna used in this research. The AV2099-4, pictured in Figure 7, is specifically designed to operate in the military UHF SATCOM bands and has a nominal antenna gain of 12 dBi [42]. These parameters were

used to calculate the RDCS range and time performance charts presented in Chapter II and Appendix A.

Figure 7. Trivec-Avant AV2099-4 Shipboard UHF Antenna.
Source: [43].

The user segment trade analysis of RDCS focused on the equipment required for both man-portable and shipboard users to operate. After a thorough trade analysis, the man-portable Harris AN/PRC-117G with a Nagoya NA-701 multiband antenna comprises the radio equipment operated by a foot-mobile user, while the shipboard portion is represented by the Trivec-Avant AV2099-4 antenna. These two systems characterize the entire user segment of RDCS.

D. PAYLOAD HARDWARE TRADE ANALYSIS

The results of the trade analysis from the user segment determined the communications equipment with which the payload portion of RDCS was then designed to be compatible. The core of the payload section is an SDR, which receives, modifies, and retransmits the radio signal. This SDR is connected to a single board computer, which provides commanding and computing functions. Based on the study conducted during the downlink frequency analysis, a filter is included in the uplink RF chain to protect the SDR from the powerful downlink signal transmission. Finally, two antennas, known as the uplink antenna and downlink antenna, connect to the SDR and enable the full-duplex capability. A block diagram of these five basic components of RDCS is given in Figure 8.

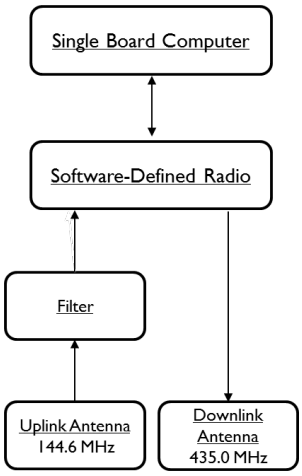

Figure 8. Initial Payload Block Diagram.

1. Single Board Computer

Although the heart of RDCS is an SDR, it requires a computer to execute commands, run configuration software, and provide the computational power necessary for signal processing. The miniaturization of computers over the last 60 years is exemplified by the single-board computing revolution. Single-board computers are capable of most traditional tasks like word processing, wireless internet browsing, and operating computer programming applications. However, unlike a traditional computer, single-board computers are typically about the size of a credit card and weight less than half a pound, making them ideal for incorporation into RDCS. There are dozens of single-board computers on the market, but one of the most capable is the Raspberry Pi (rPi) product line. The Small Sat Lab has considerable experience with these systems and has flown them many times in similar applications, including the use of an rPi to control an SDR for satellite use in the VHF band, as demonstrated by Phillip Swintek [24], and C-band, as exhibited by Bianca Lovdahl [44]. Given the time-compressed development schedule, the flight history of the rPi makes it an ideal choice for RDCS.

The primary differences between rPi models under consideration are processing power and random access memory (RAM). First and foremost, the computer requires processing power to run the SDR and is measured in GHz. In addition to processor speed, the computer needs RAM, measured in megabytes (MBs) or gigabytes (GBs), to execute

multiple processes at once, so more RAM is better for signal-processing functions. Since all rPi products are fairly small and lightweight, size and mass are not distinguishing factors. Processing speed and RAM were used to narrow the search to three rPi models: rPi 2B, rPi 3A+, and rPi 3B+. The single-board computer trade analysis is listed in Table 4.

Table 4. Single-Board Computer Comparison. Sources: [45], [46], [47].

Criteria	rPi 2B	rPi 3A+	rPi 3B+
Processor Speed	0.9 GHz	1.4 GHz	1.4 GHz
RAM	1 GB	512 MB	1 GB

The results of the trade study shows that the higher processor speed and RAM of the rPi 3B+ made it the best choice to provide the necessary signal processing power to support an SDR. Although not directly related to the relay mission of RDCS, the rPi 3B+ is also capable of operating a Raspberry Pi Camera Module V2 through a custom interface, which was included in the RDCS payload for academic and research purposes. The rPi 3B+ and camera are depicted in Figure 9.

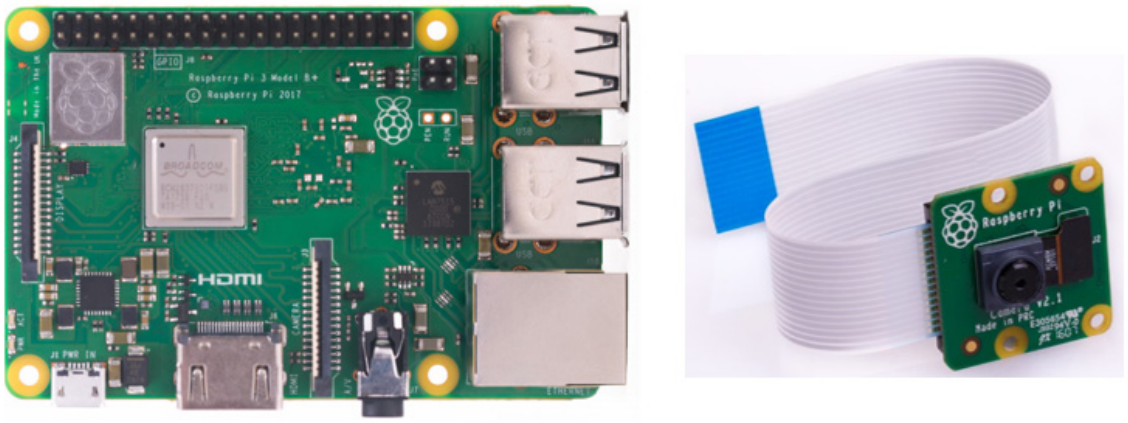

rPi 3B+ (left) and rPi Camera Module V2 (right).

Figure 9. Single Board Computer Components. Sources: [47], [48].

2. Software-Defined Radio

The main component of the RDCS payload is the SDR. SDRs are an emerging technology that have revolutionized signal processing by replacing traditional radio components like local oscillators or filters with software, which significantly reduces the size and weight of a radio. The Institute of Electrical and Electronic Engineers (IEEE) P1900.1 Working Group standards define an SDR as a "radio in which some or all of the physical layer functions are software defined" [49]. The signal-processing burden is shifted from the hardware of a traditional radio to the software on a computer. This shift allows for SDRs to be reprogrammed electronically instead of through hardware replacement, allowing for dynamic radio re-configurations, which improves a network's resiliency and spectral efficiency. There are dozens of SDRs on the market; however, the required frequency range and size considerations narrowed the analysis to two COTS products—the B205-Mini by Ettus Research and the AD9363 Adlam-Pluto Active Learning Module (PlutoSDR) by Analog Devices.

The analysis criteria focus on three design factors: mass, voltage, and transmit power. A smaller mass, measured in grams (g), results in a lighter overall payload, which increases the time to descend and therefore improves connectivity time for RDCS, assuming a constant parachute size. Furthermore, a lighter SDR is important for keeping the entire weight of the system below 1.8 kg as required by the FAA. Voltage refers to the required input voltage for the component, measured in volts (V). Voltage is directly related to power usage of the SDR, with a lower voltage requirement being preferred to maximize battery life. Finally, a higher maximum signal transmit power is more desirable as a signal of higher power will propagate further which corresponds to a longer maximum operating distance of RDCS. The results of the SDR trade analysis are depicted in Table 5.

Table 5. Software-Defined Radio Comparison. Sources: [50], [51].

Criteria	B205-Mini	PlutoSDR
Mass (g)	90.0 (with enclosure)	114
Voltage (V)	5.00	4.5 – 5.5
Transmit Power (dBm)	10	7

The Ettus Research B205-Mini, pictured in Figure 10, has a smaller mass with a higher maximum transmit power rating than the PlutoSDR, making it a more desirable option. With the higher transmit power of 10 dBm, the B205-Mini is the best choice to maximize performance. Moreover, both the rPi 3B+ and B205-Mini SDR have universal serial bus (USB) connections, making them compatible with each other and suited to function in the RDCS payload. These components represent emerging technologies that have significantly reduced the size, weight, and power required to achieve full-duplex radio relay capabilities like those of RDCS.

Figure 10. B205-Mini. Source: [50].

3. Uplink Filter

The downlink frequency analysis in section III.B.2 identifies the requirement to include a filter in the uplink path of the signal to limit the RF energy sensed by the receive portion of the SDR. Limiting the energy sensed by the uplink antenna protects the SDR circuitry and reduces noise in the receive signal. Ideally, this filter allows 100% of the uplink signal, centered on 144.6 MHz and spanning 5 kHz, to pass through and blocks out energy from higher frequencies, particularly high-powered downlink frequency. A filter that allows signals of lower frequency to pass through while inhibiting higher frequencies is known as a low pass filter (LPF).

While the exact frequency response varies for each filter, the primary consideration for an LPF is the cutoff frequency—the frequency above which signals are attenuated by the filter. The Small Sat Lab has a flight history with the Mini-Circuits SBLP-156+ LPF, which was flown on the nanosatellite technology demonstrator developed by Phillip

Swintek [24]. Swintek's demonstrator also received uplink signals in the 2-meter band, much like RDCS. The SBLP-156+, depicted in Figure 11 has a cutoff frequency of 156 MHz, which is suited to attenuate the downlink transmissions at 435.0 MHz. Based on the cutoff frequency and flight heritage, the SBLP-156+ LPF was chosen to protect RDCS uplink.

Figure 11. Mini-Circuits SBLP-156+. Source: [52].

4. Uplink and Downlink Antennas

The final building blocks of the RDCS payload are the uplink and downlink antennas. These antennas are designed for their respective frequencies and integrated into a six-inch diameter rocket. Nearly all commercially available dual-band antennas, similar to the NA-701 described in Section III.C.2.a, are stiff and inflexible, making them difficult to fit inside the payload bay and mount in a way that is conducive to radiating the surface of the earth. While several single-band COTS antennas exist, particularly in the 2-meter band, few, if any, are designed to withstand the vibrations unique to the payload configuration inside the rocket nose cone and resulting launch environment. The rigors of the launch environment thus focused the analysis on custom-built antennas, which can be reinforced to withstand vibrations.

While there are many designs for custom-built antennas, the simplicity of a half-wave dipole antenna makes it ideal for RDCS. Half-wave dipole antennas are common among amateur radio users since they are relatively easy to construct and, conservatively, have a gain of approximately 0.0 dBi. Dipole antennas consist of two parts, the feeder and radiating elements. The feeder, typically a coaxial cable, carries the RF energy to or from the radiating elements and is depicted as a bold line in Figure 12. There are two radiating

elements in a dipole antenna, each the length of one-quarter of the wavelength, where λ represents the full wavelength, making the entire antenna one-half of the wavelength long.

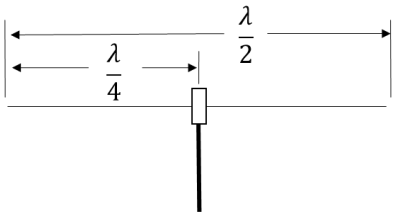

Figure 12. Half-Wave Dipole Antenna

Equation 1 was used to calculate the required element size for the antenna based on the frequencies established in section III.B, where *c* represents the speed of light in meters per second $\left(\frac{m}{s}\right)$, f is the frequency in Hertz (Hz), and λ is in meters (m) [53].

$$\lambda = \frac{c}{f} \tag{1}$$

Using Equation 1 and the relationships presented in Figure 12, the uplink and downlink antenna element lengths were calculated and are presented in Table 6 [54].

Table 6. Uplink and Downlink Antenna Element Lengths

Signal Path	f (MHz)	λ (m)	$\frac{\lambda}{2}$ (m)	$\frac{\lambda}{4}$ (m)
Uplink	144.6	2.073	1.037	0.518
Downlink	435.0	0.689	0.3445	0.172

Designing these half-wave dipole antennas completes the initial hardware selection for the payload of RDCS.

5. Initial Block Diagram

The results of the payload hardware trade analysis are shown in the block diagram of Figure 13. The rPi 3B+ was chosen for the single board computer due to its processing

power and RAM. This computer drives the core of RDCS, the B205-Mini SDR. To protect the uplink circuitry, the SBLP-156+ LPF was chosen to filter out the powerful downlink signal energy. Finally the uplink and downlink half-wave dipole antennas were chosen due to their simplicity of construction, integration, and deployment.

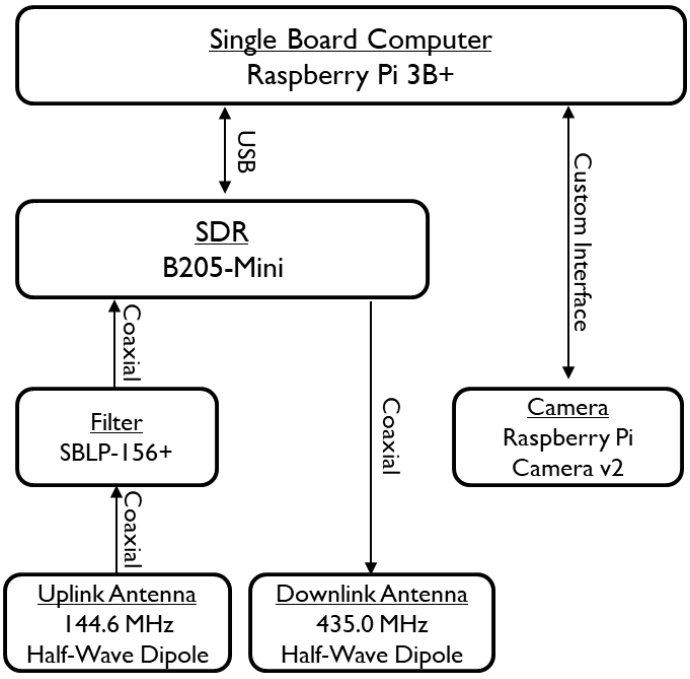

Figure 13. Payload Block Diagram.

6. Link Analysis

Once the hardware components were selected, this initial design needed to be validated with the payload CONOPS through a link analysis, consisting of two distinct methods: link budget and signal-to-noise ratio (SNR) calculation. Although quantitative in nature, understanding the quality of a link is analogous to a discussion between two people. If two people are having a conversation, but the speaker is whispering, the listener may not be able to hear what is being said, resulting in a poor link quality. For RDCS, the SDR may not be able to "hear" a transmission because the signal is received at a power level that is below the equipment's receive threshold, which results in a poor link. This received power is a significant value that can be used to quantify the quality of a link and is calculated

using a link budget, presented in more detail in section III.D.6.b. The link budget serves as the first method of quantitatively describing the quality of the link. It is an equation that accounts for the series of gains and losses experienced by a signal between transmitter and receiver and can be used to calculate the power of the signal at the receiver. The value of the received power must be above the sensitivity specifications for the receiver to ensure the signal is "heard."

To overcome the potential for receiving a low-power signal, the two people having a discussion may choose to shout at each other to ensure their voices are received at a volume level that exceeds their ears' threshold. However, ambient noise in the environment (e.g., in a bar, at a rock concert could overwhelm the discussion, and the people may still experience a poor link quality. The strength of the received signal relative to the ambient noise is known as the SNR, serves as the second method of quantitatively describing the quality of the link, and is presented in Section III.D.6.c of this work. The strength of this received signal is the same received power value calculated with the link budget. Noise for RF systems is related to the temperature of the receiver and bandwidth of received signals, with a smaller bandwidth having less noise. The strength of the signal must sufficiently exceed the noise for the signal to be intelligible.

The power of the received signal influences both evaluation methods. One of the primary factors related to the power of a received signal is the distance over which the signal propagates. If two people are having a conversation but are separated by a great distance, no matter how loud they talk, how intently they listen, or how quiet the environment, they may not be able to understand each other. This makes distance a critical element to any conversation. Similarly, the physical distances over which RDCS conducts its "conversations" is paramount to evaluating the quality of the link. Given its significance to both the link budget and SNR, the signal path distances associated with RDCS were calculated first.

a. Signal Path Distance

The first step to quantitatively describing the quality of the link was to examine the uplink and downlink signal path distances. Figure 14 depicts the geometry of RDCS, in

which the signal paths are the hypotenuse of two separate uplink and downlink triangles, which is based on a flat-earth assumption. This assumption was used for ease of understanding and concept development while incorporating conservative look angles. Signal path differences between flat- and round-earth geometry are more sensitive as look angles decrease, with values differing from 13% to 43% at the scenario's deployment altitude of 5.7 km, and are detailed in Appendix L. The differences in signal path between flat- and round-earth geometry can be minimized if less conservative look angles are used when assuming a round-earth. However, the benefit to the longer signal paths that result from a flat-earth assumption is a more robust payload design for RDCS.

The altitude of RDCS represents a common side, with the third leg being the distance over the ground (ground range) from the user to the nadir point of RDCS, or the point on the earth's surface directly below RDCS. The uplink look angle was assumed to be a minimum of 10° to account for potential terrain interference, and the downlink look angle was assumed to be a minimum of 5°, since terrain is not normally a factor for ships at sea.

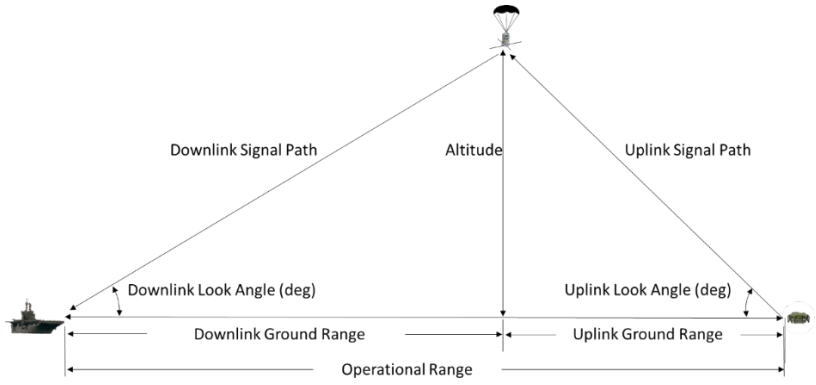

Figure 14. RDCS Geometry

The relationship between RDCS altitude, look angle, and signal path is expressed by the sine of the look angle and was used to calculate the maximum uplink and downlink signal path distances, which are summarized in Table 7. The selection of payload hardware is considered valid if the power of the received signal and SNR exceed appropriate margins

after attenuating over these distances and is determined through the link budget and SNR calculations.

Table 7. Maximum Uplink and Downlink Signal Path Distances

Signal Path	**Maximum Rocket Altitude** (km)	**Maximum Look Angle** (degrees)	**Maximum Signal Path Distance** (km)
Uplink	45.7	10°	263.3
Downlink		5°	524.6

b. Link Budget

To validate the payload hardware, the power of the received signal for both the uplink and downlink must exceed the sensitivity of the respective receivers. Due to the unpredictability of variables like environmental factors, 10 dBm or greater is considered an acceptable margin between the power of the received signal and a receiver's sensitivity threshold. The link budget, Equation 2, relates the series of gains and losses of a signal between transmitter and receiver to calculate P_r, the power of the signal at the receiver; all terms are expressed in dB [53]. Signals are initially transmitted with a power, P_t, with a particular transmitter antenna gain, G_t. However, there are always losses related to transmitter hardware including connections and cable length, which are represented as L_t. Similar to transmitter variables, there is also a gain associated with the receive antenna, G_r, as well as losses, L_r. Additionally, miscellaneous losses that may be difficult to predict are represented as L_m.

$$P_r = P_t + G_t - L_t + G_r - L_r - L_m - L_{fs} \tag{2}$$

The most significant loss in the link equation is the free-space path loss, L_{fs}. As signals propagate, their signal strength decreases substantially, which can significantly impact the power of the received signal. Free-space path loss is expressed in the units of dB and is calculated using Equation 3, where S is the distance the signal must travel measured in km and f is the frequency in GHz [53].

$$L_{fs} = 20\log_{10} S + 20\log_{10} f + 92.45 \quad (3)$$

(1) Uplink Link Budget

Equation 2 and Equation 3 were used to calculate the uplink power received and subsequent margin using values listed in Table 8, with data sources or assumptions included in the notes section of the table. The receive margin for the uplink was 9.10 dBm, which was less than the acceptable margin of 10 dBm, making the initial hardware design insufficient to function as the payload for RDCS. However, the extra 0.90 dBm required to achieve the desired margin was obtained with the incorporation of an amplifier, or amp, which is detailed in Part 3 of this section.

Table 8. Uplink Link Budget

Term	Value	Notes
Transmitter Power (P_t)	40 dBm	Given in RF-7800H-MP data sheet
Transmitter Gain (G_t)	2.15 dBi	Given in NA-701 data sheet
Transmitter Losses (L_t)	1 dB	Estimated by researcher
Receiver Gain (G_r)	0 dBi	Estimated by researcher
Receiver Losses (L_r)	1 dB	Estimated by researcher
Miscellaneous Losses (L_m)	2 dB	Estimated by researcher
Free Space Loss (L_{fs})	124.05 dB	Calculated using Equation 4
Power Received (P_r)	-85.90 dBm	Calculated using Equation 3
Receiver Threshold	-95.00 dBm	Estimated from B205-Mini data sheet
Receive Margin	9.10 dBm	Difference between P_r and receive threshold

(2) Downlink Link Budget

The downlink power received was calculated in a similar manner to the uplink and is detailed in Table 9. The downlink receive margin was below the desired 10 dBm margin by 13.63 dBm, making the downlink deficient. Similarly, this margin was overcome by adding an amp to the downlink signal path of RDCS.

Table 9. Downlink Link Budget

Term	Value	Notes
Transmitter Power (P_t)	10 dBm	Given in B205-Mini data sheet
Transmitter Gain (G_t)	0 dBi	Estimated by researcher
Transmitter Losses (L_t)	1 dB	Estimated by researcher
Receiver Gain (G_r)	12 dBi	Given by AV2099-4 data sheet
Receiver Losses (L_r)	1 dB	Estimated by researcher
Miscellaneous Losses (L_m)	2 dB	Estimated by researcher
Free Space Loss (L_{fs})	139.63 dB	Calculated using Equation 4
Power Received (P_r)	-121.63 dBm	Calculated using Equation 3
Receiver Threshold	-118.00 dBm	Given in RF-7800H-MP data sheet
Receive Margin	-3.63 dBm	Difference between P_r and receive threshold

(3) Payload Amplifier Hardware Analysis

The lack of margin for both the uplink and downlink indicates the initial hardware selections are inadequate to support RDCS communicating effectively from the expected rocket altitude of 45.7 km. To overcome these deficits, amps were added the uplink and downlink signal paths. An amp increases an input signal by a specific amount, which is normally a function of the input frequency. While there are many types of RF amps available, the Small Sat Lab has a flight history with projects by both Swintek [24] and Lovdahl [44] using wideband and low-noise amplifiers (LNAs) manufactured by Mini-Circuits. In these projects, an LNA was used on the uplink portion of payloads to increase the power of received signal while introducing minimal additional noise. Similarly, a wideband amp was used on the downlink side of the payloads to increase the power of the transmitted signal.

Each LNA and wideband components with flight history was evaluated to ensure utility for RDCS. The Small Sat Lab has a flight history with the ZX60-P103LN+ LNA, which is pictured in Figure 15 and was used by Swintek [24]. This LNA has a small form factor and weighs less than one-tenth of one pound, making it ideal for RDCS. The LNA is capable of providing approximately 18 dBm of additional power to the receive signal at the uplink frequency of 144.6 MHz [55]. With all other variables remaining the same, the

addition of this LNA on the uplink side significantly improved the link budget by increasing the receive margin well above the required 10 dBm, as summarized in Table 10.

Figure 15. Mini-Circuits ZX60-P103LN+ LNA. Source: [55].

Table 10. Uplink Link Budget with Amplifier

Term	Value	Notes
Initial Power Received	-85.90 dBm	Calculated in Table 8
LNA	18 dBm	Given in ZX60-P103LN+ data sheet
New Power Received (P_r)	-67.90 dBm	Addition of P_r and LNA
Receiver Threshold	-95.00 dBm	Estimated from B205-Mini data sheet
New Receive Margin	27.10 dBm	Difference between P_r and receive threshold

The Small Sat Lab also has a flight history with a wideband amp, the ZX60-V82+, which was used by Swintek to increase the power of the downlink signal [24]. This component is nearly identical to the LNA in size and weight with the capability to provide approximately 16 dBm of additional power at the downlink frequency of 435.0 MHz [56]. With the wideband amp, the downlink margin also exceeded the 10 dBm threshold requirement, as detailed in Table 11.

Table 11. Downlink Link Budget with Amplifier

Term	Value	Notes
Initial Power Received	-121.63 dBm	Calculated in Table 9
Wideband Amp	16 dBm	Given in ZX60-V82+ data sheet
New Power Received (P_r)	-105.63 dBm	Addition of P_r and wideband amp
Receiver Threshold	-118.00 dBm	Given in RF-7800H-MP data sheet
New Receive Margin	12.37 dBm	Difference between P_r and receive threshold

c. Signal-to-Noise Ratio

The final element to the overall link analysis is the SNR. This parameter represents the energy of the signal relative to the noise of the environment. Generally, an SNR of 10 dBm or greater is considered sufficient to ensure a quality link. Noise (N), measured in Watts (W), was calculated using Equation 4 [53].

$$N = kTB \tag{4}$$

Noise is a function of the ambient temperature T with the units of Kelvin (K); the bandwidth of the signal, B, in Hz; and Boltzman's Constant, k, in the units of Joules per Kelvin $\left(\frac{J}{K}\right)$. The temperature was estimated to be 290 K, which is the approximate value for the temperature of the earth, and the bandwidth of the FM voice signal was limited to 5 kHz. Only one noise calculation was completed as the values for each term applied to both the uplink and downlink. Once the noise was calculated, it was converted to dBm using Equation 5 [53]. This equation uses one milliwatt, or 1 x 10–^{3} Watts, as the dB reference unit to convert the noise value to dBm.

$$N(dBm) = 10 * \log\left(\frac{N(W)}{1x10^{-3}(W)}\right) \tag{5}$$

Subsequently, once both the signals (new P_r's from Table 10 and Table 11) and noise values were in the same units, Equation 6 was used to determine the SNR. In this equation, S is the signal strength and N is the noise strength, both measured in dBm [53].

$$SNR(dBm) = S - N \tag{6}$$

The calculations for the SNR demonstrate that both the uplink and downlink margins are well above the required 10 dBm margin with the inclusion of amps, as shown in Table 12.

Table 12. Uplink and Downlink SNR

Signal Path	**Signal Power** (dBm)	**Noise**					**SNR** (dBm)
		k (J/°K)	T (°K)	B (Hz)	Noise (W)	Noise (dBm)	
Uplink	-67.90	1.38 x 10–^{23}	290	5000	2.00 x 10–^{23}	-136.99	69.08
Downlink	-105.63						31.36

d. Maximum Range

The excess margin in both received power and SNR for the uplink and downlink indicates that the payload is capable of communicating further than required from the design altitude of 45.7 km. The downlink received-power margin is only 12.57 dBm, just 2.57 dBm above the required margin, which is substantially lower than the other margins. This makes the link budget for the downlink the equation that determines the actual maximum range of RDCS. Signal path distance, corresponding free-space path loss, maximum altitude, and ground ranges were calculated and are summarized in Table 13. These values correspond with the maximum performance values presented in Chapter II.

Table 13. Maximum Range Calculation

Signal Path	**Look Angle**	**Signal Path Distance** (km/miles)	**L_{fs}** (dBm)	**Maximum Altitude** (km/ft)	**Maximum Ground Range** (km/miles)	**Maximum Operating Range** (km/miles)
Uplink	10°	(346/215)	127	60/196,000	340/211	1026/638
Downlink	5°	(688/428)	142		686/426	

7. Payload Hardware Summary

A payload hardware trade analysis was conducted to determine the most suitable components for the single-board computer, SDR, uplink filter, and both uplink and downlink antennas. The results of the initial link budget revealed a receive-margin deficit for both the uplink and downlink, which was overcome with the addition of an LNA to the uplink chain and a wideband amp to the downlink signal path for RDCS. The final payload hardware block diagram is depicted in Figure 16. These components are the core of RDCS and will ensure it has the sufficient link quality to operate effectively.

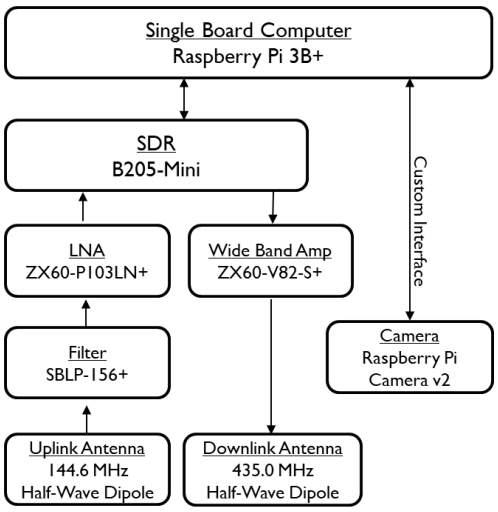

Figure 16. Final Payload Hardware Block Diagram

E. PAYLOAD SOFTWARE

While the hardware is critical to the design of RDCS, the software serves an equally important role. For the payload to function properly, the software has to be compatible with both the SDR and rPi. There are several software programming environments to program the B205-Mini, and the industry standard is GNU Radio. GNU Radio is open source software that provides a visual programming environment through the use of graphical user interface (GUI) blocks that generate scripts in the programming language Python 2.7, which is compatible with the rPi. Furthermore, the Small Sat Lab has extensive flight experience with GNU Radio, including projects created by Swintek [24] and Lovdahl [44].

The only difference between Swintek's project and RDCS is the downlink frequency, making the final radio software, known as a flow graph, from his project a suitable starting point for RDCS. The initial flow graph for RDCS is pictured in Figure 17. The receive block, labeled "UHD: USRP Source" and commonly referred to as the source block, is outlined in green in Figure 17 and represents the signal input to the SDR. This block is configured to the receive frequency of 144.6 MHz. Other configuration settings for the source block included the antenna port, sample rate, and gain.

After the signal is received, it passes through a digital LPF, squelch, and automatic gain control (AGC), which are outlined in blue. This digital filter functions like a bandpass

filter by narrowing the incoming signal to a band 5 kHz wide, centered on 144.6 MHz, which reduces noise. Configuration settings include the sample rate, transition width, and gain. Next, the signal reaches the power squelch block, which digitally removes all energy below the configured -75 dB. This block reduces the noise received by the signal, which improves link quality. After the squelch, the signal passes through the AGC. The AGC digitally modifies the power, either with an increase or decrease in energy, to a normalized value configured in the "Reference" setting of the block. The reference setting is normalized by GNU Radio to the capabilities of the SDR; if the Reference in the AGC is set to .5, or 50% of the SDR's capability, signals below this threshold are increased to 50% while signals below are reduced to 50%. Without the AGC, an uplink signal transmitted a long distance from RDCS would sound weaker to the downlink user when compared to a signal transmitted closer. The AGC is useful for ensuring the input to the sink block is at a constant power level, despite the user distance and corresponding signal energy at the source block. This ensures a predictable and repeatable downlink transmission.

Finally, the signal reaches the transmit block, named "UHD: USRP Sink" and commonly referred to as the sink block, which is outlined in green. This block is tuned to the downlink frequency of 435.0 MHz and transmits the signal from RDCS. The sink block has similar configuration settings to the source block, including antenna port, sample rate, and gain. Blocks outlined in orange in Figure 17 represent variables, some with GUIs that could be manipulated in real-time while flow graphs are executed, which facilitates rapid configuration changes for software validation and troubleshooting. The remaining boxes outlined in red are functions that do not modify the signal for RDCS, but are useful for inclusion in the first flow graph to facilitate software validation. GNU Radio's intuitive programming environment, availability, and flight history make it an ideal choice for programming the B205-Mini.

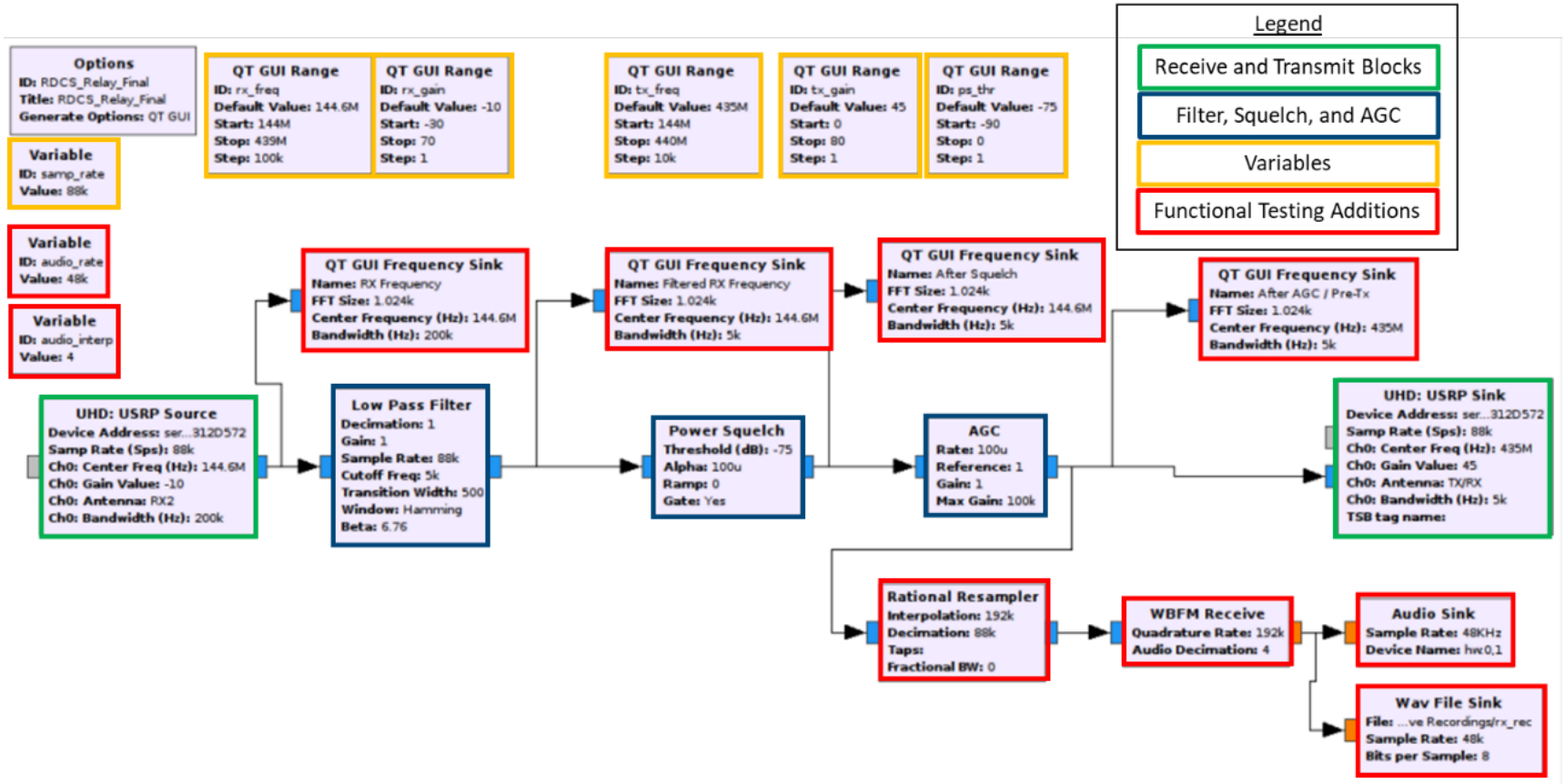

Figure 17. Initial GNU Radio Flow Graph

The other payload software function is to command the rPi camera, which is mounted outboard to view the horizon. This camera is programmed to collect two-minute-long video clips with a resolution of 2592 x 1944, which corresponds to a 4:3 aspect ratio and approximately 15 frames per second (fps). Its main purpose is to record RDCS separation from the rocket and primary parachute deployment. The camera and radio scripts are imbedded in the startup sequence of the rPi 3B+ to eliminate the need for the operator to initiate these processes. With this feature, once the payload receives power from the bus and began its boot scripts, the radio and camera functions begin immediately. The startup, radio, and camera scripts are contained in Appendix G.

In summary, the core of RDCS, the B205-Mini SDR, is programmed using GNU Radio, an open-source software package with a user-friendly GUI. Using this fairly intuitive programming environment, the LPF, squelch, and AGC blocks manipulate the signal to reduce noise and raise the signal power to the highest applicable level before transmission by the sink block. GNU Radio generates a Python 2.7 script from these blocks which is then executed by the rPi 3B+ to provide the necessary signal processing functions central to RDCS.

F. BUS DESIGN

After the payload hardware and software were designed, the analysis turned to the bus. The bus is responsible for administrative functions like housing the payload, running startup scripts, distributing power, transmitting telemetry, and facilitating recovery. There are a myriad of COTS or custom combinations of parts that could have been used as a bus for RDCS, but two main factors dominated the bus trade analysis: schedule and integration. Schedule refers to the limited time available for the project, for which approximately six months were allotted between initial concept and field demonstration. Given this constraint, a ready-made solution was more preferable than a custom-built bus. The second factor, integration, involves the challenges associated with integrating the payload with the bus and the rocket payload bay. Schedule and integration drove the analysis to select a bus that was compact and light-weight. Both of these considerations are addressed by the Small Sat Lab's custom high-altitude balloon (HAB) Bus.

1. HAB Bus

The HAB Bus, depicted in Figure 18, is a custom product designed and built by the engineers of the Small Sat Lab. It is designed to support research by providing all of the necessary bus functions for payloads ascending to altitude via HAB and was the delivery platform of choice for both Swintek [24] and Lovdahl [44]. The HAB Bus includes a structure, electrical power system (EPS), and command and data handling (C&DH) system. The complete HAB Bus weighs less than 1 kg, which makes it an ideal candidate for incorporating into RDCS [57].

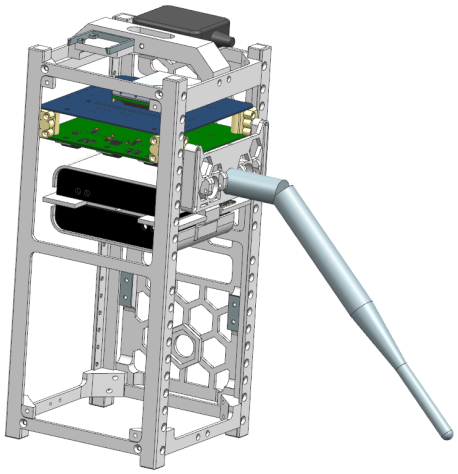

Figure 18. Small Sat Lab HAB Bus Nominal Configuration.

a. Structure

The HAB Bus provides the means to secure all of the subsystem elements into a single flight article. These components include the side rails, cross bars, side panels, parachute mount, and camera mount. It has dimensions of approximately 10 x 10 x 20 cm and fits inside the rocket payload bay [57]. The structure, the white portions of Figure 18, are made of polycarbonate formed by a three-dimensional (3D) printer through a process known as additive manufacturing. This process allows for parts to be developed using computer aided design (CAD) software and then made by a 3D printer. All CAD development for the HAB Bus and RDCS was completed using Siemens NX software. The

side rails are 20 cm long with mounting holes spaced 10 cm apart. Four cross bars, two on the top and two on the bottom, connect these side rails to form the structure's 10 x 10 x 20 cm rectangle. The parachute mounting panel on the top of the structure also includes mounting points for the C&DH GPS and rPi camera mount. The structure forms the skeleton of the bus.

b. EPS

The HAB Bus also includes an EPS subsystem, the green board in Figure 18, which uses linear regulators to distribute power for the payload and bus. The EPS can be powered by either solar panels, batteries, or a combination of the two. The batteries consist of 10 AA Energizer Ultimate lithium batteries, which provide 48 Watt-hours (Whrs) of energy at -10°C [57]. These batteries are contained in the black and white housing in the middle of the structure from Figure 18. The batteries are powered through a switch mounted on a small panel that also serves as the mounting point for the C&DH antenna.

c. C&DH

The final section of the HAB Bus is the C&DH subsystem, the blue board in Figure 18, which provides bus controlling and telemetry. Bus controlling, including start-up scripts and payload commanding, is accomplished by a Raspberry Pi Zero, which is mounted to the C&DH board. Along with the C&DH board, the rPi Zero controls an rPi Camera Module V2, similar to the payload rPi 3B+. The bus camera is positioned vertically and programmed to capture two-minute-long video clips at 90 fps at a resolution of 640 x 480. The primary purpose of this camera is to view the HAB burst and facilitate post-flight analysis. Much like the payload software, the camera script is imbedded in the startup sequence of the bus controller for automatic camera operation. Telemetry is provided through a Microhard n920X2 wireless modem, which is mounted to the C&DH board and includes a fixed antenna that extends beyond the structural frame, as shown in Figure 18. This telemetry stream includes GPS location information, provided by a Byonics GPS5 unit depicted in Figure 19, and general health and status data. Telemetry is received on the ground by an n920X2 connected to a laptop. This ground station presents the telemetry stream into its individual elements and displays the information in a GUI. The C&DH

system also includes functions like balloon release, parachute release, and a universal asynchronous receiver/transmitter (UART) connection to the payload, which was not required for RDCS.

Figure 19. HAB Bus GPS Unit. Source: [58].

2. HAB Bus Design Changes

The HAB Bus is ready-made, possesses all of the requirements necessary for RDCS, and has extensive flight history in the Small Sat Lab, making it an ideal choice. However, the HAB Bus is designed for a balloon, not a rocket. To adapt the HAB Bus to the launch vehicle and environment, design changes to all three subsystems are required, as is the addition of thermal mitigation. While the RDCS bus is a unique design, it remains heavily based on the Small Sat Lab HAB Bus.

a. Structure

The RDCS bus' side rails, parachute mount, and side panels are modified to mitigate vibration effects, facilitate rocket integration, or streamline the assembly process. These structural components consist exclusively of 3D-printed polycarbonate.

(1) Side Rails

The first subsystem to receive design changes is the side rails, in the form of spacers and nut cages. Spacers are added to the outside of the side rails to facilitate rocket integration and the nut cages are added to ease maintainability.

The structural cross section of RDCS is a 10 x 10 cm square, as depicted in cross section view of Figure 20, in which the black circle represents the rocket body and the white square represents the 10 x 10 cm square of the HAB Bus; thus, integrating the original side rails with the payload bay is essentially trying to fit a square peg into a round hole.

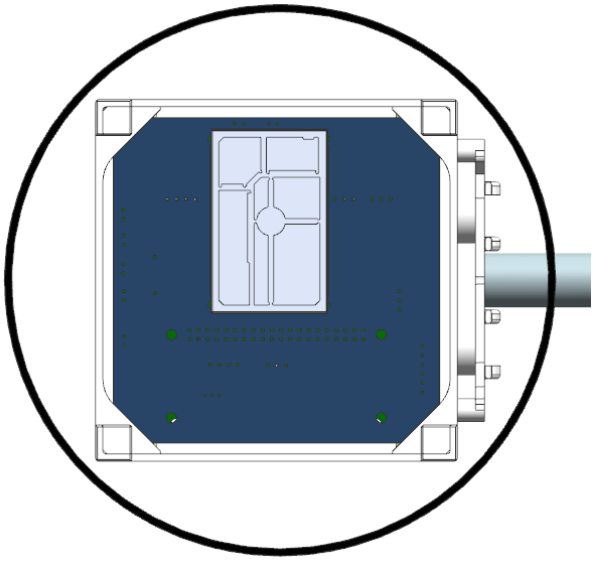

Figure 20. Top-Down View of HAB Bus Inside Payload Bay

Additionally, systems inside the rocket payload bay are not physically attached to the rocket to facilitate a simpler deployment. Spacers are therefore added on the outside edges of the side rails to minimize movement inside the payload bay and are depicted in red in Figure 21. These polycarbonate pieces are sized with a radius to match inner diameter of the rocket body and added to the top and bottom of the side rails in NX. By adding the spacers to the two side rails in CAD, each side rail with its four spacers are a single integrated piece, adding strength and reducing weight when compared to using spacers that required fasteners. Figure 21 depicts the spacer location as viewed along the long-axis of the rocket and an isometric view of the RDCS structure. These spacers are used to secure the square peg of RDCS in the round hole of the rocket.

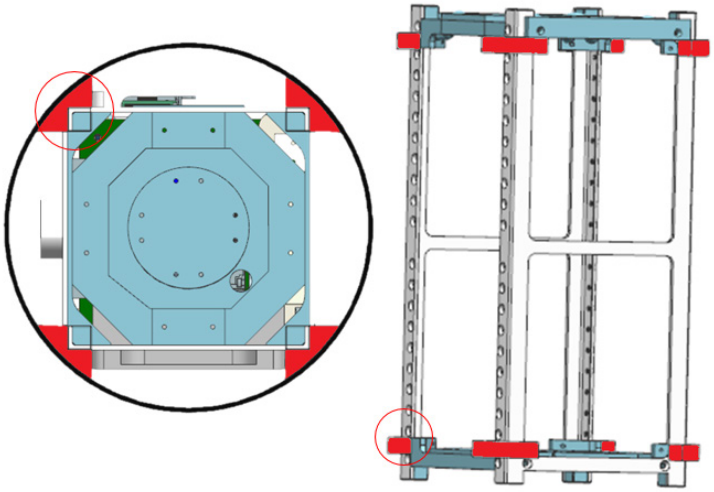

RDCS Bus Spacers Nadir Face (left) and Isometric View (right)

Figure 21. RDCS Bus Spacers

The other modification to the side rails is the addition of 3D-printed nut cages, which are included to improve maintainability. Nearly all of RDCS is assembled using #2-56 machine screws to join the various pieces. Screws are either inserted directly into pieces, relying on the threads of the screw to grip the tapped hole in the plastic, or secured with a stainless steel nylon lock nut. Lock nuts form a stronger attachment, so this method of fastening is used wherever possible. For all instances using lock nuts, which is nearly exclusively when securing components to the side rails, nut cages are incorporated, as shown in Figure 22. These nut cages prevent the nuts from slipping when torque is applied. The cages are rectangles, which measure 10 x 7.5 x 4 mm, and are extruded on the inside surface of the side rail, centered on the specific holes used to secure components. In the middle of this rectangle, there is a hexagon-shaped cavity with the exact dimensions of a lock nut, which allows the lock nut to be inserted prior to securing components to the side rail. Since cages are only added to the required holes, each side rail is a customized for a particular side of RDCS and is labeled as either “A” or “B” for identification. Nut cages allow screws to be installed with a single screwdriver from the outside of RDCS; non-captive nuts require access to the inside of RDCS with a nut driver to manually restrict the

nut from rotating when applying torque. Incorporating nut cages significantly reduces the time to install and remove panels, which dramatically improves maintainability.

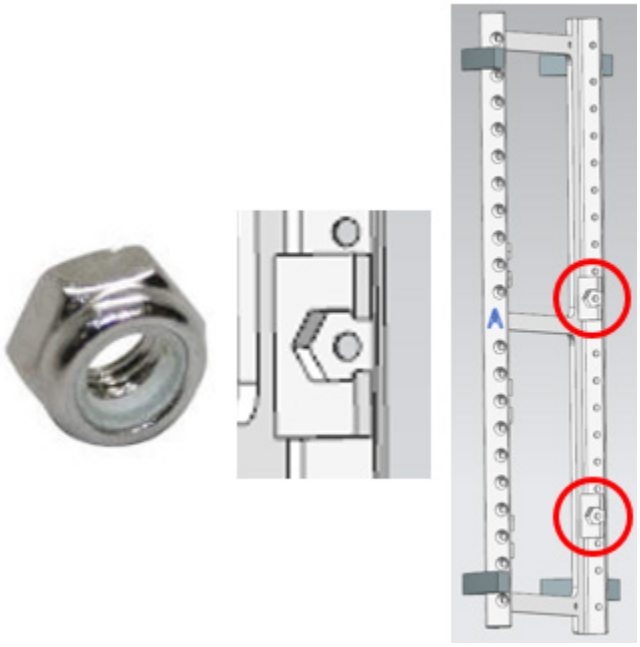

Stainless Steel Lock Nut (left), Nut Cage Example (middle), and Side "A" Rear Nut Cage Locations (right)

Figure 22. Side Rail Nut Cages. Source: [59].

(2) Parachute Mount

The second structural component of the HAB Bus modified for RDCS is the parachute mount. The HAB Bus parachute mount has a flight history of breaking under aggressive deployment conditions. Given this history and the potential for RDCS to be deployed by a rocket in an aggressive manner, the parachute mount is redesigned, as shown in Figure 23. The number of attachment points to the structure is doubled from 6 to 12. For the HAB Bus, cross bars and the parachute mount are all printed as individual pieces and joined with fasteners. By contrast, the cross bars for RDCS, highlighted in teal in Figure 23, are fully integrated into the mount, which is then 3D printed as a single piece. These changes address the previous failures experienced by the Small Sat Lab.

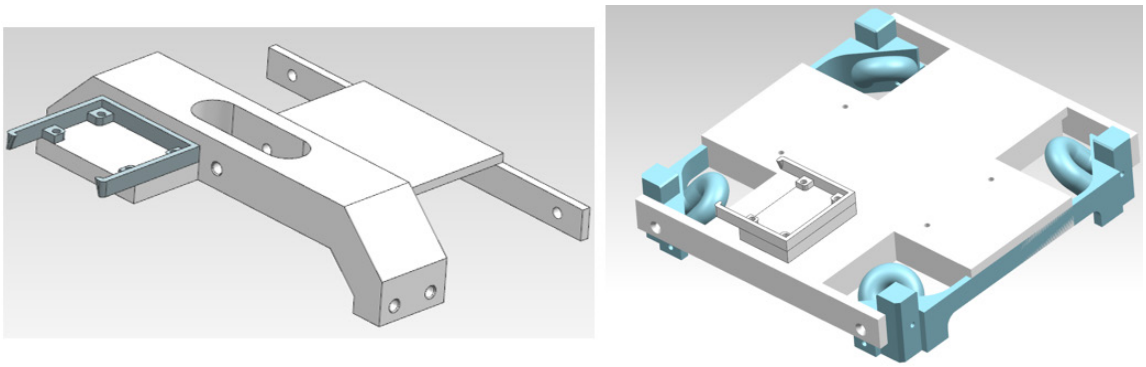

HAB Bus Parachute Mount (left) and RDCS Bus Parachute Mount (right)

Figure 23. Parachute Mount

(3) Side Panel

The final modified structural component is the honey-combed side panel, shown in Figure 24. This honey-combed pattern is designed to allow the panel to retain its rigidity for structural support while minimizing weight. However, these holes would leave RDCS exposed to the harsh environment of near-space. To protect components from wind and debris, this panel is printed solid as shown in Figure 24. An rPi camera mount is included for the payload camera and oriented out towards the horizon.

HAB Bus Side Panel (left), RDCS Side Panel with rPi camera (Right)

Figure 24. Structure Side Panel

b. EPS

The HAB Bus battery compartment, EPS switches, and switch panel are likewise modified to reduce the effect of vibrations related to the rocket launch environment. Secondary reasons include protecting RDCS from the outside environment and streamlining operations. Unlike structural changes, which are all made with polycarbonate, the switch change requires completely new hardware. However, none of these changes significantly impact the EPS system functions or design.

(1) Battery Compartment

The HAB Bus battery compartment has a known issue with batteries becoming unseated during flight while systems were attached to HABs. Given the increased vibration environment of a rocket, this characteristic of the HAB Bus battery compartment is unacceptable for RDCS. The housing is redesigned from being a single case containing all 10 AA batteries to comprising two identical cases with five batteries each, labeled Battery Box A and Battery Box B. Figure 25 depicts the RDCS battery box design, consisting of three polycarbonate pieces: one box capped with two identical lids. The batteries are secured in the case with 3M Scotch Weld epoxy to withstand the vibrations associated with the rocket and soldered together in series. Although the new battery box does not substantially modify the electrical configuration of RDCS, it is made to address the known issue of batteries becoming unseated in flight.

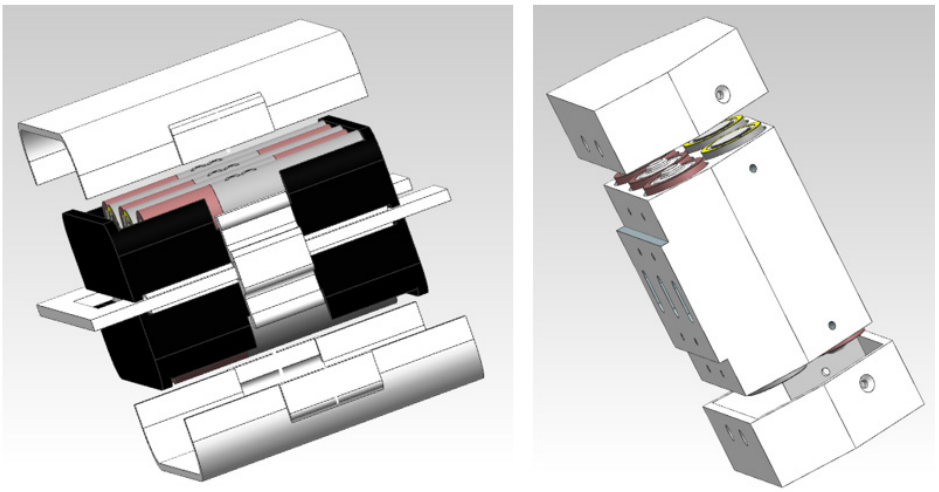

HAB Bus Battery Box (left) and RDCS Battery Box

Figure 25. Battery Box (Exploded View)

(2) EPS Switches and Panel

The HAB Bus switches and panel are modified to mitigate vibration effects, facilitate rocket integration, or simplify operations. The HAB Bus EPS switch panel consists of two single-pole double throw (SPDT) switches and the C&DH antenna mounting slot, which is depicted in Figure 27; one switch connects the battery pack to the power circuit of the EPS board and the other provides the option to enable solar panels. These switches are held in place by two cotter keys. Five aspects of this switch panel are redesigned to support RDCS. First, because RDCS does not incorporate solar panels, this switch is removed. The remaining battery switch is replaced with two separate FingerTech Mini Power Switches, see Figure 27, one for each battery pack.

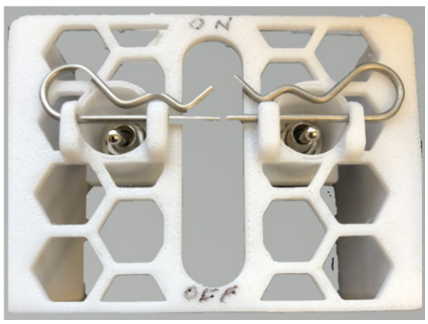

Figure 26. HAB Bus Switch Panel

Size Comparison (left) and Cross-Section (right).

Figure 27. FingerTech Switch. Source: [60].

These switches are actuated using a screw to physically connect both electrical contacts, making them less susceptible to becoming unseated due to vibrations than the cotter key retention system. One switch is connected to Battery Box A and labeled "BATT A," as indicated in Figure 28. The other switch, labeled "BATT B," is directly connected to Battery Box B. Light-emitting diodes (LEDs) are incorporated into the switch panel to provide operators with a visual indication of battery and RDCS status, which are viewed from the outside of RDCS. The mounting holes for the LEDS are above and below their respective switches, as shown in Figure 28. First, "BATT A" switch is engaged, and the top LED, connected to the C&DH system, emits a flashing light. This flashing light serves two functions. It indicates that C&DH subsystem processes are in progress, much like a traditional computer flashes while in use, and it also indicates that Battery Pack A is supplying power to the bus. Next, "BATT B" switch is engaged, and the second LED,

which is wired directly to Battery Pack B, emits a steady light. This indicates that Battery Pack B is supplying power to the bus.

The fourth change is to enlarge the switch panel to cover an entire face of the 10 x 10 x 20 structure of RDCS and fill in the hexagon-shaped holes of the structure, as depicted in Figure 28. These changes are designed to limit heat loss from the wind and atmosphere while RDCS is in flight. The final change is to relocate the C&DH antenna to its own panel and is further explained in Section III.F.2.c(1).

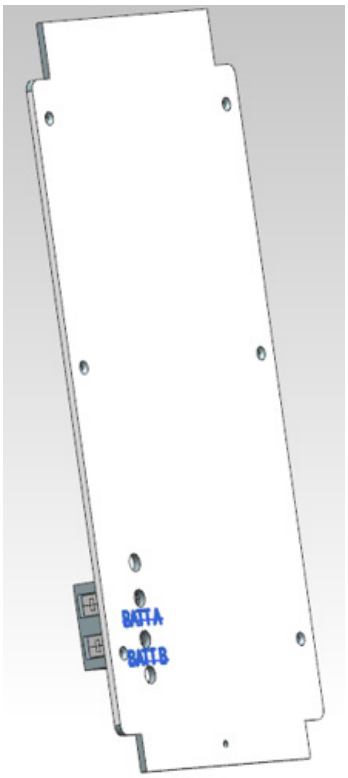

Figure 28. RDCS Switch Panel

While no significant changes have been made to the electrical system, modifications to the battery housing and switch panel address the launch environment, thermal considerations, and operations. A block diagram of the RDCS EPS system is depicted in Figure 29 and a full schematic is included in Appendix B.

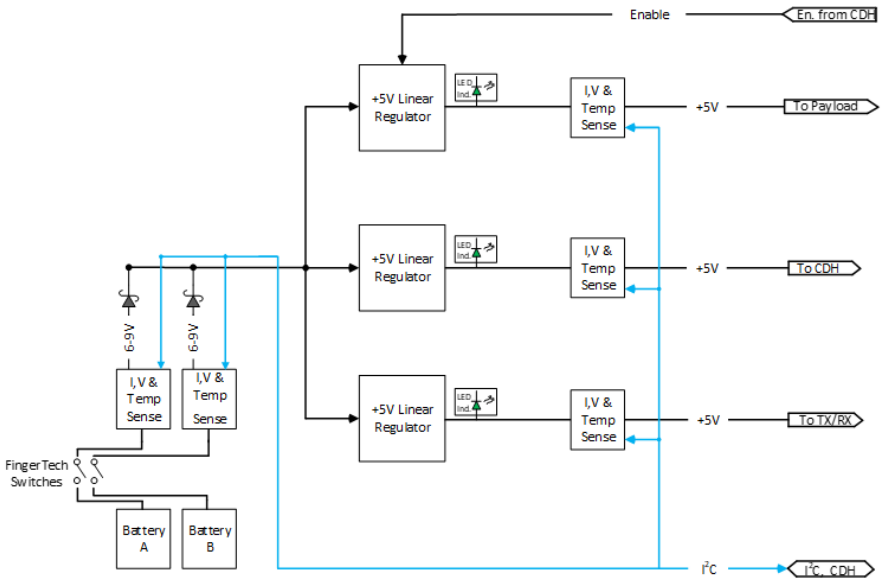

Figure 29. RDCS EPS Block Diagram. Adapted from [57].

c. C&DH

The C&DH subsystem of the HAB Bus requires modification to the MHX antenna and the addition of three covers. Antenna modification is required to facilitate RDCS integration, as the radiating element on the HAB Bus exceeded the diameter constraints imposed by the rocket payload bay. A cover is added to the GPS for security and two more are added to provide environmental protection around the C&DH antenna. Although more than cosmetic changes, none of the modifications change the functional attributes of the C&DH system as it normally operates in the HAB Bus.

(1) Antenna

The HAB Bus antenna extends beyond the allowable limits of the payload bay and needs modification. This antenna is a helical design intended to operate at 915.0 MHz, which is a frequency compatible with the telemetry radio. The new antenna needs to be designed for the same frequency, fit inside the rocket for launch, and then be positioned in an orientation that is to conducive to radiating the ground during operations. A simple yet effective design that meets all three of these requirements is a quarter wave monopole antenna, diagramed in Figure 30. The radiating element extends out from the feeder with

four radials mounted orthogonally and function as the ground plane. For a monopole antenna, both the radiating element and radius of the ground plane are one-quarter the length of design wavelength [61].

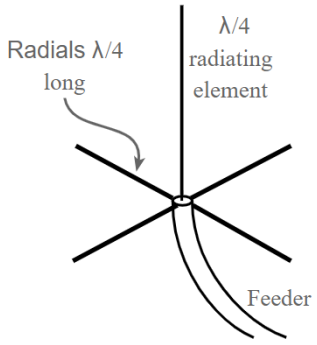

Figure 30. Quarter-Wave Monopole Antenna. Source: [61].

Similar to the antenna design of section III.D.4, Equation 1 yielded the wavelength, λ, associated with 915.0 MHz. This value is divided by four to determine the ideal radial lengths for the ground plane and radiating elements. These calculations are summarized in Table 14.

Table 14. C&DH Monopole Antenna Element Size

Signal Path	f (MHz)	λ (m)	$\frac{\lambda}{4}$ (m)
Telemetry	915.0	0.328	0.082

Although the ideal ground plane for a quarter-wave monopole antenna with a 915.0 MHz design frequency is a circle with a 16.4 cm diameter, this is too large to fit in the rocket. Consequently, the ground plane is modified to a 16.4 x 10 cm rectangle and made from a $1/32$ inch (0.794 mm) thick aluminum sheet, which allows the ground plane to also function as a structural panel for RDCS. To fit the 8.2 cm radiating element inside the payload bay, the radiating element is made of measuring tape material as depicted in Figure 31. The element is then bent to fit inside the rocket, much like the payload antennas, which

then naturally unfold after deployment due to its elastic properties. The feeder is a coaxial cable secured to the rear of the antenna plate with the negative portion grounded to the aluminum and the positive line connected to the radiating element. While the new C&DH does not affect the overall functional design of the system, it does allow for integration in the rocket.

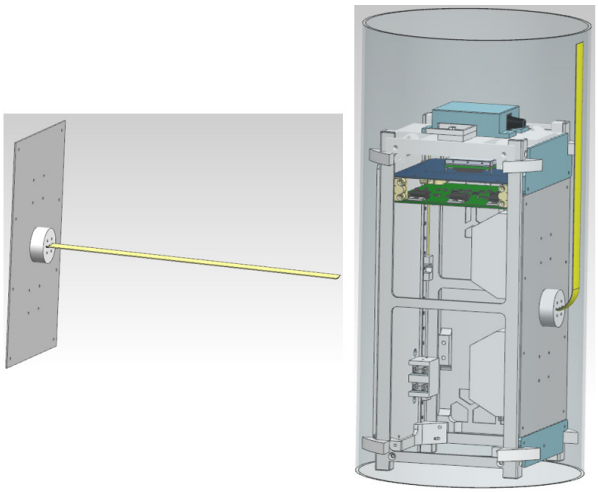

Deployed Configuration (left) and Stowed Configuration (right)

Figure 31. C&DH Antenna Design

(2) Covers

Three covers are added to augment some of the C&DH subsystem components and are colored in teal in Figure 31. The cover attached to the parachute mount on top of the bus is incorporated to secure the GPS receiver. The GPS cover includes four attachment points to the parachute mount and is constructed entirely out of 3D-printed polycarbonate. The other two covers, fitting above and below the antenna plate, are designed to protect internal components from the outside environment. Both covers near the ground plane are attached flush with the side rails using two screws each. Although modifications are made to the C&DH antenna and covers are added, there is no significant change to the operation of the subsystem from the HAB Bus. The C&DH functional bock diagram is depicted in Figure 32.

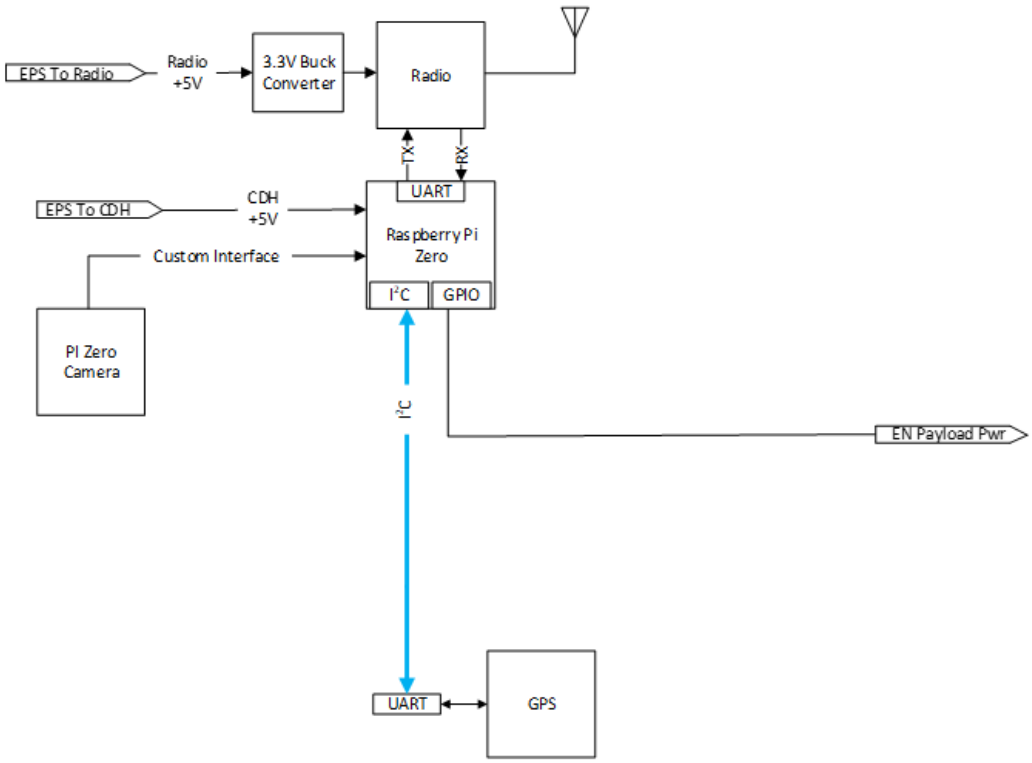

Figure 32. RDCS C&DH Block Diagram. Adapted from [57].

d. Thermal Mitigation

The RDCS bus also needed thermal mitigation to function in the cold temperatures of the near-space environment as the HAB Bus does not include any organic thermal protection components and includes panels with holes. These panels allow for heat loss from the wind and cold environment, primarily due to conduction. Cold temperatures have the most detrimental effect on the batteries and electrical components of RDCS. Table 15 estimates the current and energy capacity from the 10-battery power supply of the HAB Bus as a function of internal temperature. Current is measured in milliamps (mA), which decreases as temperature decreases. Energy capacity is measured in Watt-hours (Whrs), which also reduces with decreasing temperature. A sufficient decrease in energy capacity could result in RDCS malfunctioning in flight, effectively ending its utility and result in mission failure.

Table 15. Estimated Available Capacity vs. Temperature. Source: [57].

Temperature (°C)	**Current** (mA)	**Energy Capacity** (Whrs)
-10	3200	48.0
-20	2900	43.5
-30	1800	27.0
-40	1000	15.0

The batteries are not the only components sensitive to cold temperatures. Table 16 is a summary of the published operating temperature ranges for various components from both the bus and payload of RDCS. While the range for the majority of the hardware is -40 to 85°C, the B205-Mini SDR has a noticeably more restrictive operating temperature range. The coldest expected temperature of the near-space regime is approximately -60°C, as explained in Section A.3 of this chapter, and it is imperative that the loss of heat be prevented for both the payload and bus.

Table 16. Component Operating Temperature Ranges.

Section	**Component**	**Approximate Operating Temperature Range** (°C)
Bus	Bus Controller	-40 to 85 [62]
	Radio	-40 to 85 [63]
Payload	Computer	-40 to 85 [47]
	SDR	0 to 40 [50]
	Amplifiers	-40 to 85 [55], [56]
	LPF	-55 to 100 [52]

The batteries and payload components produce heat in their normal operation, so the primary objective of the thermal mitigation steps is to contain this self-generated heat to prevent excessive cooling. To prevent heat loss from the power supply, each battery box is wrapped in thermally insulating HT-340 polymide foam produced by Boyd Corporation with properties summarized in Table 17. The low density, measured in kilograms per cubic meter $\left(\frac{kg}{m^3}\right)$, makes the foam lightweight and the low coefficient of thermal conductivity,

measured in Watts per meter Kelvin $\left(\frac{W}{mK}\right)$, make the flame retardant and non-conductive foam an ideal choice. The foam is also used to line the inner side of the external panels to contain the heat produced by the various components and prevent excessive cooling.

Table 17. HT-340 Polymide Foam Properties. Source: [64].

Property	Value
Density (kg/m^3)	6.4
Thermal Conductivity (W/mK)	0.046

Because both the batteries and SDR are the most sensitive to temperature and mounted in locations that have minimal separation from the outside environment, these components warrant additional thermal mitigation. The batteries are mounted to the aluminum C&DH antenna ground plane, which conducts heat much like a radiating plate, and the SDR is mounted only 4 mm from the switch panel, which provides limited space from the environmental elements. To add an additional insulating measure, the inner surface of the ground plane and switch panel are lined with DuPont 5 mil Kapton tape. The coefficient of thermal conductivity for 1 mil of Kapton tape is 0.12 $\frac{W}{mK}$, and DuPont lists insulation as an application of Kapton tape [65]. Figure 33 is a depiction of the thermally insulating foam and tape used to protect the battery box and SDR.

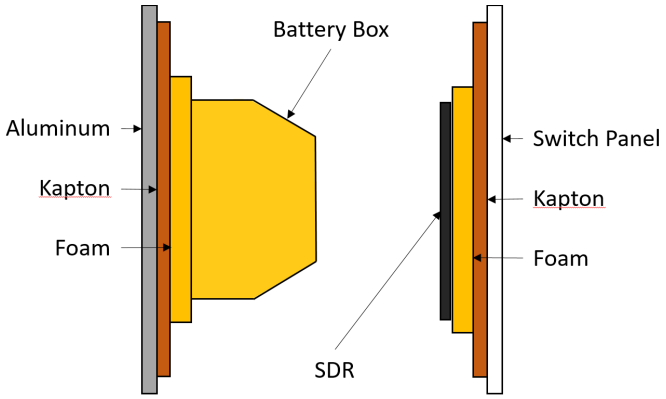

Diagram not to scale

Figure 33. Thermal Mitigation for Batteries and SDR

In brief, to prevent the cold temperatures of the near-space regime from adversely affecting RDCS, thermal mitigation steps are taken to prevent heat loss for both the bus and payload. The inside surfaces of the entire structure are lined with thermally insulating foam to prevent heat loss. Additional measures are added to protect the batteries and SDR, given their heat sensitivity and particular placement inside the structure.

e. Summary

All of the changes to the HAB Bus are to address structural, thermal, operator, or rocket integration concerns. The 3D-printed structure is modified with spacers and nut cages while the size of the parachute mount is increased. The electric subsystem has notable design modifications to supply the same power specifications to a new form factor. To fit the C&DH in the rocket, it is modified to a custom-built monopole antenna made of measuring tape. Additionally, thermally insulting material is used to contain the heat generate by components and limit cooling. Although RDCS is a unique design, it is based heavily off the Small Sat Lab's HAB Bus.

3. Recovery Components

The recovery equipment is the final section of the bus design analysis. There are three separate elements to RDCS recovery: tracking, safety parachute, and primary parachute. To facilitate real-time tracking and recovery, as part of the academic research,

a tracking sensor is installed. Next, in the event the primary parachute did not deploy properly, a safety parachute is also included. The final recovery element is the primary parachute. Its function is to minimize the descent rate, which is critical to prolonging connectivity time for users. While not all components are required if the system were ever to be operationalized, they provide necessary recovery, safety, and tracking capabilities to facilitate academic research.

a. Tracking

The tracking capability is an example of a non-essential component to RDCS that is much more useful for this demonstration. Tracking functions are accomplished by the SPOT Trace pictured in Figure 34. It is mounted internal to RDCS in a compartment, circled in red in Figure 34, which is integrated into a side panel. This panel is derived from the HAB Bus side panel but has been filled, much like the switch panel, for thermal considerations. The SPOT Trace passes all messages with satellites in LEO to users, which offers a nearly worldwide tracking capability. Users can monitor their devices on the company website. The Trace is also capable of providing location information in the form of GPS coordinates every 2.5 minutes that can be viewed using Google Maps. The Trace is powered by four AAA batteries and completely independent of the bus EPS. This device has a significant flight history in the Small Sat Lab and is known to support recovery efforts by operating for days, if required, which is long after the bus is expected to run out of power.

SPOT Trace (left) and Trace Mounting Panel (right).

Figure 34. Tracking Equipment. Source: [66].

In-flight, the Trace is intended to be a backup to the C&DH Byonics GPS, which is managed by the C&DH system.

b. Safety Parachute

Similar to the Trace, a safety parachute is included to facilitate retrieval in a non-operational setting. This parachute reduces the descent velocity of RDCS as it approaches the ground. The Small Sat Lab has a flight history with the Rocket Man 4Ft. High Altitude Balloon Parachute, pictured in Figure 35. Given the FAA weight constraint, the heaviest RDCS can weigh is approximately 1.8 kg, which corresponds to a descent rate at impact of approximately 5.18 $\frac{m}{s}$ [67], an acceptable impact speed. The safety parachute is released by the Jolly Logic Release Mechanism, pictured in Figure 35, which is a self-contained and independently powered device that is programmed to release the parachute at approximately 300 m (1000 ft) [68]. The mechanism is enabled on the ground prior to launch. Once its internal barometer senses an ascent above the trigger altitude of 300 m,

the mechanism arms; then, when RDCS descends below this trigger altitude, the mechanism is designed to release the safety parachute, which decreases the descent velocity to reduce the force of the impact with the ground. Given the safety parachute's CONOPS, it always deploys during the descent at 300 m. In the event RDCS does not deploy from the rocket properly, the safety chute still deploys and will reduce the speed of the system at impact. The "always-on" nature of the safety parachute provides the additional margin of safety necessary to conduct the academic research for RDCS.

Rocket Man 4Ft (left) and Jolly Logic Release Mechanism (right).

Figure 35. Safety Parachute. Source: [69] , [68].

c. Primary Parachute

Unlike the SPOT Trace and safety parachutes, this primary parachute is necessary for RDCS even if it were to be operationalized. The main function of the primary parachute is to increase the drag of RDCS, decrease its descent velocity, and prolong its time at altitude. By selecting the largest parachute able to fit inside the rocket payload bay, RDCS achieves the maximum time at altitude, thereby increasing connectivity time for the user.

(1) Parachute Selection

The space used by the rocket parachute with its rigging, safety parachute with its rigging, and RDCS leaves approximately 9 cm of available length for the payload parachute in the rocket payload bay. Equation 7 defines the volume of a cylinder, V ,

calculated in cubic centimeters (cm^3), where r is the radius of cylinder measured in centimeters (cm) and h is the height of the cylinder measured in cm. This equation was used to calculate the remaining volume of the payload bay, approximately 1680 cm^3 [70].

$$V = \pi r^2 h \tag{7}$$

Given this constraint, and the flight history of the Small Sat Lab with Rocket Man products, the largest parachute that fits in the allotted space of the payload bay is the 9Ft Rocket Man, which has a packed volume of approximately 1545 cm^3 [67]. It looks very similar to the parachute of Figure 36 and attaches to the parachute mount.

Figure 36. Rocket Man Parachute. Source: [67].

(2) Calculating Descent Profile

The descent profile of the parachute is directly related to the time to descend and paramount to understanding the connectivity window capability of RDCS. Parachutes function by creating a drag force through aerodynamic braking, which is opposite the acceleration due to gravity, the force known as weight, as depicted in Figure 37.

Figure 37. Free Body Diagram. Adapted from [69], [71].

Aerodynamic drag is explained in Equation 8 where D represents drag in Newtons (N), ρ represents air density in kg per cubic meter $\left(\frac{kg}{m^3}\right)$, V represents descent velocity in meters per second $\left(\frac{m}{s}\right)$, A represents the cross-sectional area of the parachute in square meters (m^2), and coefficient of drag, C_D, is a dimensionless value. The standard density of air at the surface of the earth is 1.225 $\frac{kg}{m^3}$, and a typical value for the coefficient of drag for rocket parachutes is 1.75 [71].

$$D = \frac{1}{2}\rho V^2 A C_D \tag{8}$$

Weight, represented as W and measured in N, is a force described by Newton's Third Law and given in Equation 9, where m is the mass of an object measured in kg and g is the acceleration due to gravity measured in meters per second squared $\left(\frac{m}{s^2}\right)$ [71].

$$W = mg \tag{9}$$

Parachutes keep these two forces are equal, a condition known as terminal velocity. Mathematically, terminal velocity is expressed by setting Equation 8 and Equation 9 equal to each other. This new expression is then algebraically manipulated to solve for the descent velocity of RDCS and is presented as Equation 10 [71] .

$$V = \sqrt{\frac{2mg}{\rho A C_D}} \tag{10}$$

All of the input variables to Equation 10 are known at the surface of the earth except the cross-sectional area of the parachute. However, the Rocket Man website states that a 15 lb payload (6.8 kg) will experience a descent rate of 15.84 feet per second (fps), or 4.82 $\frac{m}{s}$, at impact under a 9Ft Rocket Man parachute [67]. Using this published information and Equation 10, the cross-sectional area for the parachute is 2.67 m^2.

However, air density and gravity are not constant throughout the descent of RDCS. Equation 11 is the calculation for atmospheric density is a function of altitude. Z represents the altitude in the units of km, H represents the scale height in the units of km, ρ_0 represents the density of air at the surface of the earth in the units of $\frac{kg}{m^3}$ [72]. Equation 11 shows that the density of the air decreases exponentially with altitude. Correspondingly, the descent rate of RDCS will decrease as it descends.

$$\rho = \rho_0 e^{\frac{-Z}{H}} \tag{11}$$

Similarly, gravity does not remain constant with altitude, but is expressed by Equation 12, where μ represents the Earth Gravitational Constant expressed in cubic meters per second squared$\left(\frac{m^3}{s^2}\right)$, R_e is the radius of the earth measured in meters, and z is the altitude from the surface of the earth in meters. Thus, the acceleration due to gravity decreases the greater the distance from the earth [73].

$$g = \frac{\mu}{\left(R_e + z\right)^2} \tag{12}$$

The descent profile for RDCS was calculated using Equation 10, Equation 11, and Equation 12 through numerical integration with a custom program, contained in Appendix C, written in Matrix Laboratory (MATLAB). Figure 38 is a plot of the predicted descent velocity of RDCS during operation, summarized in Table 18. Figure 38 confirms the conclusion that the descent rate decreases over time as RDCS decreases in altitude.

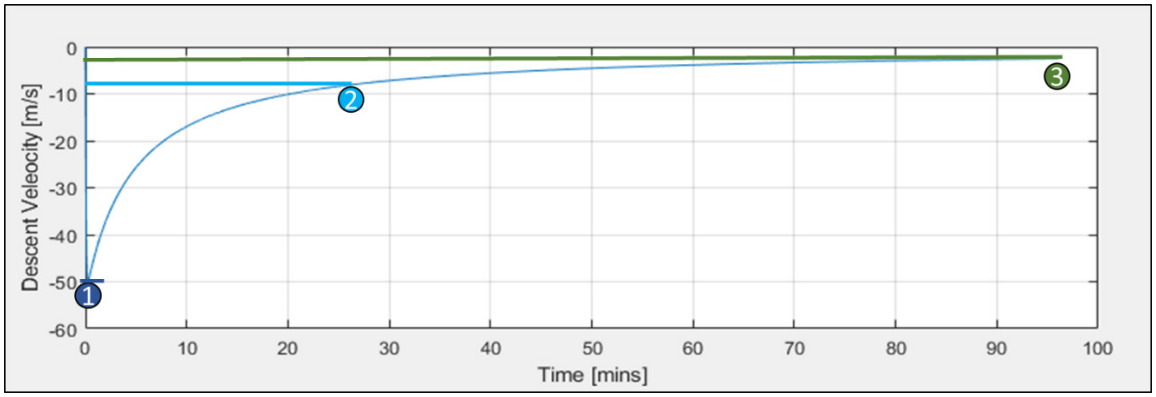

Figure 38. Predicted Descent Velocity as a Function of Time

Table 18. Predicted Descent Velocity Summary

Label	Condition	Value
–	Initial Free Fall	14 seconds
1	Maximum Descent Velocity	-50 m/s (-165 fps)
2	Average Descent Velocity	-7.9 m/s (26 fps)
3	Impact Velocity	-2.5 m/s (-8.1 fps)

Figure 39 depicts the change in altitude over time from the maximum altitude, summarized in Table 19. Since altitude corresponds to a link capability for RDCS, this data was critical to developing the performance charts depicted in Figure 2 and further detailed in Appendix A.

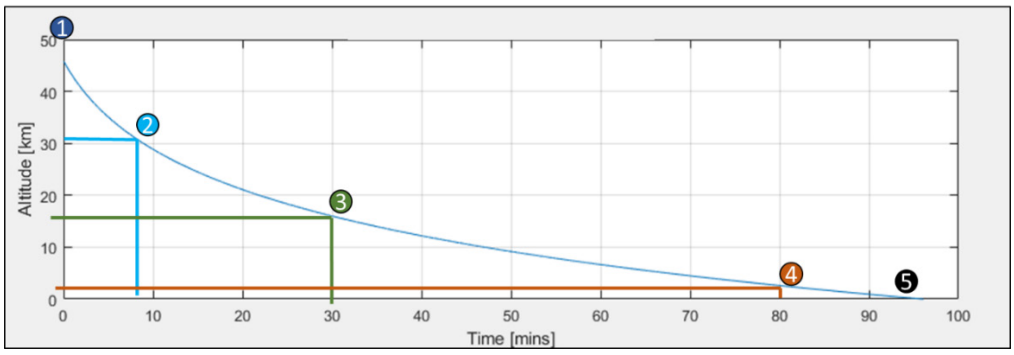

Figure 39. Predicted Altitude as Function of Time.

Table 19. Descent Summary

Altitude (km)	Altitude (ft)	Descent Time (mins)	Notes
45.7	150,000	0	Deployment Altitude
30.5	100,000	8.5	
15.2	50,000	31.8	
2.4	7,800	81.4	Altitude for 25 mile operational range
0	0	96	

The 9Ft Rocket Man parachute was chosen to maximize the time aloft for RDCS, extending its operational utility. It is the largest parachute option given the available volume remaining in the rocket payload bay. The parachute is predicted to produce an average descent velocity of -7.9 $\frac{m}{s}$ and an impact velocity of -2.5 $\frac{m}{s}$. It allows for nearly 81 minutes to conduct operations further than the minimum 25 mile operational range derived from the MOC and discussed in Chapter I. Other recovery equipment includes the SPOT Trace and safety parachute, which all serve critical roles for safety and academic research functions. The recovery components are the final elements of the RDCS design and trade analysis, with remaining portions focusing on integration, test, and demonstration.

G. PAYLOAD AND BUS INTEGRATION

The bus and payload were initially designed in CAD using NX software to design for size and fit. The payload was designed first, then the bus. Through an iterative process known as rapid prototyping, parts were designed, printed, assembled, and checked for fit and functionality. Required modifications were noted, applied to the CAD file, and then parts were reprinted. This process continued until each piece was correctly designed for form, fit, and function.

1. Payload

The payload was designed and built first. While the trade analysis of Section III.D determined the hardware that comprises RDCS, the analysis does not address the specifics

of fitting the payload inside the bus. Since space is the primary factor for constructing the payload, emphasis is placed on a compact form factor. There are two portions to the payload construction, the payload mount and the payload antenna plate.

a. Payload Mount

The payload mount serves as the attachment point for all of the hardware identified in the trade analysis and is built exclusively out of 3D-printed polycarbonate. The mount consists of two parts, the platform and the cover, and is pictured in Figure 40 with all of the components identified from the trade analysis. The LPF, LNA and wideband amp were attached to the cover portion of the mount and secured with lock nuts. Due to space considerations on the underside of the cover, nut cages are not featured in the payload cover. The cover is attached to the platform portion at three separate locations to reduce the effects of vibrations. Underneath the cover, the rPi is screwed in to the platform, while the SDR is fastened to the opposite side of the platform. Four legs, each with two screw holes, are designed to attach the payload to the side rails for a vertical mount. The camera cable is routed from the rPi and up through the cover to facilitate mounting on the side panel to capture horizontal video.

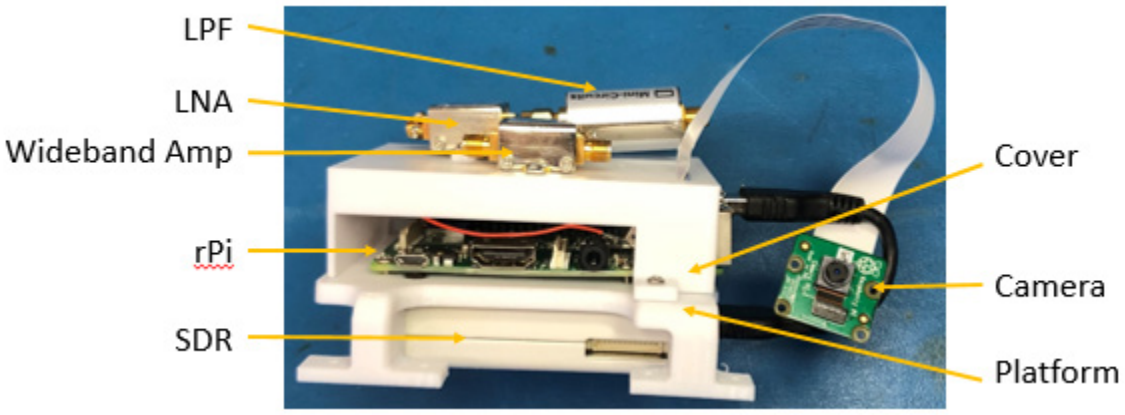

Figure 40. Payload Mount

b. Payload Antenna Plate

The other section of the payload is the antenna plate, depicted in Figure 41, which serves as the attachment piece for both uplink and downlink antennas. Similar to the parachute mount, the cross bars, colored in teal in Figure 41, are fully integrated into the plate and printed as a single piece. Because the antenna elements are too long to fit inside the rocket without bending, the elements are made of size 18 piano wire. This wire is flexible enough to return to its original shape after bending to fit inside the rocket, but stiff enough retain its shape during operation. Due to this flexible behavior, no additional mechanisms are required to deploy the antennas for operation. Both antennas are mounted to the same plate, as depicted in Figure 41, with the VHF elements mounted to the top-facing side and the UHF to the bottom side.

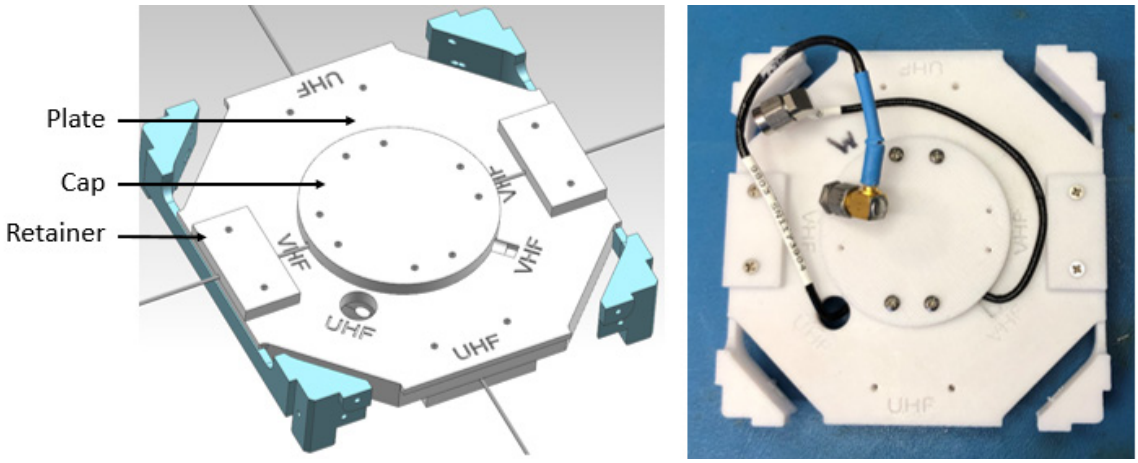

CAD Model (left) and Polycarbonate Hardware (right)

Figure 41. Payload Antenna Plate.

The top and bottom of the plates are exactly the same, just rotated 90° to minimize antenna pattern overlap. The middle of each antenna is centered on the plate underneath the circular cap. There are channels built into the plate and caps to allow for each respective feeder cables to be routed to the radiating elements. The cable routing through the VHF channel connects the VHF antenna to the LPF. The cable that runs through the UHF channel connects the wideband amp to the UHF antenna. From the caps, radiating elements

route through slots to the rectangular retainers, which have troughs to guide the piano wire elements and serve as mounting points for the elements. JB Weld epoxy in the troughs secures the retainers and piano wire to the antenna plate. Figure 42 is a depiction of the fit-check of the flight ready antenna plate in a bus engineering design unit (EDU).

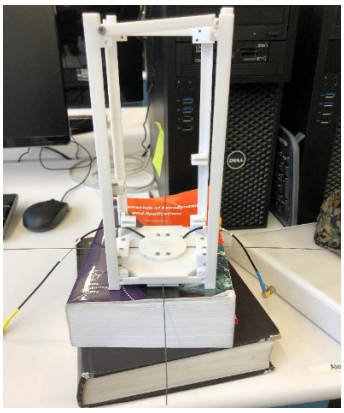

Figure 42. Antenna Plate Fit Check

2. Bus

The bus was built after the payload. A bus EDU was used to conduct checks to ensure appropriate clearance between components and the fit of parts within the structure. Figure 43 is a depiction of the bus under construction. Once bus construction was the complete, the next step was to integrate the payload, route the wiring, and install the foam.

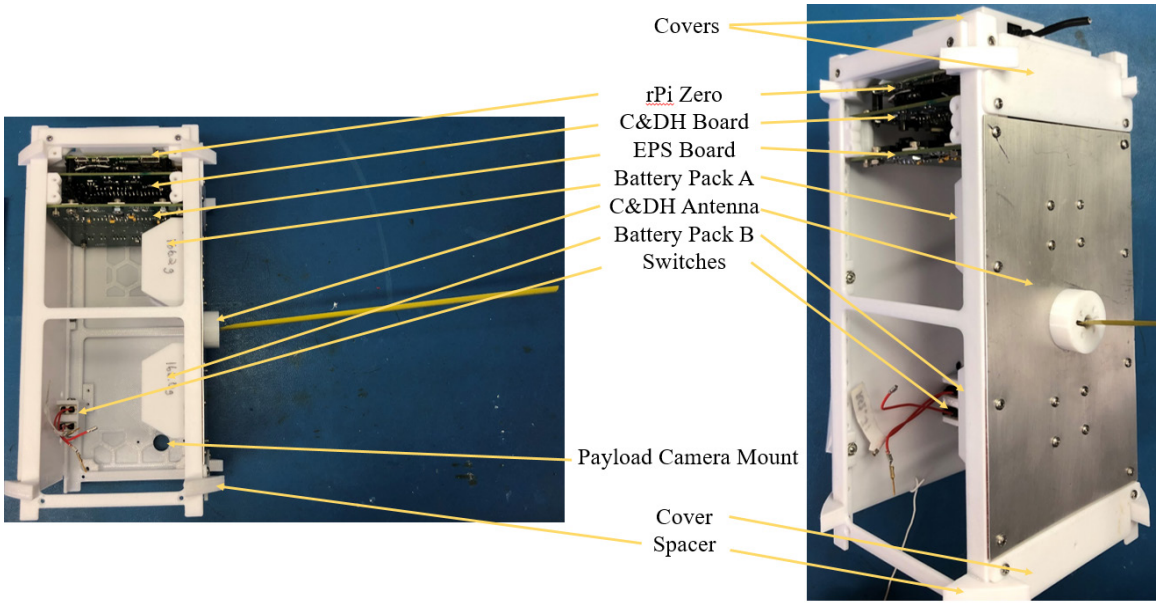

Bus Side View (left) and Isometric View (right)

Trace mounting panels has been removed to view interior

Figure 43. Bus Construction

3. Integration

The first step to completing the build was to integrate the payload and bus. The payload was mounted vertically with the SDR facing the switch panel and amplifiers closest to the center of the structure. Figure 44 depicts the fit check of the payload, circled in yellow, and bus. The next steps to integration were the wire routing and foam installation, shown in Figure 45. Once the wiring and foam were complete, the final step was to tune each antenna. Using a Keysight FieldFox RF Analyzer, each antenna was tuned to their respective frequencies by trimming the outside edges of each element. The antennas were then wrapped in Kapton tape to electrically isolate them from one another and other conducting materials. The final step of integration was to estimate the mass, power, and data properties of the system.

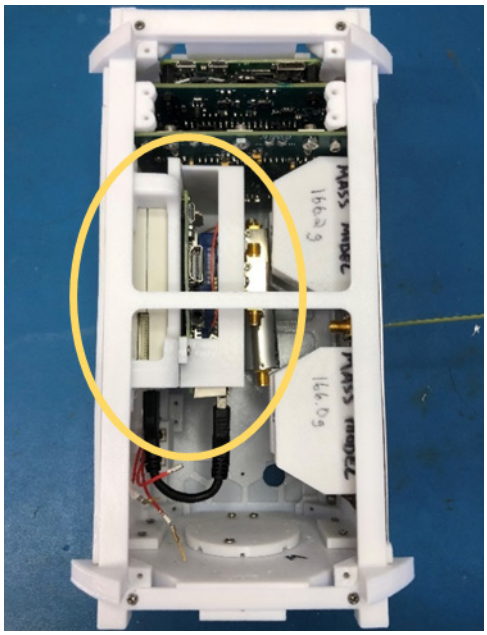

Figure 44. Payload Installation

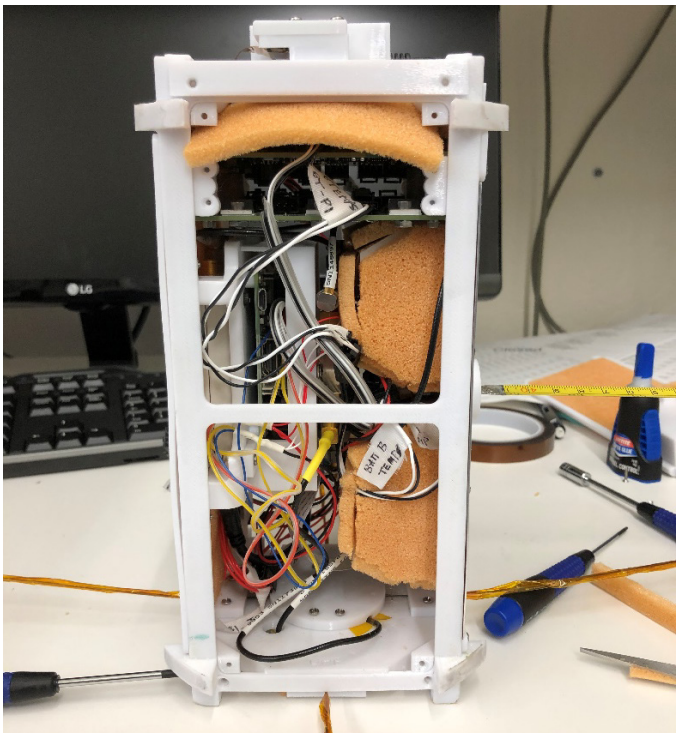

RDCS Antennas having Kapton tape applied just prior to vibration testing

Figure 45. Integrated RDCS

4. Budgets

Once RDCS was assembled, the mass, power, and data budgets were calculated to ensure all requirements associated with these metrics were met. For the mass budget, the entire system is restricted by the FAA to no more than approximately 1.8 kg, not including the recovery equipment. To maximize lift capacity, the rocket requires RDCS to be as light as possible. All components of the system were weighed, including a 10% margin for each subsystems, and found to meet the limitations. Table 20 is a summary of the mass budget with detailed mass values contained in Appendix D.

Table 20. RDCS Mass Budget Summary

Calculated Value (lbs)	**Constraint**	**Source**
2.31	< 4 lbs	FAA
3.75	Light as possible	Rocket

The power budget constraint is the power supply's 48 Whrs of maximum available energy for the bus and payload. To calculate energy usage, the products' maximum current, I, measured in amperes (A), and voltage, V, measured in volts (V), were multiplied together according to Equation 13 to determine power consumption, P, in Watts (W).

$$P = IV \tag{13}$$

Each component's power was then multiplied by the entire operating time, t_o, measured in hours, and estimated duty cycle (DC) expressed as a percentage of total operating time to determine energy consumption.

$$E = Pt_o(DC) \tag{14}$$

The entire time of operation, t_o, from launch, through 196,000 ft, and all the way to touchdown was calculated to be approximately 96 minutes. Factoring in approximately 15 minutes for ground operations, the planned operating time for RDCS was approximated as 110 minutes. The results of the power budget analysis are summarized in Table 21 with detailed values contained in Appendix E.

Table 21. RDCS Power Budget Summary

Calculated Value (Whrs)	**Constraint** (Whrs)	**Source**
36.73	< 48	Batteries

The final budget was the data budget to ensure sufficient space was available on both the bus controller and payload computer to store the video recorded onboard during flight. The bus has 10 GB of available storage and the payload has 24 GB, making these storage capacities the constraints for the data budget. Using the data rate associated with each particular camera's settings and time of operation, the total expected data for each computer was calculated to be within limits as summarized in Table 22. A complete data budget is enclosed in Appendix F.

Table 22. RDCS Data Budget Summary

Calculated Value (GB)	**Constraint** (GB)	**Source**
4.54	< 10	Bus Storage
18.54	< 24	Payload Storage

H. CONCLUSION

RDCS is designed to operate with current existing hardware and provide BLOS communication to tactical users. The design is heavily influenced by constraints imposing size, weight, and volume limitations. First, a frequency trade analysis was conducted to understand the most suitable choice of uplink and downlink frequency, which considered factors like compatibility with operational systems, availability of COTS hardware, and spectrum availability, which ultimately resulted in the choice to design for the 2-meter and 70-cm amateur bands. Next, the user segment was examined to determine a radio and antenna combination for a foot-mobile user and shipboard antenna for those afloat. These systems define the external system in which RDCS was required to operate.

These conditions constrained the design choices regarding the two major components of RDCS: payload and bus. After a thorough hardware trade study and link analysis, specific components were chosen for incorporation with the payload. Further analysis determined that RDCS had excess capability and could communicate over distances associated with a deployment altitude of 196,000 ft – well above the design altitude. The software of the SDR, the heart of the payload, was generated using GNU radio. This script receives and filters the signal, after which the signal passes through a squelch and AGC before retransmitting.

Once the payload was complete, the bus was designed. The bus for RDCS relies heavily on the Small Sat Lab HAB Bus, with modifications to the structure, EPS, and C&DH portions of the design to support rocket integration, to provide insulation, and to enhance operations. Recovery equipment on the bus includes a primary parachute, safety parachute, and tracking device. The final step to RDCS design was payload and bus integration, in which the two sections were mounted and wired together before foam thermal insulation was installed.

After thorough analysis, design, construction, and integration, RDCS was ready for testing.

IV. RDCS TESTING

The design of RDCS was validated through testing of software and hardware in both the laboratory and the field environments. The first series of tests occurred at the sub-system level with a static-load structural test and a flow-graph verification test. The first system-level test was an electrical bench test. Next, two separate field tests were required to validate the radio software with flight hardware. Once all flight-systems were validated, a functional check of the entire system was executed. Next, integration with the rocket was tested through a fit check and a deployment test. Finally, environmental testing was performed to ensure RDCS was capable of withstanding the harsh launch and operating environments associated with rockets and the near-space regime.

Much of the testing phases required over-the-air transmissions using actual radios to send and receive real FM signals. The results from Section III.C.1 have the AN/PRC-117G radio and NA-701 antenna as the foot-mobile user equipment and the Trivec-Avant AV2099-4 as the shipboard antenna for RDCS. However, this particular radio model and shipboard antenna were not readily available to the researchers. Furthermore, the AN/PRC-117G has strict handling requirements due to some of its unique capabilities, making it a less-than-ideal candidate for research purposes. A suitable proxy for the AN/PRC-117G is the Harris RF-7800H-MP, and for the purposes of this experiment, the AN/PRC-117G and the RF-7800H-MP can be considered identical [74]. In addition, the RF-7800H-MP was immediately available to researchers and did not have any handling restrictions, making it an ideal radio to substitute for the AN/PRC-117G. Since the AV2099-4 antenna was not available, the shipboard portion of the user segment was substituted with the foot-mobile equipment. Thus, all actual over-the-air operations for RDCS were conducted with the Harris RF-7800H-MP radios to perform both send and receive functions of the user segment of RDCS.

A. SUB-SYSTEM TESTING

There were two sub-system-level tests performed on RDCS prior to any modelling or construction of RDCS to verify inherited software and hardware from previous research. The first was a static-load test of 3D-printed material; the second was a flow-graph verification. The static-load test was conducted to determine the ultimate fracture threshold of polycarbonate when placed under a vertical static load. The radio software verification test was designed to confirm operation of the initial flow graph for the SDR. Sub-system testing was not conducted on the EPS or C&DH portions of the bus due the extensive HAB Bus flight history.

1. Static Load

The first test conducted for RDCS was a static-load test of a 3D-printed assembly modeled after the HAB Bus structure. Although the specific flight profile for the rocket was not known, the forces were estimated to be approximately 25 Gs. Since the Small Sat Lab did not have experience with a polycarbonate structure being subjected to forces of this magnitude, a static-load test was conducted.

The test assembly, depicted in Figure 46, was a polycarbonate structure measuring 10 x 10 x 65 mm, which included side rails and cross bars like the HAB Bus. A 4-mm-thick board with a 0.23 kg (0.5 lbs) steel mass was secured in the middle of the structure to model size and weight of the HAB Bus C&DH and EPS boards. The mass of the test board including the steel mass was 287.7 g, and the entire assembly had a mass of 343.5 g. The assembly was placed on a flat surface, and two 0.5 kg weights were stacked on top of the mass model to ensure the force of all subsequent objects was only applied the test board. These weights were used to simulate acceleration forces in a static environment. As weights were applied, the board bent. If a weight was removed, the board returned to its original position, demonstrating an elastic response. The picture on the right of Figure 46 depicts the polycarbonate response with 56.0 kg (123.5 lbs) of mass applied.

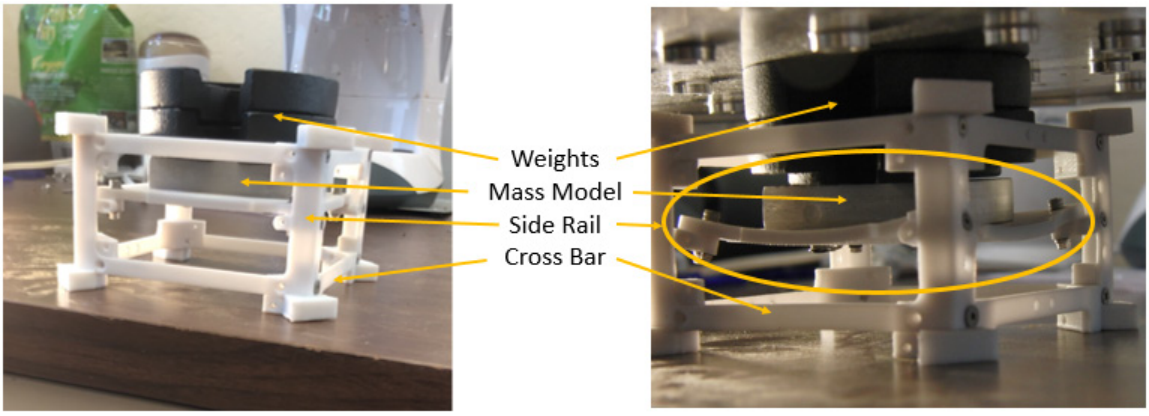

Test Assembly Setup (left) and Polycarbonate Elastic Response (right)

Figure 46. Static Load Test

The test assembly failed when 57.6 kg (126.9 lbs) of mass was applied to the mass model and board (Figure 47). The failure occurred when the test board fractured in two places. Despite the bending induced by the addition of weights, no significant damage was noted to the side rails or cross bars. As RDCS was expected to weigh approximately 1.8 kg, the ultimate yield force of 57.6 kg represents 31.7 Gs. Since this value exceeded the expected 25 Gs produced by the rocket with a factor of safety of 1.3, this static-load test was considered a success and a polycarbonate structure for RDCS was confirmed.

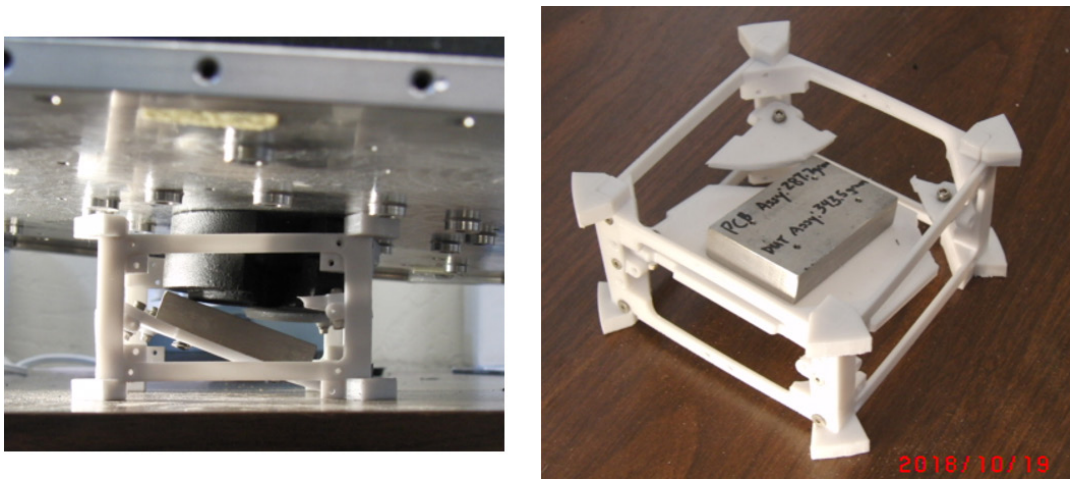

Figure 47. Static Load Test Ultimate Yield

2. Flow-Graph Verification

The next test of inherited elements was the GNU Radio flow-graph verification test to confirm the SDR was capable of conducting a full-duplex relay to in-band and out-of-band frequencies. The GNU Radio flow presented in Section III.E was very similar to the flow graph used by Swintek [24]; however, that project did not achieve a full-duplex capability. To verify the software and block configuration settings, the flow graph was used to conduct a full-duplex relay over the air. Figure 48 depicts the equipment used to conduct the verification. To simulate a payload, the laptop was used to control a B205-Mini connected to two NA-701 antennas. Speakers were connected to the laptop to verify the quality of the received transmission and assist with troubleshooting. The user segment consisted of two Harris RF-7800H-MP radios with RF-3150-AT152 antennas, which were placed five meters from the B205-Mini.

This test consisted of two phases: calibration and verification. The goal of the calibration phase was to configure the gain of the transmit block to a value that resulted in a clear transmission between the two radios. First, the transmit radio was configured for the same frequency programmed in the sink block of the flow graph, and the receive radio was tuned to the frequency programmed in the source block of the flow graph. Then, following steps similar to those presented by Swintek, the gain of the transmit block was incrementally increased until a clear FM voice transmission was heard by the researcher [24]. The result of this procedure was that a transmit gain value of 41 programmed in the sink block yielded the most audible transmission for the receive radio. This completed the calibration phase of the test.

Figure 48. Radio Flow-Graph Verification Test Setup

The next phase of the flow-graph verification was the demonstration portion, which had two objectives: 1) verify the SDR's ability to relay in-band (VHF to VHF and UHF to UHF) and 2) demonstrate the SDRs ability to relay across bands (VHF to UHF and UHF to VHF), since cross-banded transmission had never been done before in a project from the Small Sat Lab. Four frequencies were identified for this test. The two VHF frequencies were 144.6 MHz and 146.0 MHz, and the two UHF frequencies were 435.0 MHz and 439.0 MHz. Two of the frequencies, 144.6 MHz and 435.0 MHz, were chosen because they were the identified uplink and downlink frequencies from the frequency analysis of Section III.B. The other two frequencies were chosen because each was sufficiently separated from the other in-band frequency, which facilitates transmissions within the band (VHF to VHF and UHF to UHF).

The test consisted of a series of 24 transmissions between the two radios; results are summarized in Table 23. One radio was designated the transmitter and the other, the receiver, and then the roles were reversed. The receiver and sink blocks of the SDR were set to one of the identified frequencies (top row of Table 23), then the transmitter and

source block of the SDR were cycled through the transmit frequencies (first column of Table 23), making a radio transmission on each frequency. This process was repeated across all four frequencies, and the verification table was completed twice, once for each radio serving as transmitter then receiver, to complete the 24 transmissions.

Table 23. Flow-Graph Verification Table

Transmit ↓	Receive →	144.6	146.0	435.0	439.0
144.6		■			
146.0			■		
435.0				■	
439.0					■

Each radio was able to send and receive transmissions on all four frequencies using the SDR as a relay. This result demonstrated the capability of the radio flow-graph to send, relay, and receive any combination of VHF and UHF frequencies as a full-duplex system. The calibration phase revealed that a sink block transmit gain setting of 41 would produce a clear transmission for two radios spaced five meters apart.

B. SYSTEM-LEVEL FUNCTIONAL TESTING

System-level functional testing began after the conclusion of the payload and bus integration phase, described at the end of Chapter III. The first full-system test was power budget validation, the objective of which was confirming power and energy usage. Next, the radio software was validated with flight hardware through two distinct tests. Finally, a comprehensive functions check was performed to verify all systems of RDCS.

1. Power Budget Validation

The power budget was validated in the Small Sat Lab by connecting RDCS to an external power supply and monitoring total voltage and current usage. There were three separate portions of this test: payload, bus, and system, which are summarized in Table 24. A complete power budget is included in Appendix E. For each portion of the test, an Agilent E3632A DC power supply was programmed to provide to appropriate voltage and current to hardware.

The first step of the payload portion was to connect the power supply to the payload power cable, which delivered electricity to each active payload component. Next, the power supply was configured to deliver 5.00 V, which is the same voltage provided by the linear regulator from the EPS system to the payload. Then, RDCS was powered on and average current usage was monitored for 10 minutes, which was a flight representative portion of the approximately 110 minutes of entire powered time. During this period of time, the system operated under two conditions, receive-only and relay. The receive-only condition occurred when the SDR was only listening to the receive frequency without retransmitting it. In this situation, there were no signals above the squelch threshold and, consequently, there were no signals to transmit making this a receive-only condition. The second condition was relay, where the payload received a signal above the squelch value and retransmitted it. The highest observed current for each condition was used to calculate the energy usage using the same procedures detailed in Section III.G.4. These energy values were then added together to yield a maximum payload energy value, presented in Table 24.

Table 24. Power Budget Validation Summary

Section	Energy Usage (Whrs)	Constraint (Whrs)
Payload	16.21	–
Bus	14.67	–
System	41.90	48

The bus energy usage portion was determined by connecting 8.00 V of power directly the EPS board, which distributed power to the C&DH subsystem. The current was monitored for a period of 10 minutes of nominal operation, and the highest observed value was used to calculate the energy usage of the bus. The payload and bus energy usage values were added together to yield an energy usage of 30.87 Whrs, which is less than the 48 Whrs available from the power supply.

Finally, the entire system was connected to the power supply to provide a more accurate and realistic power budget. For this portion, 8.00 V was supplied to the entire system, both payload and bus, through the EPS. The payload operated in a relay condition for a period of 10 minutes, with 2.00 A being the highest current observed over this period. Using the supplied voltage and highest observed current, the power budget for RDCS was calculated to be 41.90 Whrs, or 6.1 Whrs below the battery energy constraint. Thus, although the energy usage from the whole-system power validation test was larger than both the initial power budget and the sum of the individual payload and bus measurements, RDCS possess positive energy margin. Positive energy margin indicates the 10 AA battery power supply is sufficient for RDCS to operate continuously in a relay condition for the estimated 110 minutes of operating time with energy to spare.

2. Radio Software Validation #1

Once the power budget was validated for continuous relay operations, the next step in full-system testing was to validate the relay software with flight hardware. The goal of this test was to determine the settings for each block of the radio flow graph for relays conducted over short (5 m), medium (25 m), and long (100 m) distances in preparation for an even longer test at 3 km. Although 40 dBm was identified as the design transmit power for the RDCS user segment in the initial analysis, at these distances, this setting would have resulted in an extremely strong signal which could have potentially damaged components of RDCS; thus, only 30 dBm of transmit power was used for these test distances. Table 25 is a summary of settings that were adjusted from the verified GNU Radio flow graph presented in Section IV.A.2.

Table 25. Software Validation Test #1 GNU Radio Flow Values

Range (m)	**Attenuators** (dB)	**Source Gain** (dB)	**Squelch** (dB)	**Sink Gain** (dB)
5	50	-10	-75	41
25	50	6	-75	65
100	0	28	-60	65
100	40	57	-55	65
100	50	Unsuccessful		

a. Differences from Verification Test

There were several differences in test equipment between this validation test and the pre-modeling / pre-integration flow-graph verification test. The user segment had two differences from the verification test: the flight antenna and attenuators. The RF-7800 radio was attached to the Nagoya NA-701 Multi-Band antenna instead of a standard-issue antenna, which had since been determined to be poorly suited for RDCS (see Section III.C.2). The second difference was the incorporation of attenuators, which were added to the transmit radio to reduce the signal strength received by the uplink circuitry of RDCS.

b. Test Setup

In this test, the SDR was connected to the dipole uplink and downlink antennas, both amps, and the rPi, which were all mounted inside RDCS. The rPi was controlled by a laptop via Wi-Fi to facilitate setting changes within the GNU Radio flow graph. The radios and SDR were programmed to relay from 144.6 MHz to 435.0 MHz, which were the selected frequencies from the frequency trade analysis. The transmit radio broadcasted a signal measuring 30 dBm, which attenuated through free-space loss before it was received and subsequently amplified by the LNA on RDCS. The amplified signal fed directly to the AD9364 transceiver chip in the SDR. This power of this amplified signal exceeded the chip's RF input power threshold of 2.5 dBm at distances less than 25 m [75]. Therefore, 50 dB of manual attenuators were added to the transmit radio to ensure the power of the received signal at the SDR did not exceed the limitation of the transceiver chip. A portion of the test setup is depicted in Figure 49.

Figure 49. Software Validation

c. Test Execution

The test was conducted by initially placing the user segment 5 m away from RDCS, which was operating the verified radio flow graph. Then, the transmit radio broadcasted a signal, which RDCS successfully relayed to the receive radio, completing the 5 m portion of the test.

For the second range, the user segment was moved to 25 m away and the transmit gain of RDCS was adjusted. In electrical systems, particularly amplifiers, if a setting is too close to the maximum setting, the processor can become saturated, which may result in distortion of a signal. Thus, a signal with the suitable signal strength may be unintelligible by the receiver due to the distortion as a result of saturation. Because the transmit limit of the AD9364 transceiver chip is a setting of 75 dB, the transmit gain of RDCS was set to 65 dB in GNU Radio to ensure the signal did not saturate the transceiver [75].

Finally, the receive gain in the source block of GNU Radio was incrementally increased until the signal was heard the loudest and clearest. This value was recorded and the test at a range of 25 m was considered complete.

The final distance for this user-segment test was 100 m. The user segment was located on the roof of Spanagel Hall at NPS, while RDCS was in the quad, as pictured in Figure 50. Since 100 m of separation is equivalent to 55 dB of attenuation, the attenuators were initially removed. Then, attenuators were incrementally added after each successful relay until all 50 dB of attenuators were used. Thus, the final transmission had 105 dB of attenuation, which simulated approximately 30 km of distance between the transmitter and RDCS.

Figure 50. Spanagel Roof Test. Adapted from [30].

During the first attempt, using no manual attenuators, the transmit gain remained at 65 dB and the receive gain was incrementally increased. As this gain increased above 10 dB, the received signal became very garbled and difficult to understand as the larger receive gain increased the energy of both the signal and surrounding noise floor. To reduce the noise, the squelch setting was increased to -60 dB. Then, the receive gain was again increased until the signal was repeatedly received loudly and clearly.

The second attempt at a transmission over 100 m was made with 40 dB of manual attenuation. The transmit gain was held at 65 dB and the receive gain was incrementally increased. Again, the noise began to overpower the signal, but this time at a setting of approximately 50 dB of transmit gain. The squelch setting was lowered, this time to -55

dB, to reduce the ambient noise; the receive gain was then raised to 57 dB, at which point the transmission was repeatedly considered "loud and clear" by the researcher.

The final transmission from 100 m included all 50 dB of manual attenuators. The attenuators and free-space path loss over 100 m account for approximately 106 dB loss, or approximately 30 km of simulated distance between transmitter and RDCS. The transmit gain remained at 65 dB. Next, the receive gain was incrementally increased up to the limit of 65 dB, but the signal was never received by RDCS or the receive radio, despite multiple attempts. The transmit and receive gain settings were both increased to their maximum settings of 75 dB, risking saturation, but the relay remained unsuccessful. The unsuccessful attempt completed the testing portion of this radio software validation test.

d. Post-Test Analysis

The focus of post-test analysis was the relay failure at a range of 100 m. A link budget for the failed attempt is summarized in Table 26.

Table 26. Failure Link Budget at 100 Meters Summary

Term	Value	Notes
Transmitter Power (P_t)	30 dBm	Given in RF-7800H-MP data sheet
Transmitter Gain (G_t)	2.15 dBi	Given in NA-701 data sheet
Transmitter Losses (L_t)	1 dB	Estimated by researcher
Receiver Gain (G_r)	0 dBi	Estimated by researcher
Receiver Losses (L_r)	1 dB	Estimated by researcher
Miscellaneous Losses (L_m)	2 dB	Estimated by researcher
Manual Attenuation	50 dB	Attached to transmit radio
Free-Space Loss (L_{fs})	55.65 dB	Calculated using Equation 4
Total Path Loss	105.65	Manual Attenuation + L_{fs}
Initial Power Received	-77.50 dBm	Calculated using Equation 3
LNA	18 dBm	Given in ZX60-P103LN+ data sheet
New Power Received (P_r)	-79.50 dBm	Addition of P_r and LNA
Receiver Threshold	-95.00 dBm	Estimated from B205-Mini data sheet
New Receive Margin	25.50 dBm	Difference between P_r and receive threshold

Although the calculations indicated the transmission from 100 m with 50 dB of attenuation should have been successful, the researchers were not able to conduct a clear

relay at this range with attenuators despite multiple attempts. A critical assumption of the link budget of Table 26 is that all hardware is operating nominally, which became the focus of the analysis. The transmit power of the radio was confirmed to be 10 dBm, which was measured with a Tektronic MDO3014 Mixed Domain Oscilloscope. However, when the LNA was tested with the oscilloscope, although it was receiving electrical power, it had a signal output power of -90 dBm. The researchers concluded that the LNA had been damaged, most likely during the last relay attempt at 100 m, when the transmit gain value was increased to its maximum setting. The damaged LNA acted much like a wall, blocking virtually all signal energy across the RF spectrum.

e. Uplink Filter

The damage to the LNA explains why RDCS never relayed the final transmission attempt at 100 m. The transmitted energy from RDCS at 435.0 MHz should have been blocked by the Mini-Circuits SBLP-156+, which protects the LNA, and was previously identified as a potential issue in the initial downlink frequency analysis presented in Chapter III. However, the investigation process revealed a related critical characteristic of the uplink filter: the Mini-Circuits SBLP-156+ filter was not attenuating signals adequately at the transmit frequency of 435.0 MHz.

To investigate this issue further, the filter input was connected to an EXG Analog Signal Generator and the output was connected to the oscilloscope. Using this setup, the attenuation of signals at 435.0 MHz was measured as approximately 22.5 dB; this value is commensurate with the filter data sheet. However, a link budget calculation relating the power of the RDCS transmit signal and the power received by the uplink circuity, summarized in Table 27, revealed that this level of attenuation did not reduce the signal power below the LNA's maximum RF input peak power rating of 21 dBm [55]. The researchers concluded this peak power rating was exceeded during the multiple failed attempts to complete the final transmit test at 100 m with 50 dB of manual attenuation, resulting in hardware failure.

Table 27. Effects of Transmitter on Filter and LNA

Term	Value	Notes
SDR Output Signal Power	30 dBm	B205-Mini Max Power
Wideband Amp	16 dBm	Given by ZX60-V82+ data sheet
Free Space Loss (L_{fs})	0 dB	Proximity of transmit and receive antennas
Transmit Signal Power (P_t)	46 dBm	Transmitter Power + Amp + L_{fs}
Filter Attenuation	-22.5 dBm	Measured on oscilloscope
LNA Input Power	23.5 dBm	Addition of P_t + Filter
LNA Peak Power Limit	21 dBm	Given in ZX60-P103LN+ data sheet
LNA Receive Margin	-2.5 dBm	Difference between LNA input and limit

The solution to this filter issue was to select a filter that attenuated a minimum 25 dBm at 435.0 MHz (arguably, 35 dBm would have been preferred to provide margin). The Mini-Circuits SLP-200 was immediately available to the researcher and had a measured attenuation of 64 dBm at 435.0 MHz, which was confirmed by its data sheet [76]. Furthermore, the new filter was the same shape and nearly identical in mass to the original filter, so its incorporation required no design revisions. The SLP-200 filter therefore replaced the SBLP-156+ filter as the uplink filter for RDCS. The filter replacement was made, and the link budget analysis was completed again, using the signal generator and oscilloscope, to confirm the new filter's performance in the complete RF chain. This completed the first validation test and set conditions for the second radio software validation test.

3. Radio Software Validation #2

The change in the uplink filter required a second radio software validation test to determine the optimal settings of the various blocks within the radio flow graph. Additionally, after the first radio software test, the maximum altitude of the demonstration rocket shifted to approximately 9.1 km (30,000 ft) [32]. Since RDCS was designed to operate significantly higher, the shift did not negatively impact the design; RDCS was just overpowered for this distance. However, the slant range and free-space path loss associated with this new altitude change were chosen as the design parameters to develop flow-graph settings configured for the new estimated flight altitude. Using Equation 2 and Equation 4, the new signal path and free-space path loss were calculated to be approximately 52.6 km

(32.7 miles) and 110 dB, respectively. The test consisted of two stages: laboratory and field environments. The laboratory environment used attenuators to simulate 110 dB of free-space path loss for radio flow-graph validation, and the field portion consisted of an actual over-the-air relay at a distance of approximately 3 km. While conducting the laboratory portion of this test, the researchers learned that the gains listed for blocks in GNU Radio are not absolute, but instead represent some amount relative to the SDR capabilities and are established by the GNU Radio software. This means the gains cannot be simply added and subtracted across the different blocks in a manner similar to the link budget calculation; they must be determined experimentally.

a. Laboratory Environment

The laboratory environment used attenuators to configure the uplink and downlink of the flow graph. This process started with examining the sink block of the flow graph, then the source block, and finally the blocks in between. All over-the-air testing occurred at a distance of one meter, which equates to approximately 16 dBm of free-space path loss, and varying amounts of attenuation were used during the configuration process. This process systematically examined the performance capabilities of each block using the new deployment altitude parameters as standards to complete the validation.

(1) Sink Block

The primary objective of configuring the sink block was to determine an appropriate maximum gain setting that did not result in processor saturation. In radio software validation test #1, 65 dB was used as the sink block gain setting by the researchers. However, this limit was artificially imposed by the researchers to ensure the AD9364 did not become saturated. The objective of this portion of the test was to determine the SDR's true point of saturation. The filter, squelch, and AGC were disabled to focus the analysis on the sink block.

To determine the actual point of saturation, the receive portion of the SDR was connected to the signal generator and the transmit port was connect to the oscilloscope. Next, with a fixed input signal strength, the gain setting of the sink block was incrementally increased and monitored by the researchers. The oscilloscope provided a visual indication

of saturation. Before reaching saturation, the SDR produced a signal centered on the transmit frequency of 435.0 MHz with modulation spanning approximately 5–10 kHz. However, at the point of saturation, the SDR was visually observed to modulate frequencies to a significantly higher amplitude with a bandwidth spanning over 100 MHz. The large amplitude and excessive bandwidth of the signal produced by the saturated SDR effectively eliminated the FM data of the transmission.

Having identified the point of saturation, the highest gain setting of the sink block that did not result in a saturated SDR was determined to be 72 dB. To confirm this number, a test relay using flight hardware and RF chain was conducted in the laboratory. First, the transmit radio was configured with 50 dB of attenuators to protect the AD9364, as in radio software validation test #1. The 16 dB of free-space path loss plus the 50 dB of manual attenuation resulted in a transmit attenuation of 66 dB, which is equivalent to approximately 50 meters of free-space path loss. This simulated range of 50 meters and results from radio validation test #1 were interpolated to derive a gain setting of 20 dB for the receive block. Finally, the receive radio was configured with 110 dB of attenuators to simulate the signal path distance appropriate for the new rocket altitude. The configuration for this test is summarized in Table 28. The result of this test was a successful relay, confirming 72 dB as an appropriate gain setting for the sink block in the GNU Radio flow graph for the payload.

Table 28. Sink Block Configuration Test Settings

Transmit Power (dBm)	**Manual Attenuation** (dB)	**Free-Space Path Loss** (dB)	**Source Gain** (dB)	**Sink Gain** (dB)	**Receive Attenuation** (dB)
30	50	16	20	72	110

(2) Source Block

After the sink block was configured, the next step was to determine the settings for the source block. For this test, the signal received by the SDR was monitored in GNU

Radio to determine the highest gain setting of the sink block that did not result in saturation of the SDR.

First, the transmit radio was configured with 110 dB of attenuators to simulate the new free-space path loss, as depicted in Figure 51. Then, the transmit radio broadcasted a signal, which was monitored in GNU Radio. Next, the receive gain was gradually increased to a value which was just below the point of saturation, 30 dB. These settings are summarized in Table 29. Determining this appropriate gain value completed the source block portion of radio software validation test #2.

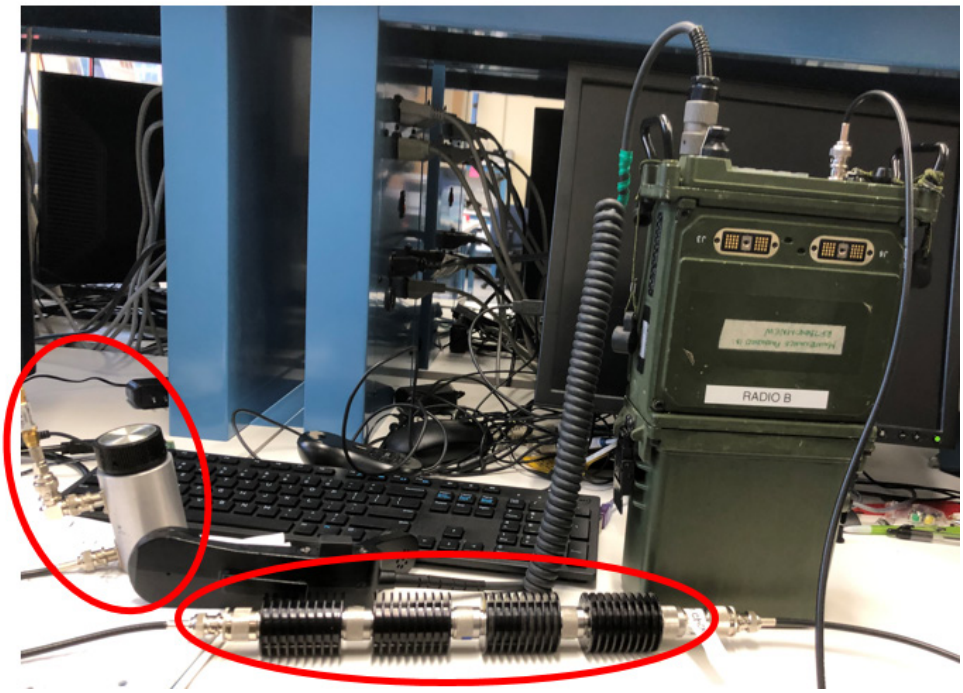

Figure 51. Uplink Attenuators

Table 29. Source Block Configuration Test Settings

Transmit Power (dBm)	**Manual Attenuation** (dB)	**Free-Space Path Loss** (dB)	**Source Gain** (dB)
30	110	16	30

(3) AGC Block

The source and sink gain settings were then used to determine the most suitable value for the AGC. For this portion of the test, the transmit and receive radios were each configured with 110 dB of manual attenuation. The squelch block was disabled to reduce complexity. The LPF was enabled and set to 1 dB, as the gain block for the LPF had no effect on the signal unless it was set to zero, in which case it eliminated the signal energy entirely.

The test consisted of the transmit radio broadcasting a signal, which was received by RDCS, monitored visually in GNU Radio for signs of saturation in the form of over-modulation, and then relayed to the other radio. This radio was being monitored by another researcher to audibly determine if the relayed signal was "loud and clear." Table 30 is a summary of the test configuration, variations of gain values for the AGC, and the results as judged auditorily by one researcher. The AGC gain settings of 1 and 0.5 both resulted in over-modulation, indicating the processor capabilities of the SDR had been exceeded. The AGC setting of 0.2 did produce an audible transmission at the receive radio, but there was considerable static in the transmission. However, the AGC setting of 0.24 resulted in a loud and clear relayed signal from RDCS.

Table 30. AGC Configuration Test Summary

Transmit Power (dBm)	**Transmit & Receive Manual Attenuation** (dB)	**Transmit & Receive Free-Space Path Loss**	**Source Gain** (dB)	**AGC Gain** (dB)	**Sink Gain** (dB)
30	110	16	30	1	72
30	110	16	30	0.5	72
30	110	16	30	0.2	72
30	110	16	30	0.24	72

(4) Squelch

The final step of the laboratory portion of software validation test #2 was to configure the squelch block. Using the settings highlighted in green in Table 30, the

squelch gain was enabled and gradually increased from -75 dB until all ambient static noise was eliminated from the relayed transmission, which occurred at -45 dB. This step concluded the laboratory portion of radio software validation test #2.

In summary, the gain settings for the radio software required validation through this second test. The test used free-space path loss associated with the distances applicable to the new rocket altitude as standards for configuration. First, the sink block was configured, followed by the source block; each were set to values just below the level that resulted in observed saturation. Next, the AGC was configured, and finally, the squelch value was determined, completing the laboratory portion of the test.

b. Field Environment

The second stage of the radio validation test #2 was the field environment. The goal of this field experiment was to test the radio relay function of RDCS using the flight version of the software. In this test, the researcher relocated the user segment to Jack's Peak, while RDCS remained stationed on the roof of Spanagel Hall. Jack's Peak is a prominent terrain feature in the vicinity of NPS, and Spanagel Hall is one of the tallest buildings on the NPS campus. From Jack's Peak, a user has a clear LOS to Spanagel Hall, circled in red in Figure 52, approximately 3.2 km away.

Jack's Peak Overview (left) and Jack's Peak LOS View (right).

Figure 52. Radio Software Validation from Jack's Peak. Adapted from [30].

First, the settings determined in the laboratory phase of test were incorporated into a single GNU Radio flow graph and compiled into a Python 2.7 script. This script was imbedded in the payload startup sequence, which already had the payload camera script, making the payload software for this test the flight version for RDCS.

Next, RDCS was relocated to the roof of Spanagel Hall, connected to an external power supply, and powered on. When the C&DH subsystem completed its start-up sequence, it directed power to the payload rPi with the flight software, which automatically initiated the radio script. The startup sequence was approximately 2 minutes long, after which RDCS was prepared to conduct relay operations. A successful relay attempt was made on the roof with the same attenuators and software settings used in the laboratory portion of the test, which confirmed flight settings a final time. Then, one researcher relocated to Jack's Peak with the user segment, consisting of the RF-7800 radio with an NA-701 antenna, configured to transmit at 30 dBm. All attenuators were removed for this field test, which was the operational configuration of the user segment. From Jack's Peak, the researchers successfully conducted multiple relays over flight frequencies between the

two radios of the user segment. This test successfully demonstrated RDCS over-the-air at ranges beyond 100 m and completed radio software validation #2.

4. Functional Check

Once the payload software was complete, the final step needed to complete system-level functional testing was a functional check. The objective of this test was a comprehensive check-out of all systems, including the user segment, ground station, and RDCS, in their respective flight configurations. The goal was to mimic, as much as possible, the setup and operations that would be used in the demonstration flight. One deviation from the demonstration configuration was the use of attenuators for both the transmit and receive radios to simulate free-space path loss and protect uplink circuitry. This was the only artificiality of the functional check; however, given the success of radio software validation test #2, researchers were confident that the incorporation of attenuators would not negate the validity of the functional check. Appendix J contains the complete functional check procedures used for this test.

First, the user segment was set up exactly as it was for the laboratory testing of radio software validation test #2. The RF-7800 radios were configured with the NA-701 antenna, each with 110 dB of attenuators attached. Next, the ground segment was configured, with a laptop connected to an n920 to receive telemetry from the bus. Finally, RDCS was configured with its bus software, which had extensive flight history, and validated payload scripts. Additionally, this test included the recovery portions of the bus: both parachutes and the SPOT Trace. First, the Trace was enabled and enclosed in the bus, just as it would be on the demonstration day. Next, RDCS was powered on by the researcher. Within less than a minute, the ground station started receiving telemetry from the bus in the form of battery temperatures and voltages. After just over one minute of operation, power was delivered by the C&DH subsystem to the payload.

After approximately two minutes, the payload was operational. This was verified by two methods. The first method was to connect to the payload rPi via Wi-Fi and verify the Python scripts were running and had not crashed or restarted. The second method was to conduct a relay with the user segment. After approximately 3 minutes of initial power

application to the bus, both methods successfully verified that RDCS was conducting operations without human intervention. After approximately five minutes, GPS location data was received from the telemetry stream, and the Trace had successfully reported its location via the SPOT phone application. This successfully completed the active portion of the functional check.

The final step was to verify camera functionality. First, to preserve battery power, the radio script and Trace were disabled. Then, the researcher navigated to the storage folders on each rPi hard drive to observe the appropriate number of two-minute-long videos. Verifying camera functionality was the final step of the functional check.

The functional check successfully demonstrated the capability of RDCS to operate all systems in its flight configuration. The system operated under its own power, and each subsystem executed all required functions as they were designed. The payload, cameras, bus, and telemetry all performed nominally. This successful functional check confirmed that RDCS could perform its designed mission if given the opportunity to deploy.

C. ROCKET INTEGRATION TEST

For RDCS to function at altitude properly, it next needed to integrate with the launch vehicle. The first portion of rocket integration was a payload bay fit check, and the second was a deployment test. The fit check was a static test that verified whether RDCS would fit inside the volume constraints of the flight version of the payload bay. The deployment test consisted of ejecting RDCS from the payload bay using the same rocket mechanism that would be used during the flight demonstration. For each of these tests, a mass model of RDCS was used instead of the flight article. A mass model was used to preserve the life of the antenna radiating elements during both the fit check and deployment test as well as critical components inside RDCS during the deployment test. The model used all of the same polycarbonate pieces as RDCS and, with the addition of weights, was within 2% of the weight of the flight article. Both tests sought to confirm the compatibility of RDCS with the rocket.

1. Payload Bay Fit Check

The fit check consisted of placing RDCS inside the payload bay to ensure proper fit, as diagramed in Figure 53. The safety parachute, mounted to the nadir face of RDCS, was inserted into the aluminum transition piece and placed on top of the rocket parachute first. Next, RDCS was stacked on top of the parachutes. Then, the primary parachute was inserted into the fiberglass nose cone. Finally, the nose cone was lowered onto the aluminum transition, encapsulating RDCS inside the payload bay.

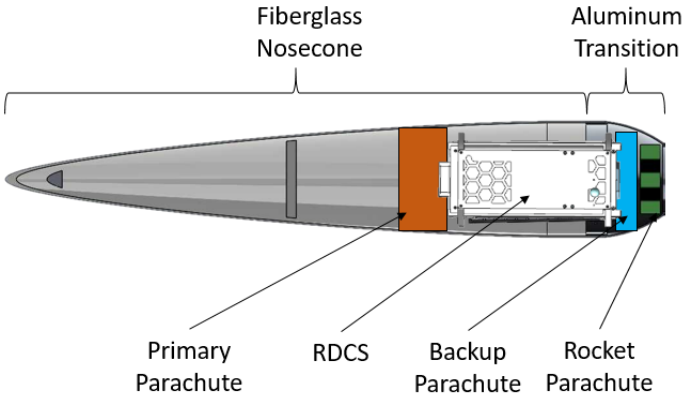

Figure 53. Payload Bay Integration. Adapted from [32].

The fit check required several attempts, as the spacers extended too far to fit inside the aluminum transition piece. However, after sanding, the spacers fit snugly inside the aluminum transition piece. A similar process of sanding was repeated for the spacers that fit inside the nose cone. Additionally, the spacers were lubricated with a synthetic silicon-based product to facilitate a snug fit while preventing the spacers from lodging inside the payload bay. Figure 54 is a picture of the fit check in progress. The side rails with these properly sized spacers were removed from the mass model at the conclusion of rocket integration testing and replaced the side rails of the flight model of RDCS.

Figure 54. Payload Bay Fit Check

After multiple attempts, the fit check of RDCS with the payload bay was complete. This configuration was used to complete the next test, the deployment test.

2. Deployment Test

The results of the fit check enabled the second rocket integration test, deployment. For this test, the mass model of RDCS was ejected from the payload bay of the rocket with the same mechanisms that would be used during flight.

The first step in this test was for the deployment mechanism of the rocket to be rigged and charged. This mechanism consisted of a 75-gram canister of CO_2, initiated by a black powder charge, both positioned below the rocket parachute. For the purposes of this test, the black powder was initiated on command; however, the flight version of the mechanism is initiated electronically by sensors inside the rocket. Next, the rocket parachute and rigging were placed inside the aluminum transition, followed by the RDCS mass model, which were stacked in the same manner described in the fit check. Also as in the fit check, silicone-based lubricant was applied the spacers to reduce the friction

between the spacers and rocket body. Finally, the nose cone was lowered on to the aluminum transition piece, which encapsulated the RDCS mass model, and was secured to the transition with nylon #4-40 shear pins. This entire system was positioned against a child's picnic bench and secured using rope.

On command, the black powder was ignited, which caused the CO_2 canisters to release their gas. The force of this expanding gas increased the pressure in the payload bay sufficiently to shear the pins between the transition and nose cone. Next, the pressure forced the rocket parachute and safety parachute forward like a plunger, ejecting the RDCS mass model. Figure 55, a frame from the deployment test video, depicts the mass model as it was ejected from the payload bay, the nose cone in flight, with the primary parachute cord still inside it. That cord is connected to the parachute mount of RDCS, which has already been ejected from the transition. The orange parachute is the RDCS safety parachute and the red parachute is the rocket parachute, both below the mass model. Additionally, the expanding CO_2 can be seen in Figure 55.

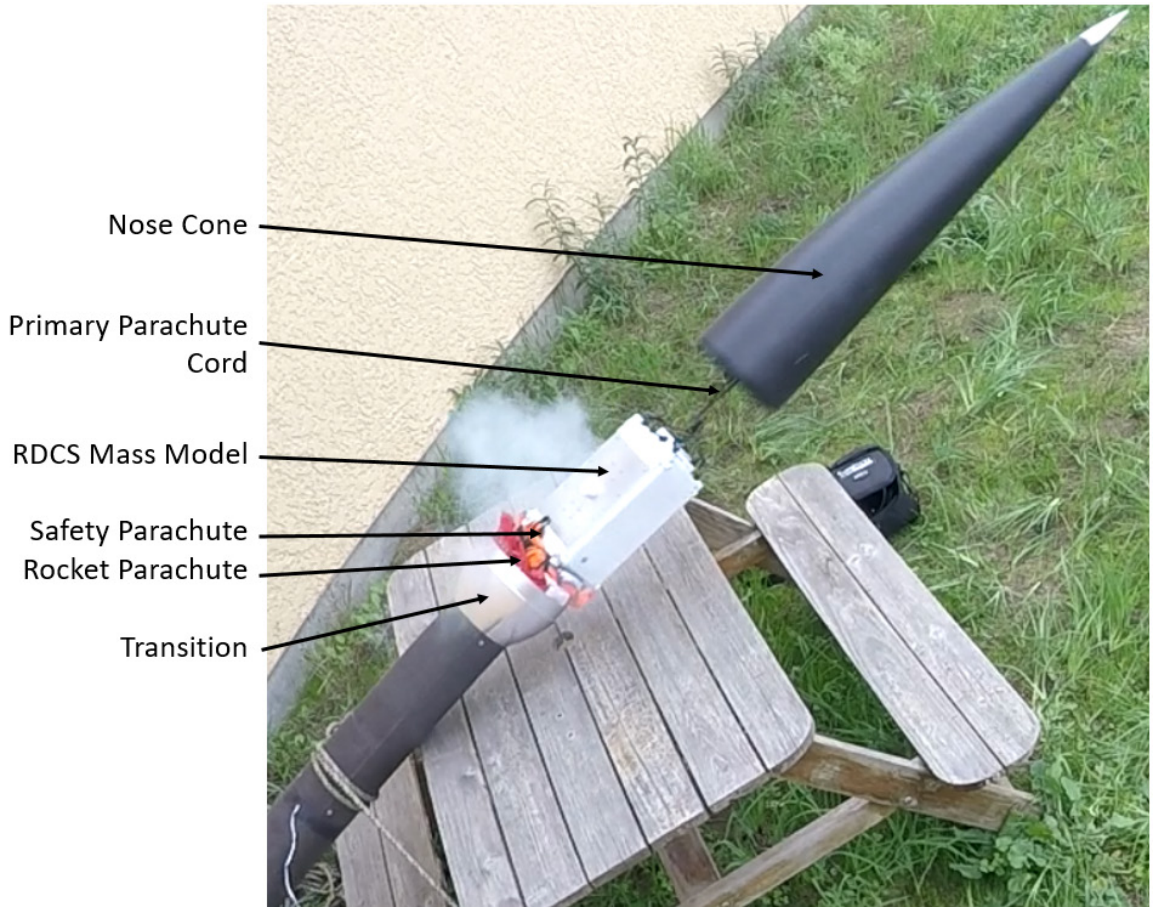

Figure 55. Deployment Test

To record forces associated with this event, a SENSR programmable accelerometer was mounted inside RDCS in place of the payload. This accelerometer, pictured in Figure 56, was mounted to a modified payload mount, which included a steel weight to ensure the weights of the mass model and flight payload mount were within 1% of each other.

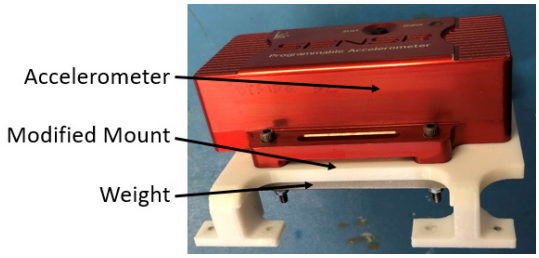

Figure 56. Mass Model Accelerometer

The sensor was programmed to initiate the event recorder mode when 1.2 Gs were exceeded for more than 0.1 seconds. When this threshold was exceeded, the sensor saved the previous one second of data and recorded for 10 seconds, making each event 11 seconds long. After each deployment test, the sensor was retrieved from inside RDCS and the data was reviewed. Figure 57 is a plot of the average, or mean, Gs experienced by RDCS as a function of time for one of the deployments. This plot depicts the first 0.16 seconds of the sequence over which the deployment occurred.

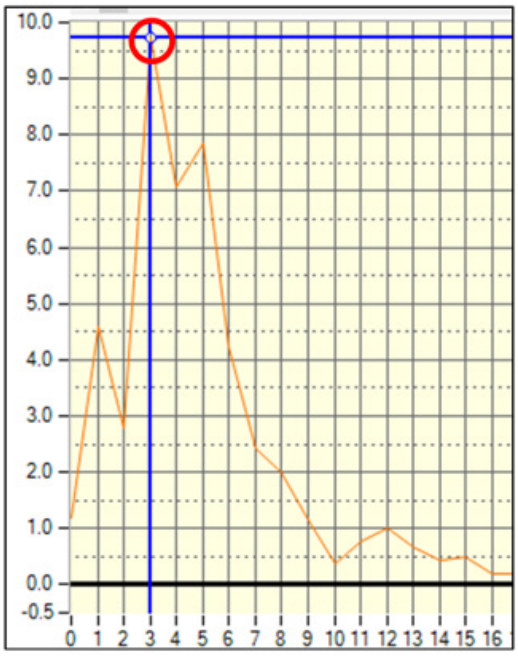

Figure 57. Payload Deployment Mean Gs vs. Time

The peak, at 9.71 Gs, represents the acceleration experienced by RDCS due to the initial force of the expanding CO_2 gas, which are the accelerations directly related to deployment design and sequence. The maximum acceleration, 9.71 Gs, is indicated by the horizontal blue line. This plot shows the onset of acceleration after 0.3 seconds which then decays over the following 0.9 seconds. At certain times during the sequence, the acceleration is less than 1.0 Gs. However, at no point does the acceleration ever become

negative. This plot and a post-deployment visual inspection were used to confirm the deployment sequence of RDCS.

Overall, five deployment tests were conducted, all of which were successful. The maximum acceleration experienced during testing was 9.71 Gs, and the entirety of forces directly related to the deployment design lasted no more than 0.2 seconds. This test series demonstrated that RDCS was compatible with the rocket deployment system and could successfully be ejected from the payload bay.

D. ENVIRONMENTAL TESTING

Upon a successful fit check and deployment testing, the final step of testing was to verify RDCS would survive the rigors of launch and high-altitude environments. High-altitude operations testing is typically conducted through the use of a thermal-vacuum chamber (TVAC) test. The launch environment verification was conducted through a vibration test in which RDCS was placed inside the rocket payload bay, which was attached to a shaker table to determine the response of RDCS. Each of these tests subjects vehicles to representative environments to ensure their designs are sufficient to operate effectively.

a. TVAC

In a TVAC test, the test article is subjected to a series of hot and cold temperatures in a near-vacuum environment for varying durations to determine the vehicle's response and performance in these conditions. The Small Sat Laboratory has extensive flight and test history with the HAB Bus, rPi's, the B205-Mini, and Mini-Circuit RF components (see Swintek [24] and Lovdahl [44]). In each case, these components performed as expected in the TVAC chamber. Neither of these projects had the thermal mitigation features, like foam, Katpon tape, and solid side panels, with which RDCS was equipped. However, the Winter 2019 SS4861 Payload Design class at NPS conducted a thermal test of an autonomously guided parafoil system also controlled by an rPi. The bus for this system included the modified battery compartment, solid side panels, and thermal-mitigation foam used for RDCS and similar to Figure 58. Using the "test by similarity" approach [77], the results of this test demonstrated that the bus design modifications for RDCS sufficiently

prevent heat loss [78]. Given the flight and test history, thermal mitigation measures, and the compressed development timeline, TVAC was not performed on RDCS.

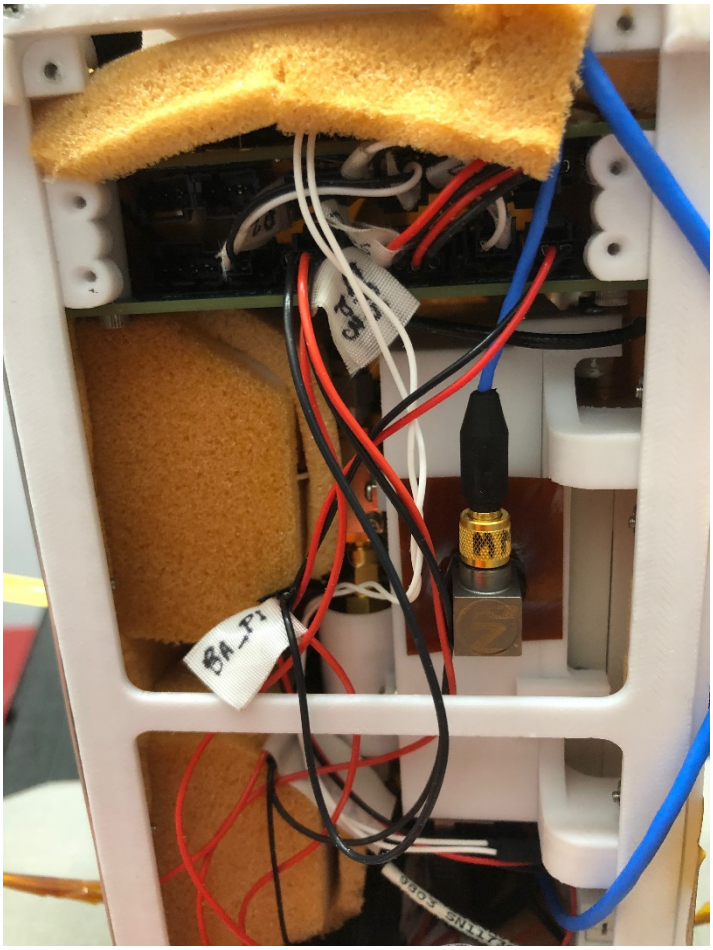

Figure 58. RDCS Thermal Foam.

b. Vibration Testing

Vibration testing was used to gain confidence that RDCS could survive the maximum predicted environment (MPE) and qualify the system for flight. This test used the flight article as the test article, a type of testing known as protoflight, which had inherent risks as there was only one functional RDCS. Due to scheduling concerns, constructing a new system, in the event the functional system was damaged during vibration testing, was considered prohibitive.

(1) Predicted Launch Environment

The first step of the vibration test was to determine the MPE. Traditionally, launch vehicles have a payload user's guide that lists detailed vibration profiles for a particular launch vehicle that give specific standards that payloads must achieve to fly on a particular vehicle. However, since the NPS rocket had never flown, there were no standards related to this particular launch vehicle against which to test RDCS. Instead, the researchers identified the NASA Sounding Rocket User Handbook [79] as a suitable source for vibrations standards based on the Improved Orion Launch Vehicle, a NASA sounding rocket, which has a similar rating to the NPS rocket. The Improved Orion Launch Vehicle is spin-stabilized and unguided. It produces approximately 20,000 pound-force (lbf) of thrust for the first six seconds and then approximately 4,000 lbf for the remaining 19 seconds until burnout at 25 seconds [79].

This profile has significantly higher thrust values than that of the NPS rocket, which produces 1,100 lbf for six seconds, after which the motor burns out [32]. Testing to the higher forces created by the Improved Orion Launch Vehicle provides margin for the growth of the RDCS program and qualifies RDCS for the NPS rocket. The Improved Orion Launch Vehicle standards include a sine sweep and random vibration test; in this case, the sine test requirements are not for the typical sine survey performed at a low level (0.25 – 0.50 g's) as a standard aerospace industry practice for determining the test article's fundamental frequencies. The sine sweep test was not applied to RDCS because sine sweep standards are based on a natural frequency particular to a rocket design. Since the NPS rocket's natural frequency was not known, the utility of conducting the sine sweep was weighed against the protoflight nature of the test and found to be unacceptable. However, the random vibration specifications were used for RDCS, and are listed in Table 31.

The parameters are categorized by axis as two separate standards: thrust and lateral. The total force applied to the test article, known as G_{rms}, is the root-mean-square acceleration as referenced to the force of gravity at the surface of the earth, or one G. The acceleration spectral density (ASD) is a measure of the mean-squared acceleration applied

as a function of frequency and measured in squared-Gs per Hertz $\left(\frac{g^2}{Hz}\right)$. These standards were used to develop the test profiles for use during the random vibration test.

Table 31. Random Vibration Standards. Adapted from [79].

Axis	**G_{rms}**	**ASD** (20-2000 Hz) $\left(\frac{g^2}{Hz}\right)$
Thrust	10.0	0.051
Lateral	7.60	0.029

(2) Test Setup

The goal of the test setup was to mimic the launch environment to the maximum extent possible while facilitating research. To mimic the launch environment, the test setup included the flight units used for the deployment test: transition, nose cone, and both parachutes. RDCS was inserted into the transition with its parachutes, just as in the deployment test. The nose cone encapsulated the payload bay with RDCS in it and was secured to the transition with #4-40 nylon shear pins. This entire assembly was attached to an aluminum adapter that was specifically designed to fit the bottom of the transition and was mounted vertically on the shaker table as depicted in Figure 59.

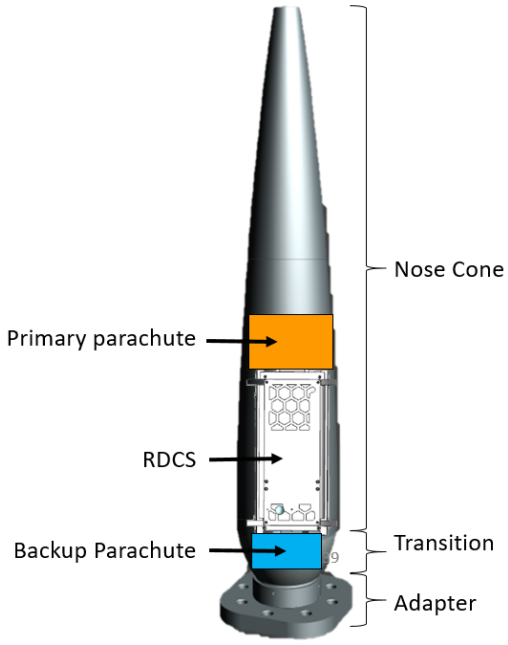

Figure 59. Vibration Test Setup

Accelerometers were placed on four locations of RDCS to collect vibration response of the vehicle. One was placed on top of the parachute mount next to the GPS cover and labeled as "zenith." The next two were placed on either side of the payload cover internal to RDCS, one on the +y side and the other on the –y side, and labeled as "payload +y" and "payload "-y." The last sensor was placed on the inside face of the payload antenna plate and labeled "nadir." Two additional accelerometers, control 1 and control 2, mounted in the base of the adapter plate, were used to ensure the force applied by the table was correctly imparted to the test assembly. Figure 60 is a depiction of the accelerometer placement for the test, and Figure 61 is a picture of some of the accelerometers used during the actual vibration test. The wires for each sensor were routed down through the transition into a channel under the adapter as depicted in Figure 62. The test article was vibrated three separate times, once for each axis. In between each axis, a functional check was performed to verify RDCS operations. The test flow is summarized in Figure 63.

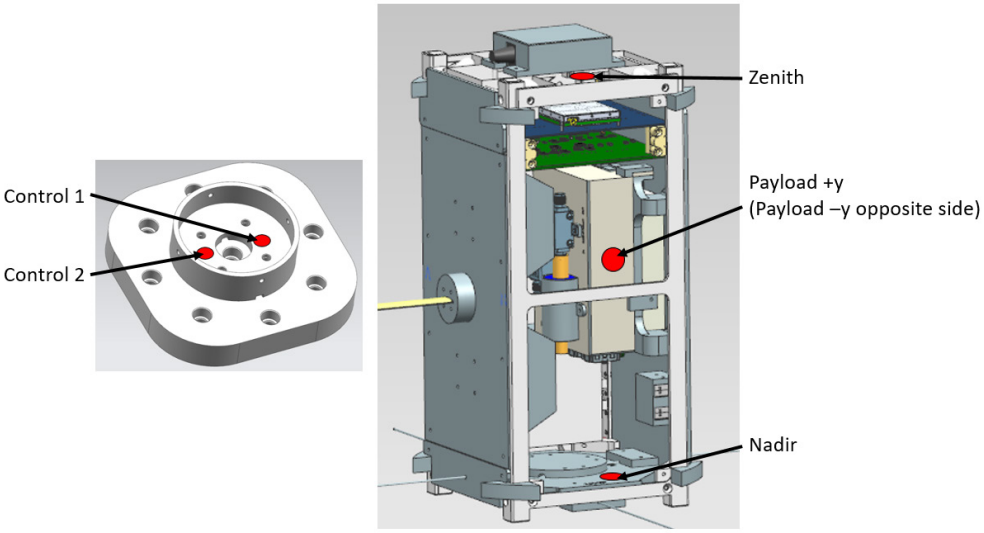

Adapter Plate (left) and RDCS (right)

Figure 60. Accelerometer Placement

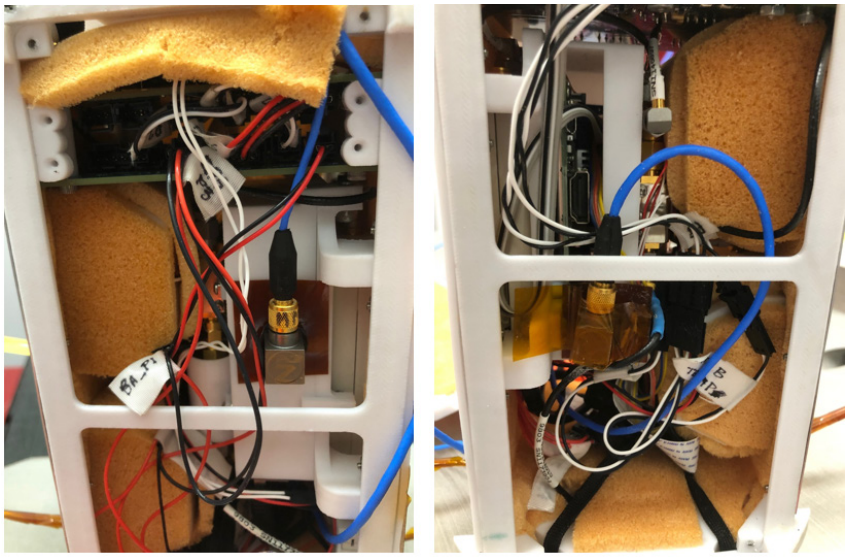

Payload +y (left) and Payload -y (right)

Figure 61. Vibration Accelerometers

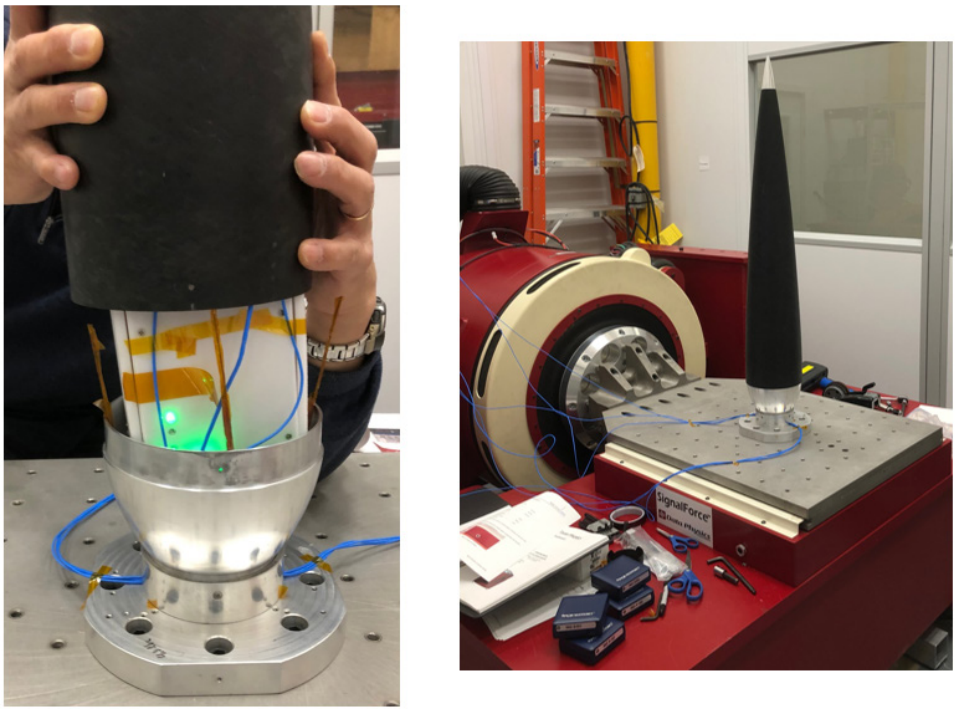

Payload Encapsulation (left) and Lateral Axis Setup (right)

Figure 62. Random Vibration Test Setup

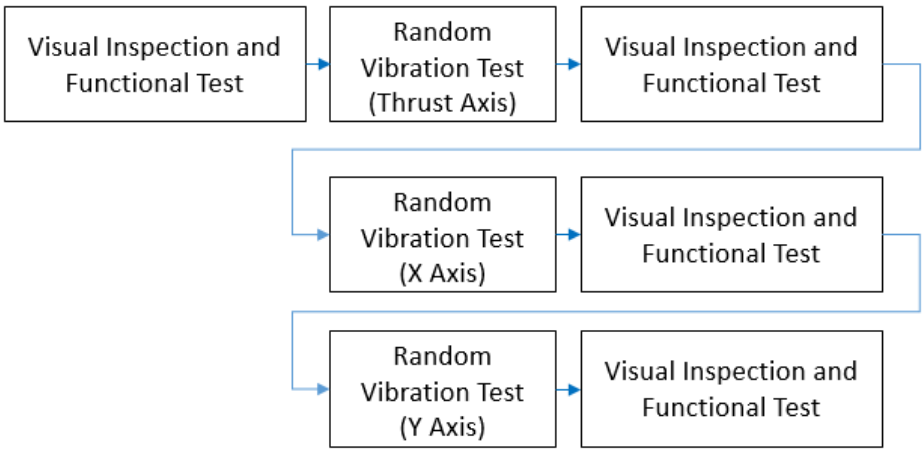

Figure 63. Random Vibration Test Flow.

(3) Results

Figure 64, Figure 65, and Figure 66 are the random vibration plots for the thrust, x, and y axis, respectively. The line labeled “NASA” in each plot is a visual depiction of the

standards which were applied to RDCS, and is the reference input for each random vibration test. The “Control” line represents the input provided by the shaker table to the test assembly, which should and does closely follow the NASA reference line. The code used for all vibration calculations is contained in Appendix I.

The industry standard for vibration testing is to conduct the most stressing case first, which for RDCS is the thrust axis. The thrust axis response is plotted in Figure 64. Each of the four payload accelerometers are independently represented in the plot. The first significant response is in the vicinity of 30 Hz, after which the response is less than the reference input.

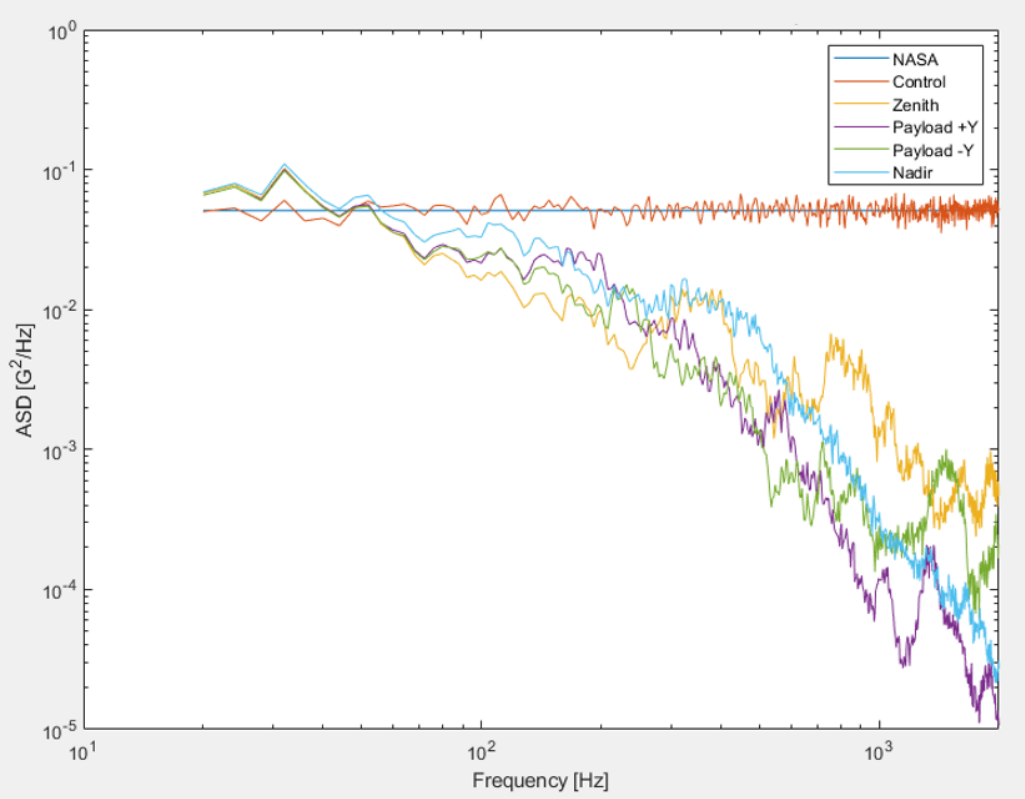

Figure 64. Thrust Axis Standards, Control, and Response Plot

The x-axis was tested second; the response is plotted in Figure 65. For this axis, the control line indicates that the ASD applied to the test assembly was the higher thrust-axis standard instead of the lower lateral-axis standard, which was attributed to operator error

during post-test analysis. Because RDCS successfully passed the x-axis random vibration test functions check at the higher thrust-axis standards, the researchers determined that a re-test of this axis was not necessary. In this test, the payload +y exhibited the most significant response between 50–110 Hz. After this peak, the overall trend was similar to the thrust axis response, particularly at the higher vibrations.

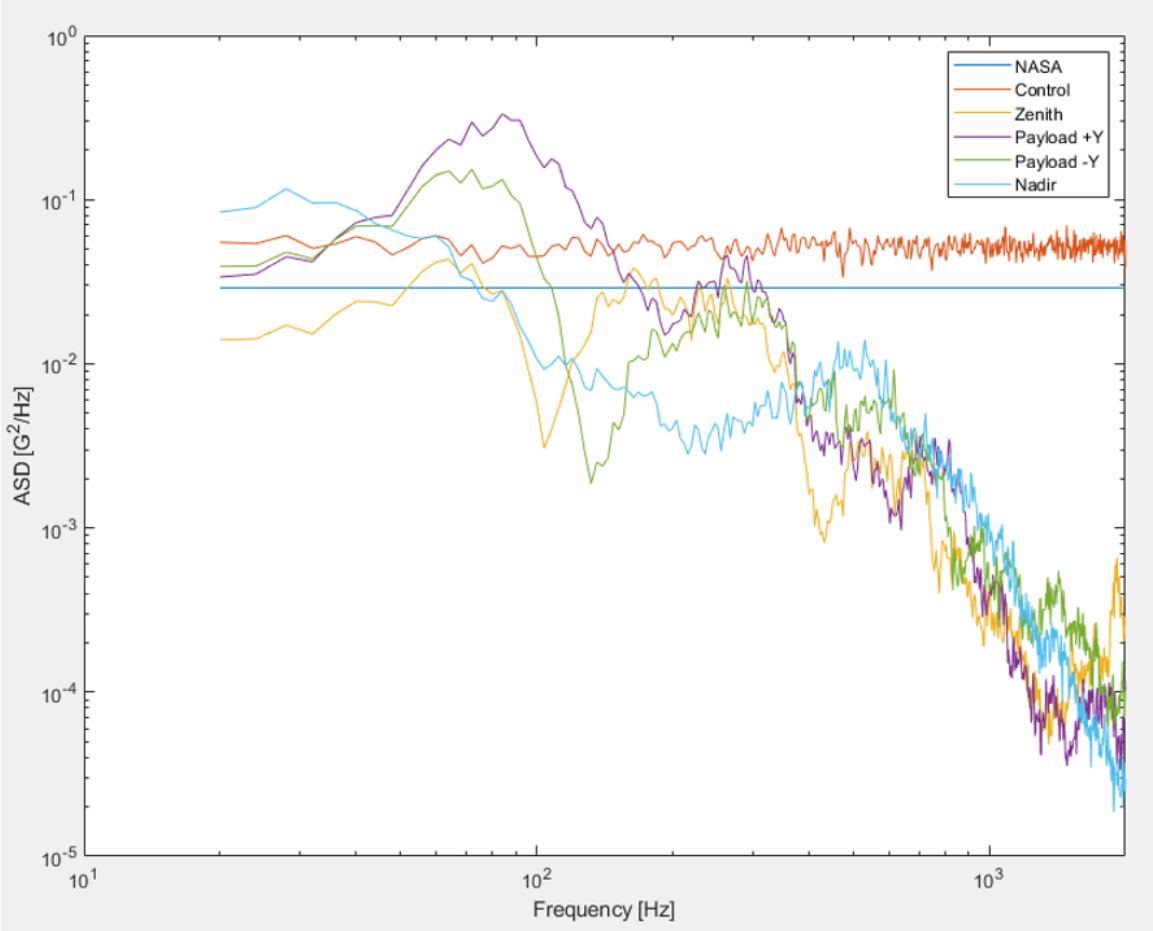

Figure 65. X-Axis Standards, Control, and Response Plot

The final axis tested was the y-axis, presented in Figure 66. In this case, the standards and control line are similar. The response of both payload sensors was similar to the response of payload +y from the x-axis over a similar frequency range. Much like the x-axis response, the higher frequency vibrations were damped for each sensor.

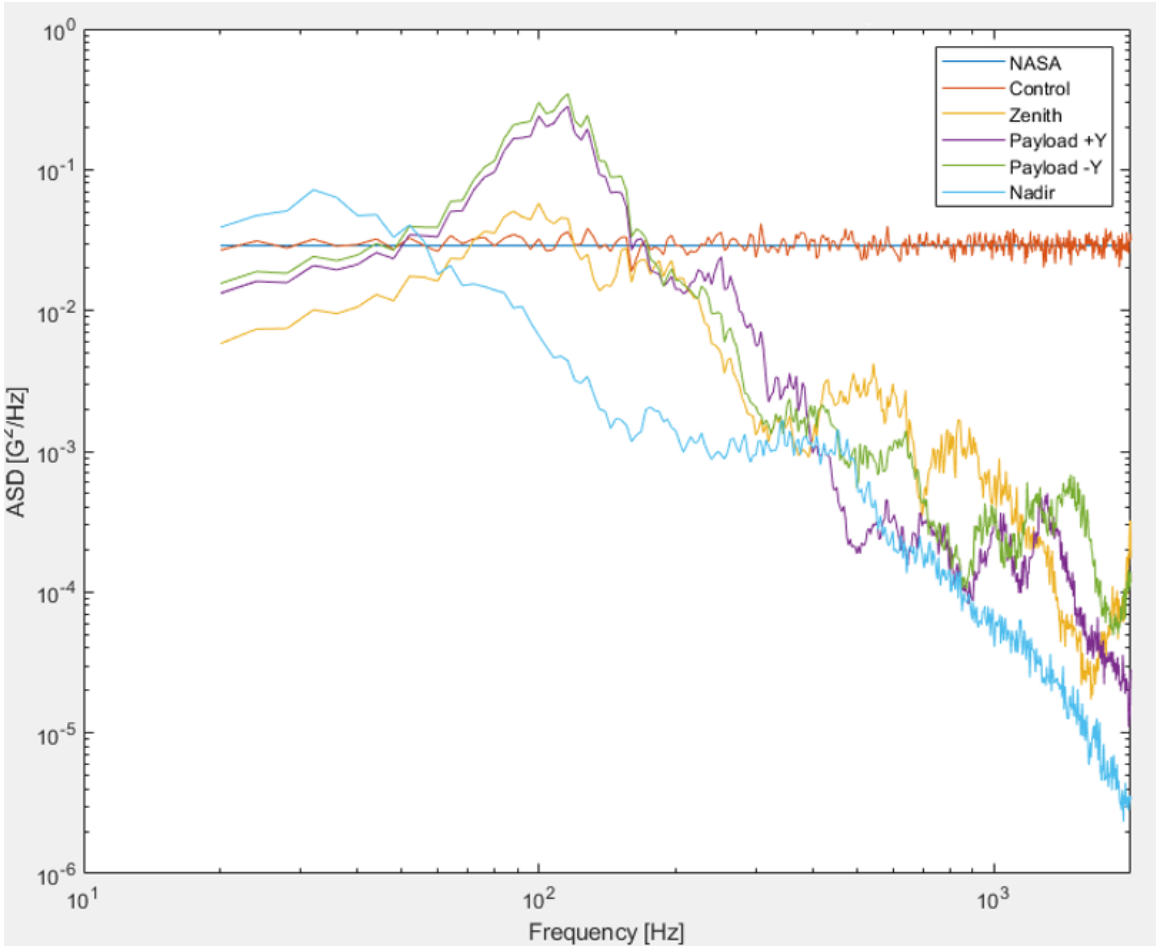

Figure 66. Y-Axis Standard, Control, and Response

The RDCS response accelerations varied depending on accelerometer placement. The measured accelerations by each accelerometer for each axis are summarized in Table 32. Control sensors were within 0.1 of the NASA Standards for each axis. The highest response was the payload +y sensor during the x-axis vibration test at 5.1 G_{rms} and the lowest response was from the nadir accelerometer during the y-axis test at 1.8 G_{rms}. In no case did the sensors experience accelerations greater than the control channel.

Table 32. Random Vibration Response

Axis	Control (G_{rms})	Zenith (G_{rms})	Payload +y (G_{rms})	Payload –y (G_{rms})	Nadir (G_{rms})
Thrust	10.1	3.0	2.8	2.7	3.3
X-Axis	10.1	2.9	5.1	3.8	3.0
Y-Axis	7.6	2.5	4.2	4.5	1.8

The amplification factor is measured in dB and given by Equation 15. $G_{response}$ represents the G_{rms} of a particular accelerometer and $G_{control}$ represents the G_{rms} of the control for the associated axis. The amplification factors for each accelerometer are given in Table 33.

$$dB = 10 * \log\left(\frac{G_{response}^2}{G_{control}^2}\right) \tag{15}$$

Table 33. Amplification Factors

Axis	Zenith (dB)	Payload +y (dB)	Payload –y (dB)	Nadir (dB)
Thrust	-24.14	-25.65	-26.53	-22.23
X-Axis	-24.98	-13.57	-19.79	-24.21
Y-Axis	-22.12	-12.20	-10.52	-29.44

The highest amplification factor was the payload –y sensor for the y-axis at -10.52 dB, and the lowest amplification factor was the nadir sensor for the y-axis at -29.44 dB. The negative numbers reveal that the response was lower than the control and that the vibrations applied to RDCS were dampened. The researchers believe the parachutes dampened RDCS during the vibration test, particularly at higher frequencies, as indicated by the low numbers associated with the zenith and nadir accelerometers, which were cushioned by parachutes. Since the test setup closely aligned with the flight configuration, the researchers believe the dampening phenomena observed during random vibration is flight representative.

(4) Conclusions

The objective of the vibration test was to determine if RDCS would withstand the MPE and qualify RDCS for flight. Since the NPS rocket MPE was not known, the test standards of a NASA sounding rocket of comparable size were used as a proxy. All three axes were tested with successful functional checks in between. The parachutes dampened much of the input accelerations created by the predicted launch environment, with no G_{rms} for any sensor exceeding the control. This successful evolution concluded the testing phase of RDCS.

E. FINAL SOFTWARE AND HARDWARE CONFIGURATION

The testing phase validated the RDCS software through two validation tests and the hardware through power, rocket integration, and vibration tests. Minor modifications were made to both software and hardware during this effort to develop a functional system certified for flight on the NPS rocket. Once the successful tests were complete, the software and hardware versions were solidified to ensure the flight-worthy configurations were identified, documented, and installed in preparation for the demonstration flight. The hardware, including bus structure, mounts, and panels had minimal changes after the bus and hardware integration phase, aside from sanding the spacers to ensure proper fit with the rocket payload bay.

The RDCS software consisted of two sections, bus and payload. The bus software consisted exclusively of Python 2.7 coding with minimal modifications to the Small Sat Lab HAB Bus software and is contained in Appendix G [57]. Those changes were primarily to the bus camera Python function, which prescribes the video clip length, frame rate, and resolution for the upward-facing bus camera.

The payload software consisted of the startup, camera, and radio scripts and is also contained in Appendix G. The startup script calls the camera and radio functions during the rPi startup sequence. Similar to the bus camera software, the payload camera script configures the camera for operations. The final radio script is contained in Appendix G, and the GNU Radio flow graph is contained in Appendix H, with gain settings summarized in Table 34.

Table 34. Final GNU Radio Flow-Graph Gain Settings

Source (dB)	**LPF** (dB)	**AGC** (dB)	**Squelch** (dB)	**Sink** (dB)
30	1	0.24	-45	72

V. RDCS DEMONSTRATION

The culmination of this research was an attempted flight demonstration of RDCS. Detailed pre-flight planning and coordination provided the opportunity to demonstrate RDCS from a target deployment altitude of 9.1 km (30,000 ft). Despite these efforts, the demonstration flight was unsuccessful due to catastrophic failure of the rocket shortly after take-off. Although RDCS was not demonstrated at altitude, this section discusses the planning and results from the attempt.

A. CONOPS

The Small Sat Lab has a standing relationship with the owners of a launch site near Mojave, California. This site, depicted in Figure 67, was required due to federal regulations regarding amateur rocket launches to altitudes like 9.1 km.

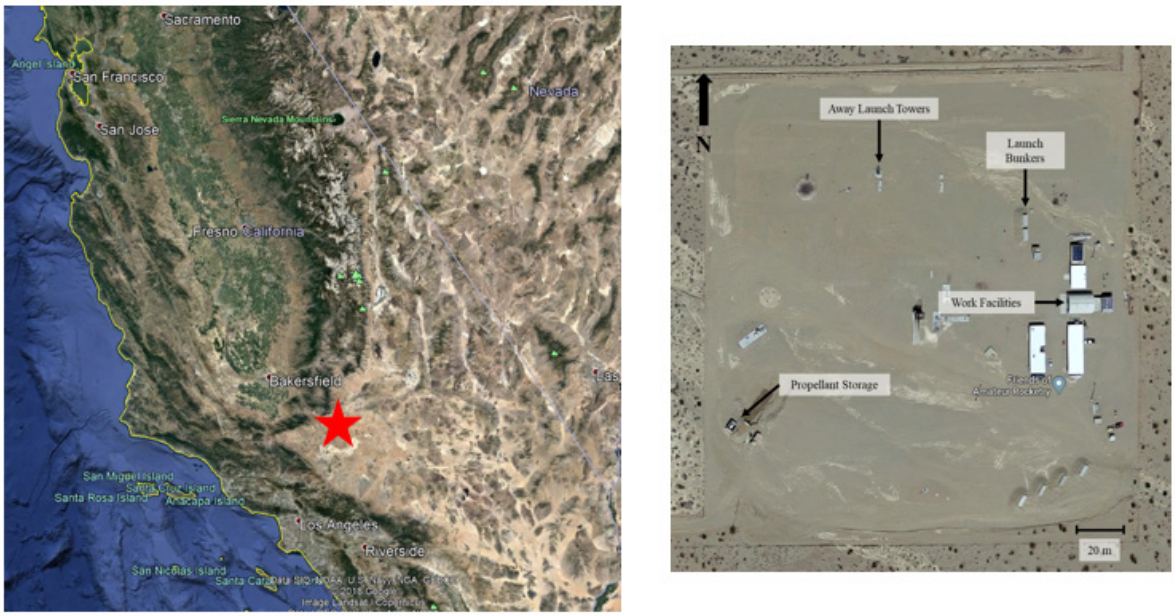

Launch Location Near Mojave, CA (left) and Launch Site (right).

Figure 67. Launch Site. Adapted from [30], [80].

The rocket was expected to travel to 9.1 km in 39 seconds and deploy RDCS. RDCS would be ejected, much as in the deployment test, and descend under parachute back to the surface of the earth. For more details regarding the launch site and rocket flight plan, see Pierce's thesis [32]. Although not designed to require recovery, the intent of the demonstration flight was to recover RDCS, if at all possible, to facilitate academic research. Using an online tool called habhub, the RDCS descent profile and location was predicted and is contained in Figure 68.

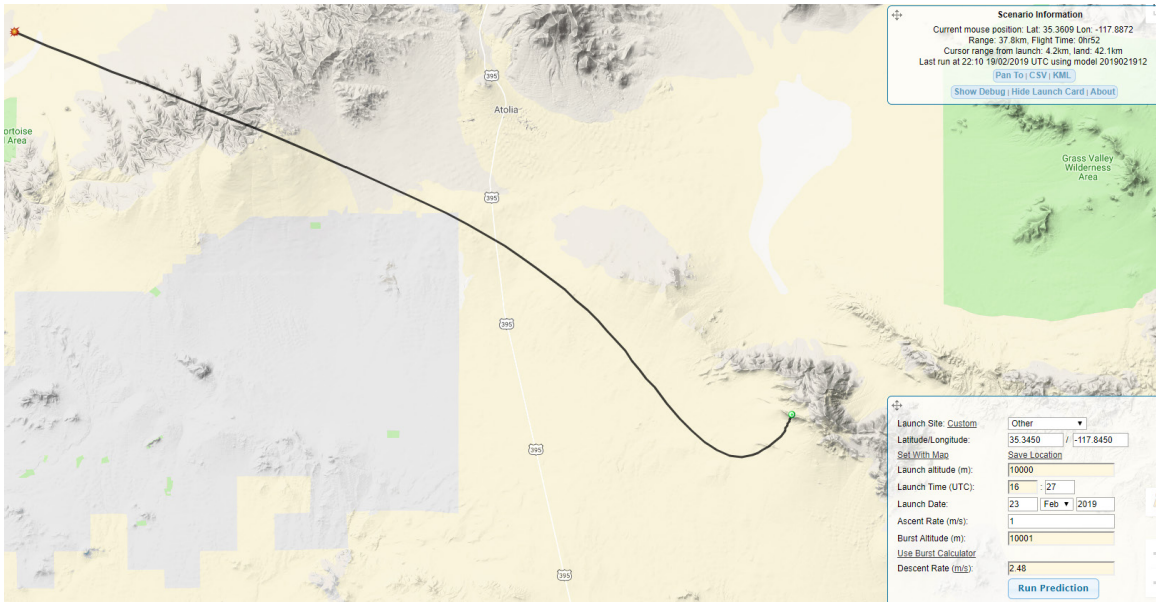

Figure 68. RDCS Descent Prediction. Adapted from [81].

Overall, the descent was expected to take approximately 52 minutes and cover 37.8 km over the ground. During the descent phase, RDCS operations would be demonstrated with the same user segment used during the functional test, without attenuators. RDCS would be tracked in flight using the GPS provided by telemetry to the ground station and the onboard SPOT Trace tracking sensor. This CONOPS is presented in Figure 69. Once RDCS impacted the ground and a location was known, a recovery team would be dispatched to recover the flight article for post-flight analysis. The combined pre-flight checklist for the rocket and RDCS is contained in Appendix K.

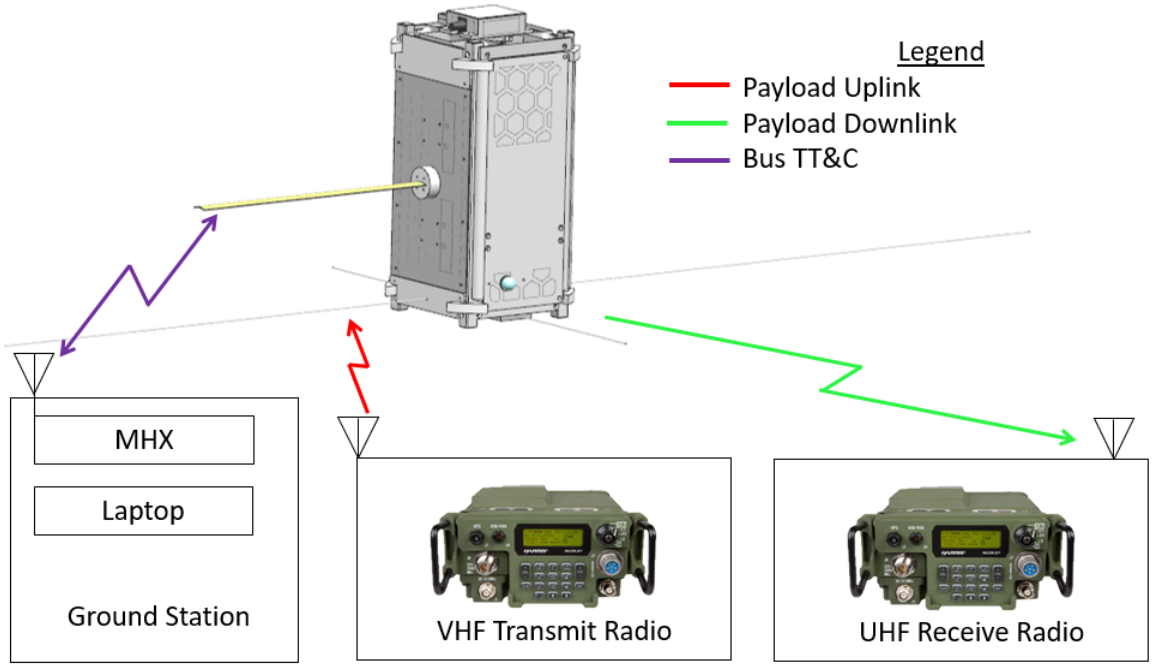

Figure 69. RDCS Demonstration Flight CONOPS

B. DEMONSTRATION

Preparations at the launch site began the day before, including rocket pre-flight checks and a final RDCS integration check. On the morning of the launch, RDCS was prepared for encapsulation in parallel with the NPS rocket as depicted in Figure 70. RDCS was encapsulated in the payload bay and the rocket was loaded on the launch rail (Figure 71). The researchers conducted a final functions check of the payload and were a "go" for launch. After final launch vehicle preparations, the rocket was launched (Figure 72).

The rocket preformed nominally for approximately 3 seconds, until it approached transonic speeds. Then, the flight path became erratic, and debris was observed in the smoke trail of the rocket. The rocket ascended to a final altitude of approximately 3,000 ft above ground level before experiencing a rapid and catastrophic fragmentation. More details regarding the rocket flight profile can be found in [32]. A final radio check with the payload was preformed approximately 5 seconds after launch but was unsuccessful.

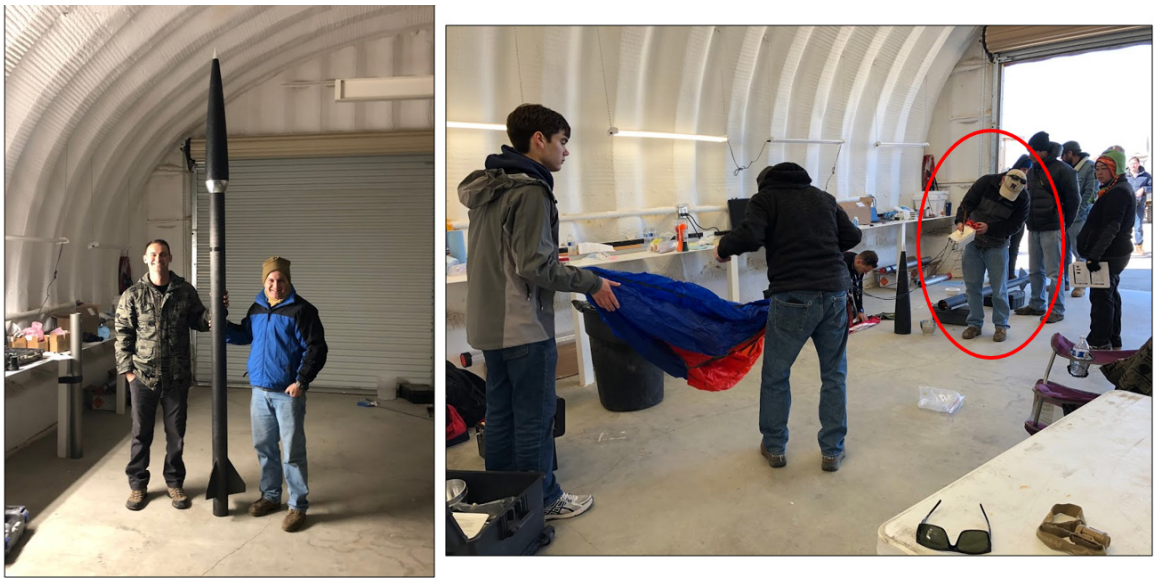

Final Integration Check (left) and RDCS Pre-flight Checks (right)

Figure 70. Pre-Flight Preparations

RDCS Encapsulation (left) and Launch Rail Loading (right)

Figure 71. Pre-Flight Events

Launch (left) and Flight Path (right)

Figure 72. Rocket Flight

C. RESULTS

Once the in-flight anomaly occurred and debris was observed, the researchers transitioned from RDCS demonstration to recovery. The debris field was spread over an area approximately 400 x 200 m to the northwest of the launch site, as depicted in Figure 73. While most of the debris collected was polycarbonate fragments no larger than a silver dollar, much of the hardware was collected, including the payload deck with rPi and SDR, uplink RF components, electrical harness, and the EPS and C&DH Board, all in Figure 74, and C&DH antenna plate.

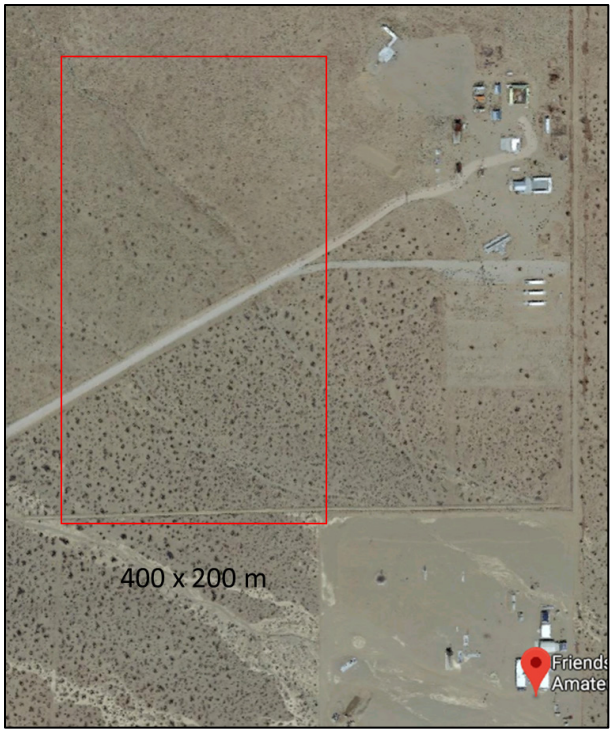

Figure 73. Debris Field. Adapted from [80].

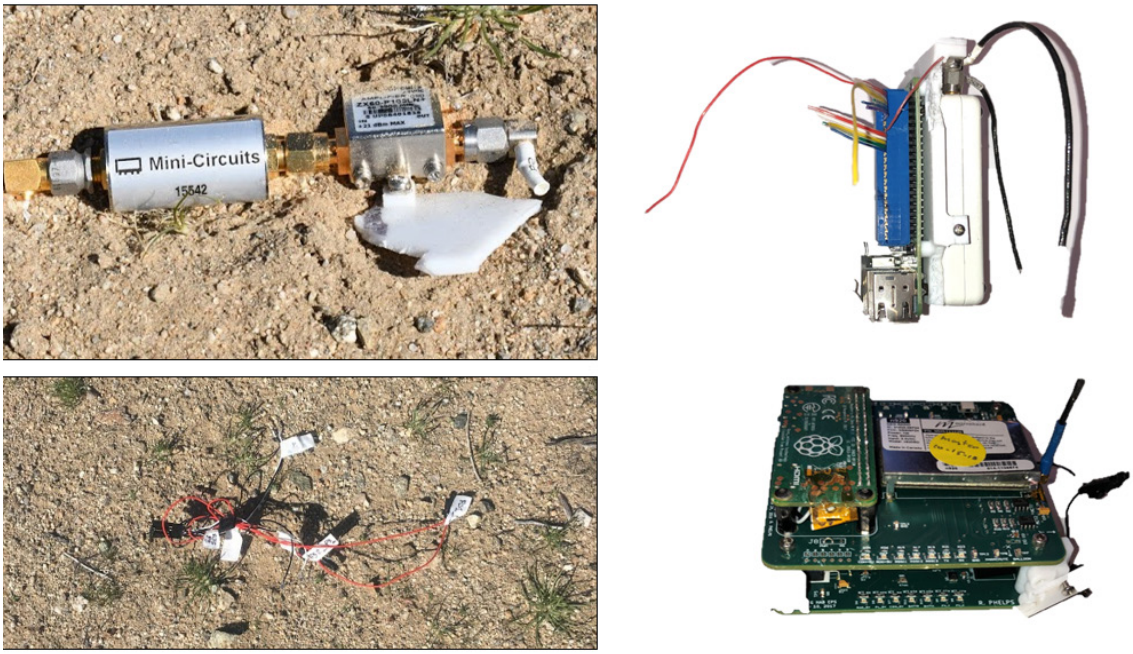

From top left to right: Mini-Circuits Components, Payload Deck, electrical harness, and EPS and C&DH Board.

Figure 74. Recovered Hardware

Rocket post-flight analysis conducted by Pierce [32] concluded that the nose cone sheared from the rocket body, which prematurely deployed RDCS at a speed of approximately Mach 1.5 (2,092 kilometers per hour or 1,300 mph). A pre- and post-flight comparison of the C&DH 1/32 inch aluminum antenna plate is presented in Figure 75, which provides a visual depiction of the forces encountered during the catastrophic failure.

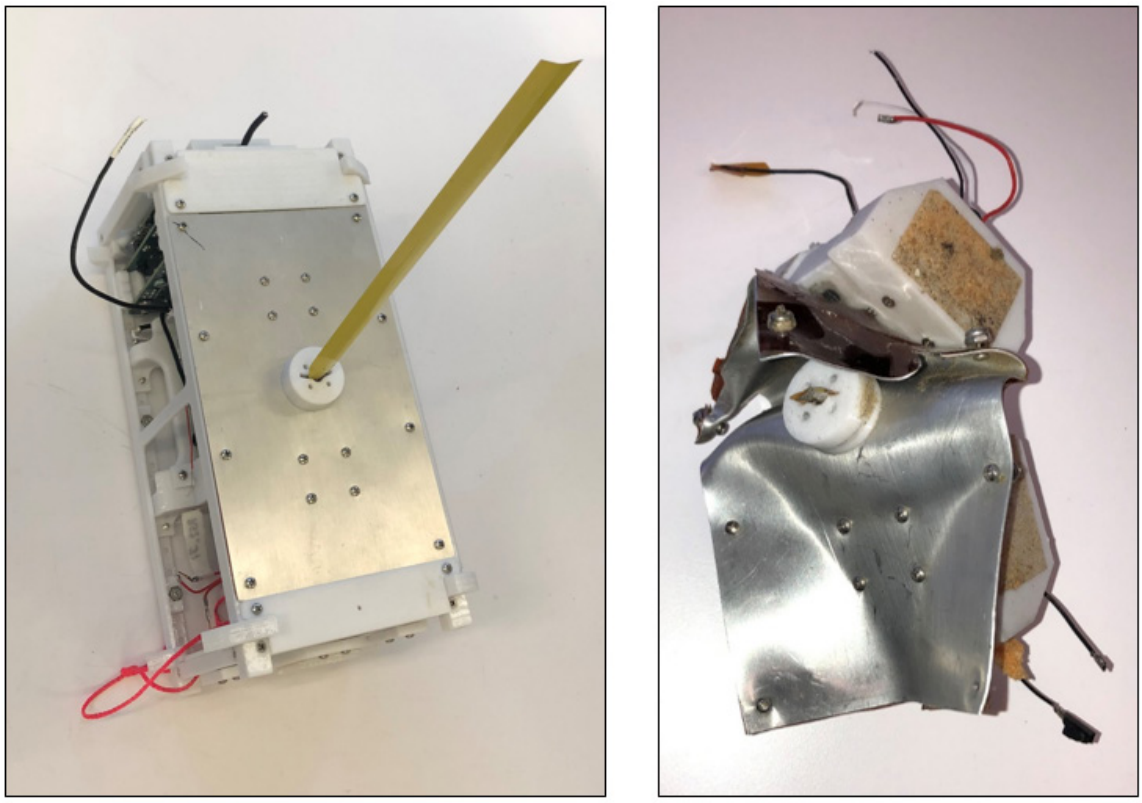

Pre-flight (left) and post-flight (right)

Figure 75. C&DH Antenna Plate

There were other effects observed that researchers conclude were due to the extreme forces associated with the premature deployment. No debris was found with foam attached, although the Kapton tape had not separated during the failure. The USB cord connecting the rPi and SDR was found to still have the USB connection from the rPi USB port lodged inside the cable's USB port.

Post-flight analysis confirmed that all fasteners that were recovered and used lock nuts retained those lock nuts, testifying to the effectiveness of nylon lock nuts. All Mini-Circuits hardware was tested using a signal generator and oscilloscope and found to be operational. However, the rPi and SDR were not functional. The secure digital cards for both the payload and bus computer were recovered intact and functional, although there was no usable video to support post-flight analysis: while each camera was functioning properly, because they were both shrouded by a parachute up to the point of rapid disassembly, the videos were two-minute clips of blackness. This analysis resulted in lessons learned regarding the durability and utility of some design features and components.

D. CONCLUSION

The demonstration flight provided the opportunity to validate RDCS pre-flight procedures and was a potential opportunity to operate RDCS in an operationally representative environment. However, RDCS never had the chance to properly deploy due to the catastrophic failure of the rocket. Debris was recovered, some of which is still functional, but all debris showed marks of the rapid disassembly in some fashion. The C&DH antenna plate depicted the extreme forces related the premature deployment of RDCS at approximately Mach 1.5. Although RDCS was not relaying communications at altitude, the demonstration flight was a step forward in the direction of operationalizing RDCS.

VI. SUMMARY AND CONCLUSIONS

RDCS, a radio relay delivered to the near-space environment by a rocket, is designed to assure communications for the battlefield commander in an uncertain future operating environment. RDCS exploits the capabilities of emerging technologies to augment narrowband SATCOM services. RDCS was demonstrated after a thorough trade analysis, design, and testing regime. While it was not tested operationally, RDCS demonstrated the potential to provide BLOS communications for the tactical commander in a contested environment.

A. SUMMARY

Modern methods of warfare rely heavily on space-based capabilities, including SATCOM for BLOS communications. However, adversaries are increasing their capability to interfere with this service, which presents a risk to leaders, particularly in the execution of C2 functions. This problem cannot be solved in the next 10 years by simply proliferating more satellites, as constellations are expensive and there is limited access to space. Potential solutions to this challenge span the orbital, near-space, and terrestrial regimes, and all of which must operate within the current SATCOM architecture to be effective in the near term. A near-space solution that is expeditionary and responsive is a rocket-delivered communications relay like RDCS.

To outline the requirements for a concept like RDCS, a CONOPS is presented in Chapter II, which includes a realistic scenario based in the South China Sea in which a shipboard battalion commander utilizes RDCS to communicate with a foot-mobile patrol nearly 375 miles away despite adversary SATCOM-jamming efforts. In this scenario, RDCS provides five minutes of connectivity for vital intelligence reports for relay to higher echelons in support of the mission. This scenario proves the use case for RDCS and helps to identify design criteria.

Based on the ranges and times presented in the CONOPS, the RDCS design was completed through a detailed mission and trade analysis, which culminated in an integrated system of hardware and software between the bus and payload. The first step of the design

phase was to define the external constraints levied by the FAA, the rocket, and the environment on RDCS. Next, the VHF uplink and downlink frequencies were selected, which had lasting impact on nearly every facet of the design. Using the frequencies, the user segment analysis identified the operationally relevant radios and antennas to communicate with RDCS. The results of the payload hardware analysis included the hardware that will receive and re-transmit signals as far as 600 miles, which were validated through a link analysis. The bus design relied heavily on the Small Sat Lab HAB Bus but included modifications to the structure, EPS, and C&DH antennas to facilitate rocket integration and expected thermal conditions at altitude. The primary parachute was thoroughly analyzed to better understand the descent profiles and time to descend, which directly impact connectivity time. The payload and bus integration resulted in a fully constructed system which, after being analyzed for mass, power, and data usage, was prepared for testing.

Testing RDCS incorporated subsystem and system-level testing, which validated hardware and software design. The software that makes up the core of RDCS, the GNU Radio flow graph, was validated through two tests encompassing both laboratory and field environments. The culmination of the hardware and software validation was an over-the-air test at a range of 3.2 km, which validated the RDCS concept. Subsequent testing included a test of the rocket integration through a fit check and deployment test, as well as environmental testing. Random vibration testing was used to verify RDCS's functionality by imparting forces modeled after NASA sounding rockets. The strategic placement of parachutes within the rocket payload bay reduced the effect of those vibrations through dampening. Finally, the testing regime validated the final software and hardware configuration in preparation for the demonstration flight.

The demonstration flight was the opportunity for RDCS to demonstrate its capabilities in an operationally relevant environment from a target altitude of 30,000 ft. However, RDCS experienced a premature deployment as the rocket suffered an anomaly at approximately Mach 1.5. This anomaly resulted in catastrophic failure of RDCS, abruptly ending the demonstration flight. However, debris recovered confirmed elements of the design beneficial to researchers.

B. CONCLUSIONS

Although the demonstration flight did not allow RDCS to operate from altitude, the detailed design, testing, and functional checks validated the concept. A system can be constructed from open-source COTS products and can operate as a short-duration radio relay to provide an augment to traditional SATCOM communications. RDCS is viable as an expeditionary near-term concept that can assure command and control for leaders in an uncertain future operating environment.

C. FUTURE WORK

There are several opportunities for future work with RDCS, with three areas of emphasis: RDCS, networks, and payloads.

There are several improvements that can be made to RDCS as a narrowband FM relay. Although functionality already exists in the C&DH software, this project did not make use of the ability to uplink commands to the payload through the C&DH system due to scheduling constraints. However, the uplink functionality could be used to switch frequencies in real-time. Furthermore, while retaining narrowband FM communications as the payload, features like frequency hopping could be added to the radio scheme to increase resiliency. Additionally, thermal effects of the foam and Kapton tape on batteries and the SDR could also be explored. Other design improvements for future work include incorporation of an internal temperature sensor, attitude control system for better antenna pointing, or steerable parachute for more precise operations and to facilitate recovery.

Another area for future work is to extend RDCS to communicate on data networks. Narrowband FM voice was chosen for this system because it is relatively simple to code with GNU Radio and fairly straight forward to determine if an audible radio signal is being demodulated properly. However, RDCS could also be used to relay information for data networks like Wi-Fi, Link-16, 4G or even 5G. The future conflict will rely heavily on the movement of digital data around the battlefield. Although RDCS is not currently designed to support these networks, a change in GNU Radio scheme and the payload hardware could support this effort.

The final area for future work is a change of the payload. The concept of deploying a payload from altitude via rocket could be extended beyond communication payloads to other mission like intelligence, surveillance, and reconnaissance. Other potential applications include a GPS augment for an area of operations or even a localized GPS jammer for training.

While most problems that can be solved from orbit are likely to be solved in the space regime, some solutions to the myriad of challenges that exist may be solved by exploiting the benefits of the near-space regime. RDCS presents a near-term, expeditionary solution that can assure communications for the commander in the contested battlespace of the future operating environment.

APPENDIX A. RANGE AND PERFORMANCE DATA SHEET

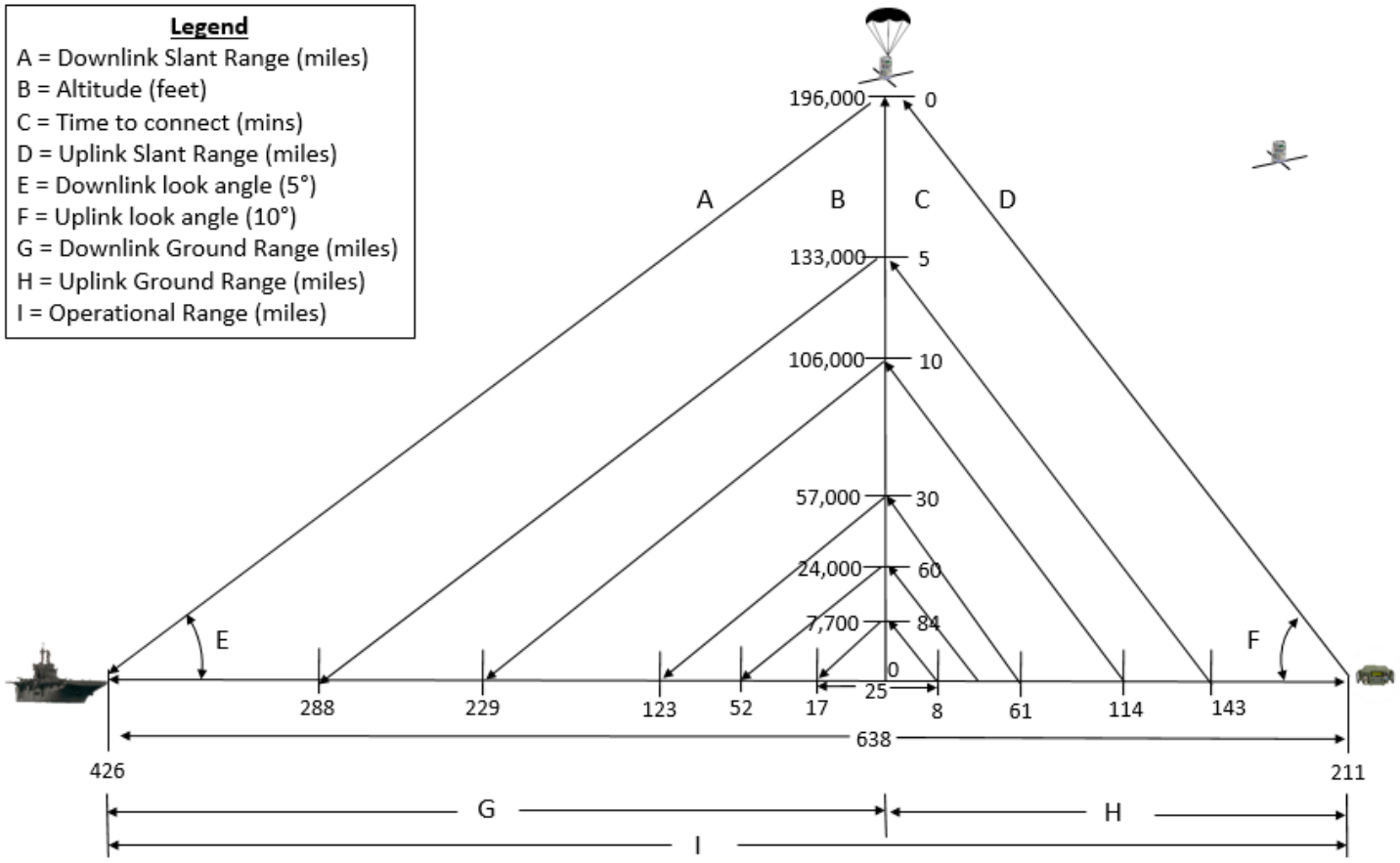

THIS PAGE INTENTIONALLY LEFT BLANK

APPENDIX B. BUS ELECTRICAL SCHEMATICS

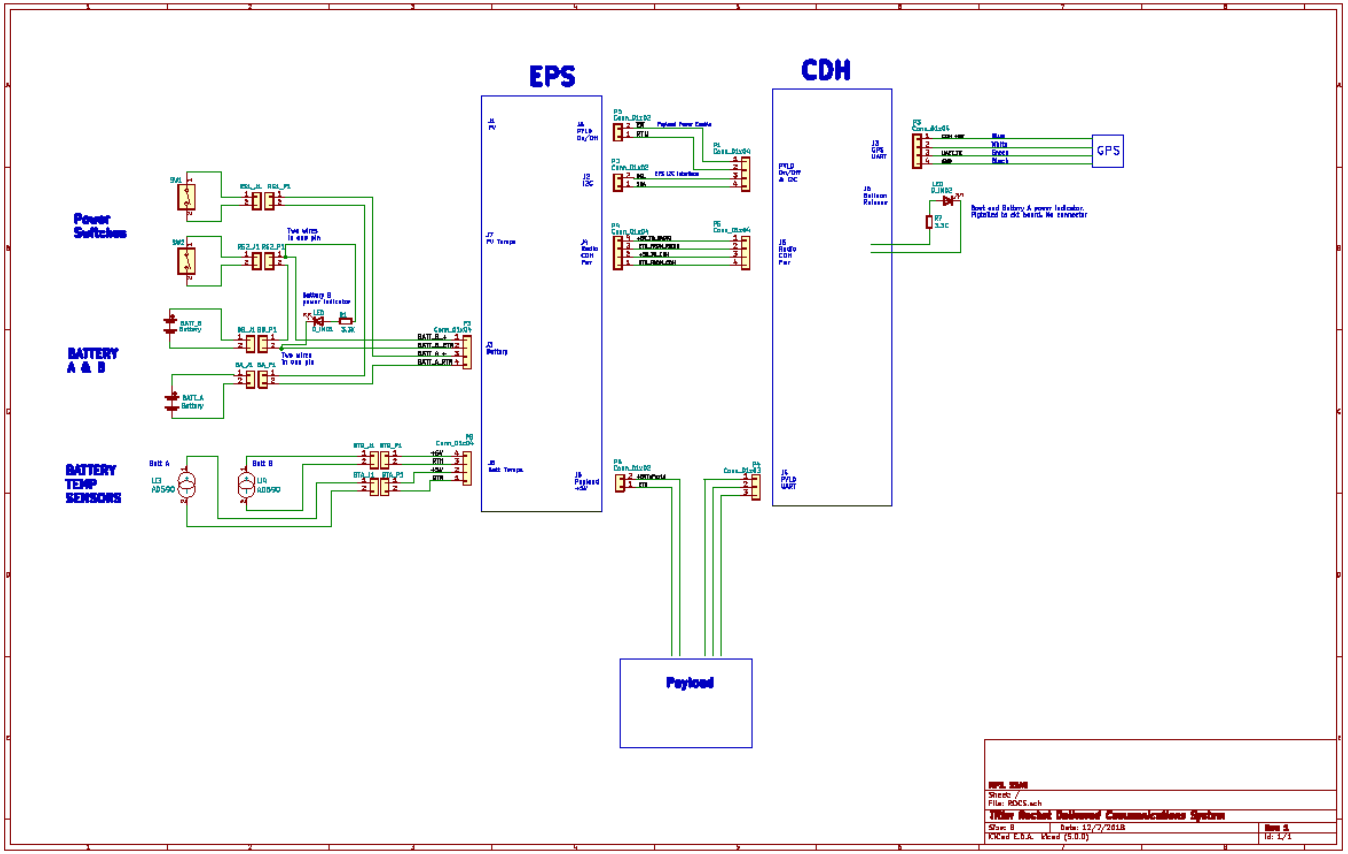

\\special\ssagcommon$\Projects\Student Theses\Thesis - Pross, John (2019 Rocket Delivered Communications System RDCS)\Write up\Archived Versions\Parts and Pieces\EPS Schematics.pdf

THIS PAGE INTENTIONALLY LEFT BLANK

APPENDIX C. MATLAB PARACHUTE CODE

RDCS Parachute Calculations

```
clear;clc;format compact
close all
```

Initialize Values

```
dt =.1;
stop=6;                                 % hrs
stop=6*60*60 ;                          % seconds
stop = stop/dt;                         % steps
Re = 6378e3;                            % m
H = 7.5e3;                              % m
g0 =9.801;                              % m/s
rho0 = 1.225;                           % kg/m^3

% Initialize Variables
Cd = 1.75;                               % 2.2 for toroid, 1.5 for dome shaped… .75 for
parasheet
A = 2.67;                               % m^2

% 150k Numbers
m = 1.8;                                % kg
z(1) = 45720;                           % m (150k ft = 45720, 196k = 60000)
```

Establish Start Parameters

```
j=1;
t(1) = 0;
v(1)=0;                                 % m/s @ altitude
rho(1)=rho0*exp(-(z(1)/H));             % kg/m^3 @ altitude
drag(1) = (.5*Cd*rho(1)*A*v(1)^2);
a(1) = -g0 + drag(1)/m;
g(1) = gravity(z);
v_terminal(1)=-sqrt((2*m*g(1))/(rho(1)*Cd*A));
```

Numerical Integration

```
for j = 2:stop

    t(j) = t(j-1) + dt;
    v(j) = v(j-1)+ a(j-1)* dt;
    z(j) = z(j-1)+ v(j)* dt;
    g(j) = gravity(z(j));
    rho(j)=rho0*exp(-(z(j)/H));
```

```
    drag(j) = (.5*Cd*rho(j)*A*v(j)^2);
    a(j) = -g(j) + drag(j)/m;
    v_terminal(j)=-sqrt((2*m*g(j))/(rho(j)*Cd*A)); % m/s @ altitude

end
```

Truncate for Values Above Earth's Surface

```
for j = 2:length(z)
    if z(j) - z(j+1) >  z(j)
        time_impact = t(j);
        z_impact = z(1:j);
        t_impact = t(1:j);
        v_impact = v(1:j);
        break
    end
end
```

Convert to English Units

```
z_impact_ft = z_impact.*3.28084;
v_impact_ft = v_impact.*3.28084;
```

Determine Time to Calculate 25 mile link

```
alt_cutoff = 7726  ;                        %ft, altitude associated with 20 mile link
[time_index]=find(z_impact_ft<alt_cutoff);
time_index=time_index(1);
time_cutoff=t_impact(time_index);
```

Plot Data

```
figure
subplot(2,1,1)
plot(t_impact./60,z_impact/1000), title('Altitude vs. Time [Metric Units]'), xlabel('Time
[mins]'),ylabel('Altitude [km]'),grid on
subplot(2,1,2)
plot(t_impact./60,z_impact_ft/1000), title('Altitude vs. Time [English Units]'),
xlabel('Time [mins]'),ylabel('Altitude [x10^3 ft]'),grid on

figure
subplot(2,1,1)
plot(t_impact/60,v_impact), title('Descent Velocity vs. Time [Metric
Units]'),xlabel('Time [mins]'), ylabel ('Descent Veleocity [m/s]'), grid on
subplot(2,1,2)
plot(t_impact/60,v_impact_ft), title('Descent Velocity vs. Time [English
Units]'),xlabel('Time [mins]'), ylabel ('Descent Veleocity [fps]'), grid on
```

```
figure
subplot(2,1,1)
plot(v_impact,z_impact/1000), title ('Altitude vs. Descent Velocity [Metric Units]'),
xlabel('Velocity [m/s]'),ylabel ('Altitude [km]'), grid on
subplot(2,1,2)
plot(v_impact_ft,z_impact_ft/1000), title ('Altitude vs. Descent Velocity [English
Units]'), xlabel('Velocity [fps]'),ylabel ('Altitude [x10^3 ft]'), grid on
```

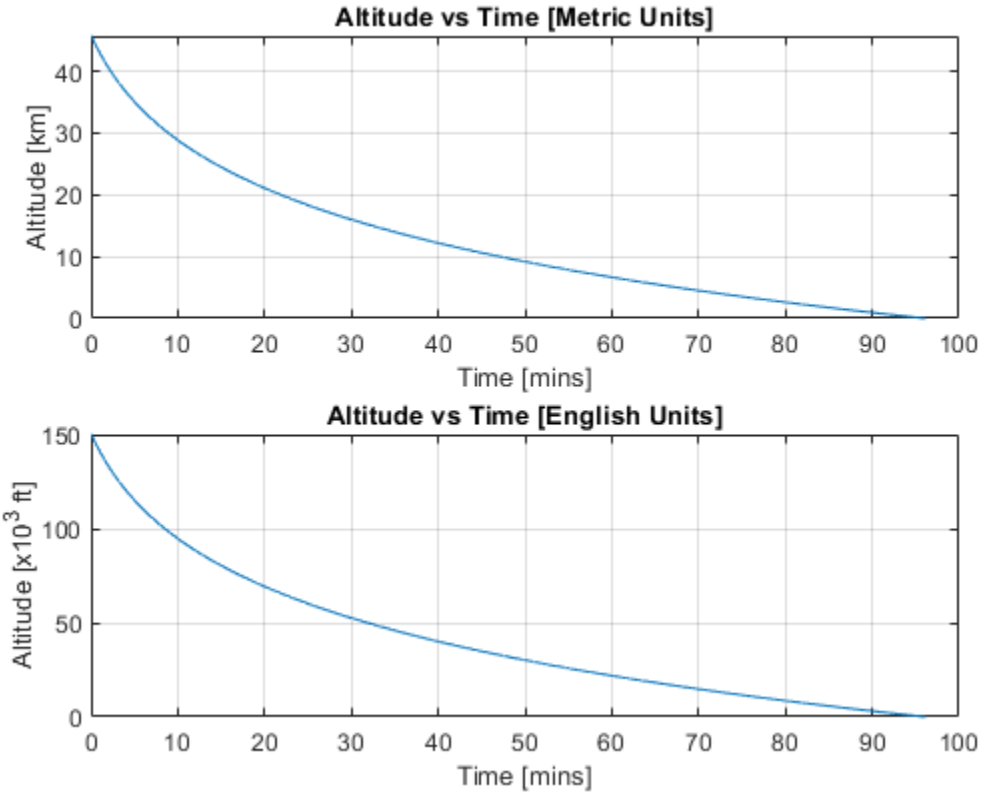

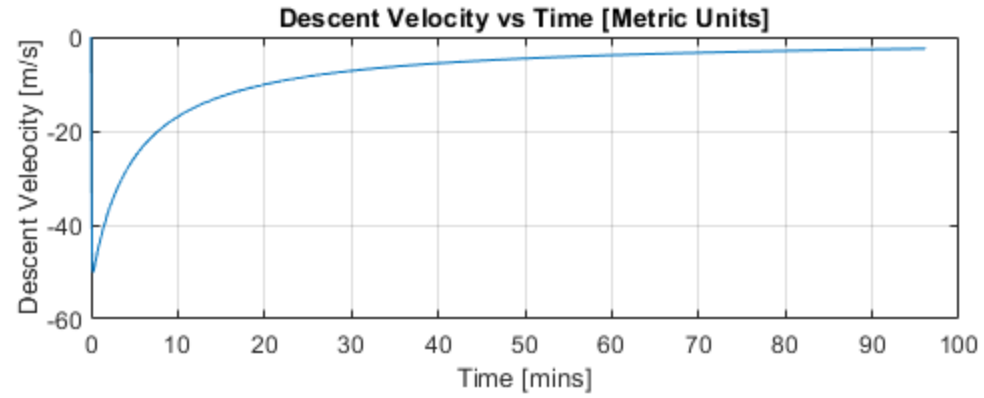
Descent Velocity vs Time [Metric Units]
Descent Veleocity [m/s]
0
-20
-40
-60
0
10
20
30
40
50
60
70
80
90
100
Time [mins]

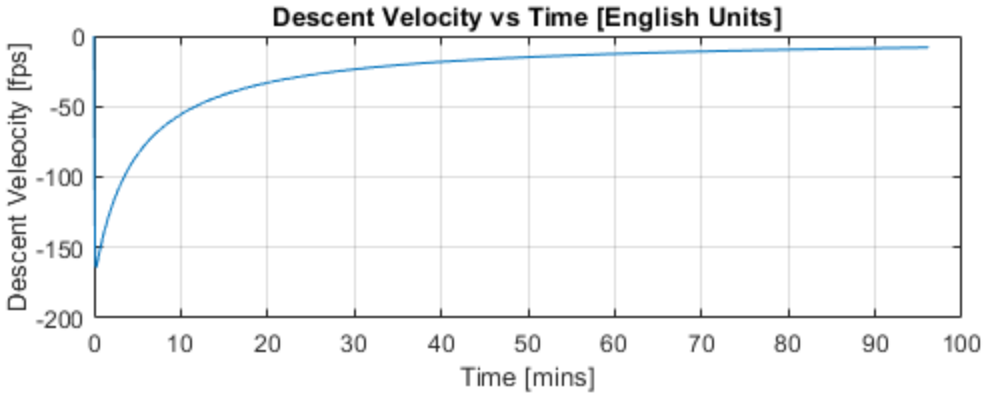
Descent Velocity vs Time [English Units]
Descent Veleocity [fps]
0
-50
-100
-150
-200
0
10
20
30
40
50
60
70
80
90
100
Time [mins]

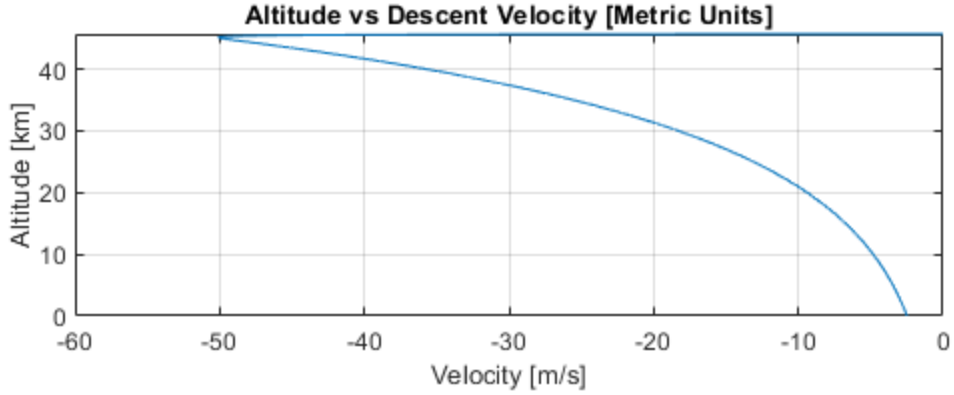
Altitude vs Descent Velocity [Metric Units]
Altitude [km]
40
30
20
10
0
-60
-50
-40
-30
-20
-10
0
Velocity [m/s]

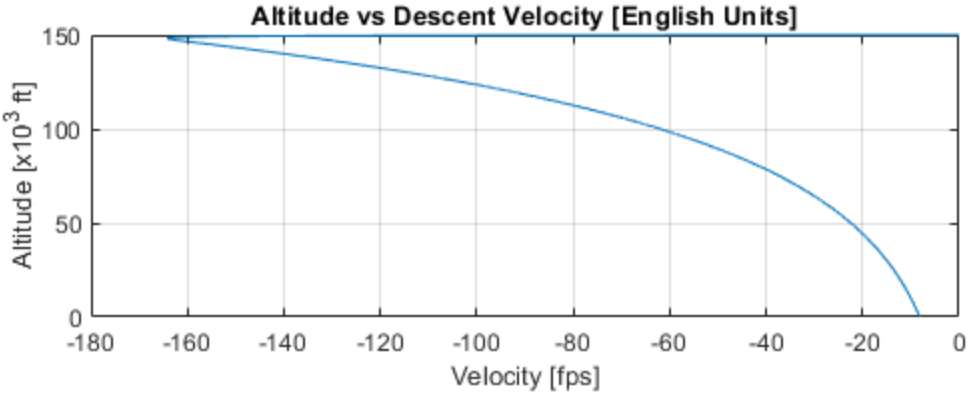
Altitude vs Descent Velocity [English Units]
Altitude [x10^3 ft]
150
100
50
0
-180
-160
-140
-120
-100
-80
-60
-40
-20
0
Velocity [fps]

Display Data

```
fprintf('\n                          Starting Altitude: %6.0f m or %6.0f ft
\n',z(1),z(1)*3.28084)
fprintf('                                RDCS Mass:  %1.1f kg or %1.1f lb
\n',m,m*2.20462)
fprintf('                                Parachute:  9 ft Rocket Man\n')
fprintf('Average descent velocity (entire envelope): %6.2f m/s or %6.2f ft/s
\n',z(1)/time_impact,z(1)/time_impact*3.28084)
fprintf('                    Descent rate at impact: %6.2f m/s or %6.2f ft/s
\n',v_impact(length(v_impact)),v_impact(length(v_impact))*3.28084)
fprintf('                        Total descent time:   %4.2f hours\n',time_impact/60/60)
fprintf('          Time to descend through %5.0f ft:  %4.2f mins\
n',alt_cutoff,t_impact(time_index)/60)
```

```
                      Starting Altitude:  45720 m or 150000 ft
                              RDCS Mass:  1.8 kg or 4.0 lb
                              Parachute:  9 ft Rocket Man
Average descent velocity (entire envelope):   7.93 m/s or  26.00 ft/s
                    Descent rate at impact:  -2.48 m/s or  -8.14 ft/s
                        Total descent time:   1.60 hours
          Time to descend through  7726 ft:  81.51 mins
```

Gravity Function

```
function [g] = gravity(z)
% This function calculates gravity as a function of altitude

mu = 3.986e14;     % m^3/s^2
Re = 6378e3;       % m
r = Re + z;        % m

g = mu / r^2;      % m/s^2
end
```

Published with MATLAB® R2018a

THIS PAGE INTENTIONALLY LEFT BLANK

APPENDIX D. MASS BUDGET

Payload	Quantity	Mass (g)	Mass (lbs)
Raspberry Pi 3B+ with harness	1	64.8	0.14
USRP B205 Mini	1	24.0	0.05
Mini Circuits ZX60-P103LN+	1	23.5	0.05
Mini Circuits ZX-V82-S+	1	23.0	0.05
Mini Cicruits SBLP-156+	1	42.0	0.09
RPi Camera Module V2.1, mount, screws	1	6.6	0.01
Antenna (Plate, Elements, 2x Coax, Screws)	1	82.0	0.18
Structure (Mount & Cover)	1	57.4	0.13
Wiring (USB, 2x Coax, Pi Cam Cord)	1	28.8	0.06
Subtotal		**352.1**	**0.78**
Margin (5%)		10%	
Subtotal		**387.4**	**0.85**

Bus	Quantity	Mass (g)	Mass (lbs)
C&DH Board, EPS Board, MHX, Raspi Zero, Double Ear	1	152.2	0.34
GPS with cover with fasteners	1	43.9	0.10
RPi Cam Module V2.1 with cover & fasteners	1	5.3	0.01
Fingertech Switches w/ connectors	2	2.2	0.00
C&DH Antenna (Ground plane, element, element mount,coax, fasteners	1	55.5	0.12
Battery Box, 5x AA, Lid, Fasteners, Epoxy)	2	273.2	0.60
Parachute Mount	1	56.2	0.12
Switch Panel, LEDs , screws,	1	54.1	0.12
Spot Tracker Panel w/ Lid	1	74.4	0.16
Raspbery Pi Cam Panel	1	48.1	0.11
Ground Plane Panel with fasteners	1	6.8	0.01
Structure (Side Rails)	2	28.0	0.06
Subtotal		**799.9**	**1.43**
Margin (5%)		10%	
Subtotal		**879.9**	**1.57**

Recovery	Quantity	Mass (g)	Mass (lbs)
Spot Tracker	1	87.9	0.19
Primary Parachute	1	340.2	0.75
Backup Release	1	17.5	0.04
Backup Parachute	1	99.2	0.22
Subtotal		**544.8**	**1.20**
Margin (5%)		10%	
Subtotal		**599.3**	**1.32**

Mass Summary			
	Mass (g)	Mass (lbs)	Constraints
Payload	387.4	0.85	
Bus	879.9	1.57	
Subtotal	**1267.2**	**2.42**	< 4 lbs (FAA Regulation)
Recovery	599.3	1.32	
Subtotal	**1866.5**	**3.75**	
Margin	5%		
Total	**1959.8**	**3.93**	Light as Possible

THIS PAGE INTENTIONALLY LEFT BLANK

APPENDIX E. POWER BUDGET

Estimated Power Requirements

Payload	Voltage (Volts)	Current (Amps)	Power (Watts)	Duty Cycle	Time (mins)	Energy (Whrs)
Raspberry Pi 3B+ [47]	5.00	1.30	6.50	100%	110	11.92
USRP B205 Mini [50]	5.00	1.20	6.00	100%	110	11.00
Mini Circuits ZX60-P103LN+ [55]	5.50	0.12	0.66	100%	110	1.21
Mini Circuits ZX-V82-S+ [56]	5.20	0.12	0.62	100%	110	1.14
Subtotal		2.74	13.78			25.27
C&DH						
Raspberry Pi Zero [62]	5.00	0.23	1.15	100%	110	2.11
GPS [58]	4.40	0.032	0.14	100%	110	0.26
MHX n920 Tx [63]	3.30	1.50	4.95	100%	110	9.08
MHX n920 Rx [63]	3.30	0.28	0.92	1%	1.1	0.02
Subtotal		2.04	7.16			11.46
Total Energy Required (Whrs)						36.73
EPS Supplied 10 x AA Energizer Lithium Cells @ -10°C (Whrs) [57]						48.00
Energy Margin (Whrs)						**11.27**
***Estimated Total Power-On Time = 100 Minutes**						

Measured Power Requirements

Sub Systems	Voltage (Volts)	Current (Amps)	Power (Watts)	Duty Cycle	Time (mins)	Energy (WHrs)	Efficiency	Required Energy (Whrs)
Payload (Rx only)	5.00	1.20	6.00	75%	82.5	8.25	0.7	11.79
Payload (Rx and Tx)	5.00	1.35	6.75	25%	27.5	3.09	0.7	4.42
Subtotal		**1.35**		**100%**	**110**	**11.34**		**16.21**
C&DH and EPS	8.00	0.70	5.60	100%	110	10.27	0.7	14.67
Total		**2.05**				**21.61**		**30.87**
Enitre RDCS System Measured								
Bus + Payload	**8.00**	**2.00**	**16.00**	**100%**	**110**	**29.33**	**0.7**	**41.90**
EPS Supplied 10 x AA Energizer Lithium Cells @ -10°C (WHrs)								48.00
Energy Margin								**6.10**

THIS PAGE INTENTIONALLY LEFT BLANK

APPENDIX F. DATA BUDGET

Data Storage Budget

Hardware	Quantity	Data Rate (GB/Hr)	Operational Time (hrs)	Storage Requirement (GB)	Storage Capacity (GB)	Margin (GB)
C&DH Raspberry Pi Zero Camera	1	2.98	1.83	5.46	10	4.54
RDCS Raspberry Pi 3 B+ Camera	1	4.98	1.83	9.13	24	14.87

THIS PAGE INTENTIONALLY LEFT BLANK

APPENDIX G. RDCS PYTHON SCRIPTS

File Location: \\special\ssagcommon$\Projects\Student Theses\Thesis - Pross, John (2019 Rocket Delivered Communications System RDCS)\Code\Final RDCS\Final Code

A. BUS STARTUP

```
from __future__ import print_function
import os
import subprocess
import shlex
import time
import traceback

import camera

#systemd notes:
# /etc/systemd/system/HAB.services is used to make this program start up after reboot
#[Unit]
#description=HAB
#
#[Service]
#WorkingDirectory=/home/pi/HAB
#ExecStart=/usr/bin/python start_HAB.py
#
#[Install]
#WantedBy=multi-user.target
# sudo systemctrl enable HAB.service
# sudo systemctrl start HAB.service


def main():
if camera.is_camera_running():
subprocess.Popen(shlex.split("/usr/bin/python camera.py"), stdin=subprocess.PIPE)
subprocess.Popen(shlex.split("/usr/bin/python master.py camera"), stdin=subprocess.PIPE)
# pnames = ["/usr/bin/python master.py camera"]
else:
# pnames = ["/usr/bin/python master.py no_camera"]
subprocess.Popen(shlex.split("/usr/bin/python master.py"), stdin=subprocess.PIPE)

subprocess.Popen(shlex.split("/usr/bin/python server_web2.py"), stdin=subprocess.PIPE)
while True:
time.sleep(1)


processes = []
```

```
40 for pname in pnames:
41 processes.append(subprocess.Popen(shlex.split(pname),
stdin=subprocess.PIPE))
42
43 # when starting the process wait a bit longer for it to start
44 time.sleep(3)
45 start = time.time()
46 while True:
47 for process in processes:
48 if process.poll() != None:
49 process = subprocess.Popen(shlex.split(pname),
stdin=subprocess.PIPE)
50 time.sleep(1)
51
52
53
################################################################################
########
54
################################################################################
########
55
################################################################################
########
56
57 if __name__ == "__main__":
58 os.system("/usr/bin/pigpiod")
59 os.system("/usr/bin/python RTC.py")
60 time.sleep(3)
61 while (True):
62 try:
63 main()
64 except:
65 s = traceback.format_exc()
66 fp = open("start_HAB_traceback.txt", "a")
67 fp.write(s+"\n")
68 fp.close()
```

B. BUS MASTER

```
1
################################################################################
########
2 #
3 # master.py
4 #
5 # HAB Bus Master program.
6 #
7 # Revision History:
8 # =================
9 # Date Who What
10 # ---------------+-------+-----------------------------------------
---------
11 # 2018-10-10 Jah Creation: Adopted from Summer 2018 HAB Bus software
12 #
```

```
13
################################################################################
########
14
15 from __future__ import print_function
16 import copy
17 import os
18 import pigpio
19 import shutil
20 import socket
21 import subprocess
22 import sys
23 import threading
24 import time
25
26 RazPi_type = 'Pi0W'
27 #RazPi_type = 'Pi0'
28
29
30 import actuators
31 import camera
32 import GPS
33 import log
34 import ADS7828
35 import MAX9611
36 import RADIO
37 import RP_LED
38 import RTC
39 import sd_capacity
40 import UART
41 import camera
42 import ADS7828
43 import flight_parameters
44 import balloon_release_logic
45
46
47
48 PAYLOAD_ENABLE_GPIO = 21
49 PAYLOAD_ENABLE = 1
50 PAYLOAD_DISABLE = 0
51
52 # Payload commands (routed to payload)
53 payload_commands = ['plreboot', 'plhalt', 'plclear', 'plstart',
'pldn', 'plst', 'pltime']
54
55
56 # Intervals (in seconds) of when to get data for particular sensors
57 VOLTAGES_INTERVAL = 5
58 CURRENTS_INTERVAL = 5
59 TEMPS_INTERVAL = 10
60 TIMEMESSAGE_INTERVAL = 10
61 GPS_INTERVAL = 3
62 GPRMC_INTERVAL = 5
63 ACTUATORS_INTERVAL = 10
64 STORAGE_STATUS_INTERVAL = 20
```

```
65
66
67 def main():
68 # these objects start threads to get the device data in a non-
blocking mode
69 # these objects should be checked regularly for queued messages so
that messages do
not queue up beyond one message
70 if RazPi_type == 'Pi0W':
71 radio = RADIO.RADIO("/dev/ttyS0", 9600, eol='\x0D') # RazPi Zero W!
72 elif RazPi_type == 'Pi0':
73 radio = RADIO.RADIO("/dev/ttyAMA0", 9600, eol='\x0D') # RazPi Zero
(no W)
74 gps = GPS.GPS(0x4C, 4800, use_PWM=True)
75 payload = UART.UART(0x4D, 9600, eol=0x0D, use_PWM=True)
76 max9611 = MAX9611.MAX9611()
77 ads7828 = ADS7828.ADS7828()
78 sd = sd_capacity.SD()
79 balloon_release =
balloon_release_logic.BALLOON_RELEASE(flight_parameters.ABSOLUTE_ALTITU
DE_UNIL_BALLOO
N_RELEASE, flight_parameters.ELAPSED_FLIGHT_TIME_UNTIL_BALLOON_RELEASE)
80
81
82 led = RP_LED.RP_LED()
83 led.queue_message(M=1, N=0, repeat=True)
84
85 USE_RTC_WATCHDOG = False # initially off, can be commanded to go on
86 rtc = RTC.RTC()
87
88 pi_gpio = pigpio.pi()
89 pi_gpio.set_mode(PAYLOAD_ENABLE_GPIO, pigpio.OUTPUT)
90 pi_gpio.write(PAYLOAD_ENABLE_GPIO, PAYLOAD_ENABLE)
91
92 # time stamps of last activites: set them to staggering starts
93 now = time.time()
94 #1: AD590 Temperatures
95 #2: EPS Temperatures
96 #3: EPS Voltages
97 #4: EPS Currents
98 #5: CDH Temperatures
99 #6: CDH Voltages
100 #7: CDH Currents
101 #8: GPS
102 #9: Balloon Actuator Voltage
103 #10: Parachute Actuator Voltage
104 #11: Message
105 #20: Payload Message
106 last_times = {1:now, 2:now, 3:now+1, 4:now+2, 5:now, 6:now+1,
7:now+2, 8:now,
9:now+3, 10:now+4}
107 last_temps_time = now
108 last_timemessage_time = now + 1
109 last_pressure_time = now + 3
110 last_voltages_time = now + 4
```

```
111 last_GPRMC_time = now + 1
112 last_actuators_time = now + 7
113 last_storage_status_time = now
114
115 last_rmc_message = None
116
117 # release start times; 0 signifies not yet done
118 b_release_start_time = 0
119 p_release_start_time = 0
120 close_start_time = 0
121 RELEASE_INDICATOR_TIME = 5
122 RELEASE_INDICATOR_DELTA_MSG = 0.1
123
124 got_gps_time = False
125 last_GPS_no_fix = 0
126
127 logger = log.LOG() # start logging system with default HAB.log
filename
128
129 fp = open("build_time.txt", "r")
130 version = fp.readline().strip()
131 fp.close()
132 msg = '\n\n-------------------------------------------------------
--'
133 radio.write_print(msg)
134 logger.log(msg)
135 msg = '11 {:<100s}'.format('%d HAB Startup, version
%s'%(time.time(), version))
136 radio.write_print(msg)
137 logger.log(msg)
138
139 if len(sys.argv) > 1 and sys.argv[1] == 'camera':
140 sock = socket.socket(socket.AF_INET, socket.SOCK_DGRAM)
141 sent = sock.sendto('video_on', ('localhost', camera.CAMERA_PORT))
142 video_on = True
143 video_available = True
144 else:
145 msg = '11 {:<100s}'.format('%d no camera available'%time.time())
146 radio.write_print(msg)
147 logger.log(msg)
148 video_on = False
149 video_available = False
150
151 last_shutdown_cmd = 0
152 last_reboot_cmd = 0
153
154 time_release_triggered = False
155 alt_release_triggered = False
156
157 # this is the main loop which should iterate quickly
158 while True:
159 # ATTENTION: make sure all code below does not block and runs
quickly!
160 now = time.time()
161
```

```
162 if USE_RTC_WATCHDOG:
163 rtc.arm_watch_dog(5)
164
165 cmd = radio.get_line()
166 if cmd != None:
167 cmd = cmd.strip()
168 cmd_lower = cmd.lower()
169 logger.log('command <%s> received.'%cmd)
170
171 if cmd_lower.split(' ')[0] in payload_commands: # note: split used
in
case command has parameters
172 cmd_payload_lower = cmd_lower.split(' ')[0]
173 if cmd_payload_lower == 'ploff':
174 pi_gpio.write(PAYLOAD_ENABLE_GPIO, PAYLOAD_DISABLE)
175 msg = '11 {:<100s}'.format('%d <ploff> received, payload powered
OFF'%(now))
176 radio.write_print(msg)
177 logger.log(msg)
178 elif cmd_payload_lower == 'plon':
179 pi_gpio.write(PAYLOAD_ENABLE_GPIO, PAYLOAD_ENABLE)
180 msg = '11 {:<100s}'.format('%d Payload <plon>, payload powered
ON'%(now))
181 radio.write_print(msg)
182 logger.log(msg)
183 elif cmd_payload_lower == 'pltime':
184 tstr = None
185 if last_rmc_message != None:
186 epoch = gps.get_datetime(last_rmc_message, override=True)
187 if epoch != None:
188 (y, m, d, hours, mins, secs) = epoch
189 tstr = '%02d%02d%02d%02d%04d.%02d'%(m, d, hours, mins, y,
secs)
190 if tstr == None:
191 tstr = time.strftime('%Y %m %d %H %M %S', time.gmtime(now))
192 (y, m, d, hours, mins, secs) = tstr.split(' ')
193 tstr = '%02d%02d%02d%02d%04d.%02d'%(int(m), int(d), int(hours),
int(mins), int(y), int(secs))
194 msg = '11 {:<100s}'.format('%d Payload <%s> relayed.'%(now, 'PLTIME
%s'%tstr))
195 radio.write_print(msg)
196 payload.write('PLTIME %s'%tstr)
197 else:
198 msg = '11 {:<100s}'.format('%d Payload <%s> relayed.'%(now, cmd))
199 radio.write_print(msg)
200 payload.write(cmd)
201
202 if cmd_payload_lower == 'plstart':
203 balloon_release.reset_start_time()
204
205
206 elif 'connect' in cmd_lower:
207 msg = '11 {:<100s}'.format('%d Radio re-connected'%(now))
208 radio.write_print(msg)
209 logger.log(msg)
```

```
210 led.queue_message(M=3, N=3, repeat=True)
211
212 elif cmd_lower == "brel":
213 actuators.b_release()
214 radio.write('11 {:<100s}'.format('%d <brel> received, Balloon
released'%now))
215 if b_release_start_time == 0:
216 b_release_start_time = now
217 elif cmd_lower == "prel":
218 radio.write('11 {:<100s}'.format('%d <prel> received, Parachute
released'%now))
219 actuators.p_release()
220 if p_release_start_time == 0:
221 p_release_start_time = now
222 elif cmd_lower == "videoon":
223 if video_available:
224 sent = sock.sendto('video_on', ('localhost', camera.CAMERA_PORT))
225 msg = '11 {:<100s}'.format('%d <videoon> received, Video on.'%now)
226 radio.write_print(msg)
227 logger.log(msg)
228 video_on = True
229 else:
230 msg = '11 {:<100s}'.format('%d <videoon> received, Camera not
available.'%now)
231 radio.write_print(msg)
232 elif cmd_lower == "videooff":
233 if video_available:
234 sent = sock.sendto('videooff', ('localhost', camera.CAMERA_PORT))
235 msg = '11 {:<100s}'.format('%d <videooff> received, Video
off.'%now)
236 radio.write_print(msg)
237 logger.log(msg)
238 video_on = False
239 else:
240 msg = '11 {:<100s}'.format('%d <videooff> received, Camera not
available.'%now)
241 radio.write_print(msg)
242 elif cmd_lower == "videoclear":
243 if video_on:
244 msg = '11 {:<100s}'.format('%d <videoclear> received, Cannot clear
video while recording.'%now)
245 else:
246 try:
247 shutil.rmtree(camera.VIDEO_DST)
248 except OSError:
249 pass
250 finally:
251 os.mkdir(camera.VIDEO_DST)
252 msg = '11 {:<100s}'.format('%d <videoclear> received, Video images
erased.'%now)
253 radio.write_print(msg)
254 logger.log(msg)
255 elif cmd_lower == "act":
256 msg = "09 {:>10d} {:>+4.2f} B rel V".format(int(now),
ads7828_data[ADS7828.BALLOON_INDICATOR])
```

```
257 radio.write_print(msg)
258 msg = "10 {:>10d} {:>+4.2f} P rel V".format(int(now),
ads7828_data[ADS7828.PARACHUTE_INDICATOR])
259 radio.write_print(msg)
260 msg = '11 {:<100s}'.format('%d <act> received, sending actuator
status.'%now)
261 radio.write_print(msg)
262 elif cmd_lower == "close":
263 actuators.b_close()
264 actuators.p_close()
265 close_start_time = now
266 msg = '11 {:<100s}'.format('%d <close> received, closing
actuators.'%now)
267 radio.write_print(msg)
268 elif cmd_lower == "reboot":
269 if now - last_shutdown_cmd > 30:
270 msg = '11 {:<100s}'.format('%d <reboot> received; must issue
another within 30 sec.'%now)
271 radio.write_print(msg)
272 logger.log(msg)
273 last_shutdown_cmd = now
274 else:
275 if video_on and video_available:
276 sent = sock.sendto('video_off', ('localhost',
camera.CAMERA_PORT))
277 time.sleep(0.1)
278 msg = '11 {:<100s}'.format('%d second <reboot> received; system
rebooting.'%now)
279 radio.write_print(msg)
280 logger.log(msg)
281 p = subprocess.Popen(['sync'], stdout=subprocess.PIPE,
stderr=subprocess.PIPE)
282 results, err = p.communicate()
283 p.wait()
284 time.sleep(1)
285 p = subprocess.Popen(['reboot'], stdout=subprocess.PIPE,
stderr=subprocess.PIPE)
286 results, err = p.communicate()
287 p.wait()
288 while True:
289 time.sleep(1)
290 elif cmd_lower == "halt":
291 if now - last_reboot_cmd > 30:
292 msg = '11 {:<100s}'.format('%d <shutdown> received; must issue
another within 30 sec.'%now)
293 radio.write_print(msg)
294 logger.log(msg)
295 last_reboot_cmd = now
296 else:
297 if video_on and video_available:
298 sent = sock.sendto('video_off', ('localhost',
camera.CAMERA_PORT))
299 time.sleep(0.1)
300 msg = '11 {:<100s}'.format('%d second <shutdown> received; system
halting.'%now)
```

```
301 radio.write_print(msg)
302 logger.log(msg)
303 p = subprocess.Popen(['sync'], stdout=subprocess.PIPE,
stderr=subprocess.PIPE)
304 results, err = p.communicate()
305 p.wait()
306 time.sleep(1)
307 p = subprocess.Popen(['halt'], stdout=subprocess.PIPE,
stderr=subprocess.PIPE)
308 results, err = p.communicate()
309 p.wait()
310 while True:
311 time.sleep(1)
312 elif cmd_lower == "rmc":
313 if last_rmc_message == None:
314 msg = '11 {:<100s}'.format('%d <rmc> received, no RMC available to
set time.'%now)
315 radio.write_print(msg)
316 logger.log(msg)
317 else:
318 epoch = gps.get_datetime(last_rmc_message, override=True)
319 if epoch != None:
320 (y, m, d, hours, mins, secs) = epoch
321 tstr = '%02d%02d%02d%02d%04d.%02d'%(m, d, hours, mins, y, secs)
322 p = subprocess.Popen(['date', '--utc', tstr],
stdout=subprocess.PIPE, stderr=subprocess.PIPE)
323 results, err = p.communicate()
324 p.wait()
325 now = time.time() # need to update now
326 tstr = time.strftime('%Y-%m-%d %H:%M:%S', time.gmtime(now))
327 msg = '11 {:<100s}'.format('%d <rmc> received, syncing PI time
to RMC time (%s).'%(now, tstr))
328 radio.write_print(msg)
329 logger.log(msg)
330 got_gps_time = True
331 logger.rename_with_datetime(now) # update log file name
with date/time stamp in name
332 msg = '11 {:<100s}'.format('%d Payload <%s> relayed.'%(now,
'PLTIME %s'%tstr))
333 radio.write_print(msg)
334 payload.write('PLTIME %s'%tstr)
335
336 # Jah
337 # elif cmd_lower == 'wdog':
338 # USE_RTC_WATCHDOG = True
339 # msg = '11 {:<100s}'.format('%d watch dog timer enabled.'%now)
340 # radio.write_print(msg)
341 # logger.log(msg)
342
343 else:
344 # invalid command
345 msg = '11 {:<100s}'.format('%d command <%s> is invalid.'%(now,
cmd))
346 radio.write_print(msg)
347
```

```
348
349 # check if payload has something to relay to radio
350 payload_msg = payload.get_line()
351 if payload_msg != None:
352 payload_msg = payload_msg.strip()
353 logger.log(payload_msg)
354 radio.write_print(payload_msg)
355
356
357 # check MAX9611 IVT sensors for data
358 data = max9611.get_data()
359 if data != None:
360 max9611_data = copy.deepcopy(data)
361 fname = os.path.join('logs', 'max9611.log')
362 try:
363 if not os.path.exists(fname):
364 max9611_fp = open(fname, 'w')
365 s = 'EPOCH, Date/Time,'
366 for device in max9611.devices:
367 s += '%s T,%s V,%s I,'%(device, device, device)
368 max9611_fp.write(s + '\n')
369 else:
370 max9611_fp = open(fname, 'a')
371 s = '%1.3f, %s,'%(now, time.strftime('%Y-%m-%d %H:%M:%S',
time.gmtime(now)))
372 for device in max9611.devices:
373 s += '%d,%1.2f,%1.2f,'%(data[device]['T'], data[device]['V'],
data[device]['I'])
374 max9611_fp.write(s + '\n')
375 max9611_fp.close()
376 except IOError:
377 pass
378
379 # check ADS7828 for A/D data
380 data = ads7828.get_data()
381 if data != None:
382 ads7828_data = copy.deepcopy(data)
383
384 # check if release indicators need to send messages
385 if now - b_release_start_time < RELEASE_INDICATOR_TIME:
386 msg = "09 {:>10d} {:>+4.2f} B rel V".format(int(now),
ads7828_data[ADS7828.BALLOON_INDICATOR])
387 radio.write_print(msg)
388 logger.log(msg)
389 else:
390 b_release_start_time = 0 # reset it
391
392 if now - p_release_start_time < RELEASE_INDICATOR_TIME:
393 msg = "10 {:>10d} {:>+4.2f} P rel V".format(int(now),
ads7828_data[ADS7828.PARACHUTE_INDICATOR])
394 radio.write_print(msg)
395 logger.log(msg)
396 else:
397 p_release_start_time = 0 # reset it
398
```

```
399 if now - close_start_time < RELEASE_INDICATOR_TIME:
400 msg = "09 {:>10d} {:>+4.2f} B rel V".format(int(now),
ads7828_data[ADS7828.BALLOON_INDICATOR])
401 radio.write_print(msg)
402 logger.log(msg)
403 msg = "10 {:>10d} {:>+4.2f} P rel V".format(int(now),
ads7828_data[ADS7828.PARACHUTE_INDICATOR])
404 radio.write_print(msg)
405 logger.log(msg)
406 else:
407 close_start_time = 0 # reset it
408
409 gps_msg = gps.get_line()
410
411 if gps_msg != None:
412 led_message = False
413 if ("$GPGGA" in gps_msg):
414 msg = '11 {:<100s}'.format('%d %s'%(now, gps_msg.strip()))
415 logger.log(msg)
416 s = gps.parseGPS(gps_msg)
417 if s != '':
418 if now - last_GPS_no_fix > 10:
419 radio.write_print(s)
420 logger.log(msg)
421 last_GPS_no_fix = now
422 if s[0:2] != '11 ': # messages coming back with '11 ....' are
failures or GPGGA without a fix
423 # led.queue_message(M=4, N=0, repeat=True)
424 led_message = True
425 elif ("$GPRMC" in gps_msg):
426 last_rmc_message = gps_msg[:] # make a copy in case 'use_rmc'
command
sent
427 if now - last_GPRMC_time > GPRMC_INTERVAL:
428 msg = '11 {:<100s}'.format('%d %s'%(now, gps_msg.strip()))
429 radio.write_print(msg)
430 logger.log(msg)
431 last_GPRMC_time = now
432 if not got_gps_time:
433 epoch = gps.get_datetime(gps_msg)
434 if epoch != None:
435 (y, m, d, hours, mins, secs) = epoch
436 tstr = '%02d%02d%02d%02d%04d.%02d'%(m, d, hours, mins, y, secs)
437 p = subprocess.Popen(['date', '--utc', tstr],
stdout=subprocess.PIPE, stderr=subprocess.PIPE)
438 results, err = p.communicate()
439 p.wait()
440 now = time.time() # need to update now
441 msg = '11 {:<100s}'.format('%d GPS time synched.'%now)
442 radio.write_print(msg)
443 logger.log(msg)
444 got_gps_time = True
445 logger.rename_with_datetime(now) # update log file name
with date/time stamp in name
446 led.queue_message(M=3, N=0, repeat=True)
```

```
447 led_message = True
448 if not led_message:
449 led.queue_message(M=2, N=0, repeat=True) # GPS message but
neither of the 2 conditions above
450
451
452 # check for automatic balloon release
453 if gps.valid and balloon_release.is_altitude_too_high(gps.alt) and
not
alt_release_triggered:
454 alt_release_triggered = True
455 logger.log("Automatic balloon release, altitude (%d m) is above %d
m"
%(gps.alt, balloon_release.release_altitude))
456 actuators.b_release()
457 radio.write_print('11 {:<100s}'.format('%d altitude (%d m) above %d
m,
Balloon released'%(now, gps.alt, balloon_release.release_altitude)))
458 b_release_start_time = now
459 elif got_gps_time and balloon_release.is_release_time() and not
time_release_triggered: # no need to do this in addition to the one
above
460 time_release_triggered = True
461 logger.log("Automatic balloon release, elapsed time is greater than
%d
seconds"
%(flight_parameters.ELAPSED_FLIGHT_TIME_UNTIL_BALLOON_RELEASE))
462 actuators.b_release()
463 radio.write_print('11 {:<100s}'.format('%d elapsed time is greater
than %d
seconds, Balloon released'%(now,
flight_parameters.ELAPSED_FLIGHT_TIME_UNTIL_BALLOON_RELEASE)))
464 b_release_start_time = now
465
466
467 if now - last_times[1] > TEMPS_INTERVAL:
468 msg = "01 {:>10d} {:>+4d} {:>+4d} {:>+4d} {:>+4d} EPS TEMPS
C".format(int(now), ads7828_data['BAT_A'], ads7828_data['BAT_B'],
ads7828_data['PV_X'], ads7828_data['PV_Y'])
469 radio.write_print(msg)
470 logger.log(msg)
471 last_times[1] = now
472
473 if now - last_times[2] > TEMPS_INTERVAL:
474 msg = "02 {:>10d} {:>+4d} {:>+4d} {:>+4d} {:>+4d} {:>+4d} {:>+4d}
{:>+4d}
EPS TEMPS C".format(int(now), max9611_data['Battery_A']['T'],
max9611_data['Battery_B']['T'], max9611_data['PV_X']['T'],
max9611_data['PV_Y']['T'], max9611_data['Radio_EPS']['T'],
max9611_data['CDH_EPS']['T'], max9611_data['Payload']['T'])
475 radio.write_print(msg)
476 logger.log(msg)
477 last_times[2] = now
478
479 if now - last_times[3] > VOLTAGES_INTERVAL:
```

```
480 msg = "03 {:>10d} {:>+4.2f} {:>+4.2f} {:>+4.2f} {:>+4.2f} {:>+4.2f}
{:>+4.2f} {:>+4.2f} EPS VOLTS V".format(int(now),
max9611_data['Battery_A']['V'], max9611_data['Battery_B']['V'],
max9611_data['PV_X']['V'], max9611_data['PV_Y']['V'],
max9611_data['Radio_EPS']['V'], max9611_data['CDH_EPS']['V'],
max9611_data['Payload']['V'])
481 radio.write_print(msg)
482 logger.log(msg)
483 last_times[3] = now
484
485 if now - last_times[4] > CURRENTS_INTERVAL:
486 msg = "04 {:>10d} {:>+4.2f} {:>+4.2f} {:>+4.2f} {:>+4.2f} {:>+4.2f}
{:>+4.2f} {:>+4.2f} EPS CRNT A".format(int(now),
max9611_data['Battery_A']['I'], max9611_data['Battery_B']['I'],
max9611_data['PV_X']['I'], max9611_data['PV_Y']['I'],
max9611_data['Radio_EPS']['I'], max9611_data['CDH_EPS']['I'],
max9611_data['Payload']['I'])
487 radio.write_print(msg)
488 logger.log(msg)
489 last_times[4] = now
490
491 if now - last_times[5] > TEMPS_INTERVAL:
492 p = os.popen('vcgencmd measure_temp').readline()
493 cpu = int(float(p.replace("temp=","").replace("'C\n","")))
494 msg = "05 {:>10d} {:>+4d} {:>+4d} {:>+4d} CDH TEMPS
C".format(int(now),
max9611_data['CDH']['T'], max9611_data['Radio']['T'], cpu)
495 radio.write_print(msg)
496 logger.log(msg)
497 last_times[5] = now
498
499 if now - last_times[6] > VOLTAGES_INTERVAL:
500 msg = "06 {:>10d} {:>+4.2f} {:>+4.2f} CDH VOLTS V".format(int(now),
max9611_data['CDH']['V'], max9611_data['Radio']['V'])
501 radio.write_print(msg)
502 logger.log(msg)
503 last_times[6] = now
504
505 if now - last_times[7] > CURRENTS_INTERVAL:
506 msg = "07 {:>10d} {:>+4.2f} {:>+4.2f} CDH CRNT A".format(int(now),
max9611_data['CDH']['I'], max9611_data['Radio']['I'])
507 radio.write_print(msg)
508 logger.log(msg)
509 last_times[7] = now
510
511 if now - last_times[9] > ACTUATORS_INTERVAL:
512 msg = "09 {:>10d} {:>+4.2f} B rel V".format(int(now),
ads7828_data[ADS7828.BALLOON_INDICATOR])
513 radio.write_print(msg)
514 logger.log(msg)
515 last_times[9] = now
516
517 if now - last_times[10] > ACTUATORS_INTERVAL:
518 msg = "10 {:>10d} {:>+4.2f} P rel V".format(int(now),
ads7828_data[ADS7828.PARACHUTE_INDICATOR])
```

```
519 radio.write_print(msg)
520 logger.log(msg)
521 last_times[10] = now
522
523 if now - last_timemessage_time > TIMEMESSAGE_INTERVAL:
524 if got_gps_time:
525 msg = '11 {:<100s}'.format('%d %s (synched with GPS)'%(now,
time.strftime('%Y-%m-%d %H:%M:%S %Z')))
526 else:
527 msg = '11 {:<100s}'.format('%d %s (not synched with GPS)'%(now,
time.strftime('%Y-%m-%d %H:%M:%S %Z')))
528 radio.write_print(msg)
529 logger.log(msg)
530 last_timemessage_time = now
531
532 if now - last_storage_status_time > STORAGE_STATUS_INTERVAL:
533 data = sd.get_data()
534 if data != None:
535 (fs, size, used, avail, cap, mount) = data
536 avail = float(avail)/1024.0
537 sd_msg = 'SD available %1.2f Mbytes'%avail
538 if video_available:
539 if video_on:
540 sd_msg += ' (camera is ON)'
541 else:
542 sd_msg += ' (camera is OFF)'
543 else:
544 sd_msg += ' (NO camera detected)'
545 msg = '11 {:<100s}'.format('%d %s'%(now, sd_msg))
546 radio.write_print(msg)
547 logger.log(msg)
548 last_storage_status_time = now
549
550 time.sleep(0.01)
551
552
553 if __name__ == "__main__": # read from radio is not working
554 os.nice(-19) # run at highest priority
555 main()
556
```

C. BUS RADIO

```
1 from __future__ import print_function
2 import threading
3 import time
4 import Queue
5 import serial
6 import sys
7 import time
8
9
10 class RADIO(object):
11 def __init__(self, port, baudrate, eol='\x0A'):
12 self.eol = eol
```

```
13 self.buff = ""
14 self.ser = serial.Serial(port=port, baudrate=baudrate, bytesize=8,
parity='N',
stopbits=1, timeout=0, xonxoff=0, rtscts=0)
15 self.ser.flushInput()
16 self.ser.flushOutput()
17 self.queue = Queue.Queue()
18 self.thread = threading.Thread(target=self.enqueue_output,
args=(self.queue,))
19 self.thread.daemon = True
20 self.thread.start()
21
22
23 def enqueue_output(self, queue):
24 # run forever, looking for a line and putting it in the queue
25 while True:
26 queue.put(self.build_line()) # this blocks!
27
28
29 def build_line(self):
30 while True:
31 n = self.ser.inWaiting()
32 if n == 0:
33 time.sleep(0.05)
34 continue
35 data = self.ser.read(n)
36 # for d in data:
37 # print('%02X '%ord(d), end='')
38 # print()
39 self.buff = self.buff + data
40 i = self.buff.find(self.eol)
41 if i >= 0:
42 s = self.buff[:i]
43 self.buff = self.buff[i+len(self.eol):]
44 return s
45
46
47 def get_line(self, timeout=0.01):
48 try:
49 line = self.queue.get(timeout=timeout)
50 except Queue.Empty:
51 return None
52 else:
53 return line
54
55
56 def write(self, data, send_eol=False):
57 if send_eol:
58 self.ser.write(data+self.eol)
59 else:
60 self.ser.write(data)
61
62
63 def write_print(self, data, send_eol=False):
64 print(data)
```

```
65 self.write(data+'\r\n', send_eol)
66
67
68 if __name__ == "__main__":
69 # this only happens when this module is NOT imported, but is run as
'sudo python
radio.py'
70 radio = RADIO("/dev/ttyAMA0", 9600, '$')
71 # radio = RADIO("COM6", 9600, eol='@@@')
72
73 count = 0
74 while True:
75 no_msg = True
76
77 msg = radio.get_line() # this is NOT blocking!
78 if msg != None:
79 no_msg = False
80 tstr = time.strftime('%Y-%m-%d %H:%M:%S')
81 t = time.time()
82 print("%1.3f: %s" %(t, msg))
83 radio.write('%d'%count)
84 count += 1
85
86 if no_msg:
87 time.sleep(0.05)
88
```

D. BUS CAMERA

```
1 from __future__ import print_function
2 import os
3 import select
4 import socket
5 import threading
6 import time
7
8 import picamera
9
10 CAMERA_PORT = 12345 # UDP port for camera on/off messages
11 VIDEO_DST = 'videos'
12
13 BITRATE = int(10E6)
14 QUALITY = int(30)
15 VIDEO_SEGMENT_LENGTH_SECS = 60*2
16 #VIDEO_SEGMENT_LENGTH_SECS = 15
17 #VIDEO_SEGMENT_LENGTH_SECS = 60*1
18
19
20 #Default: 37.16 Mb 46 sec ==> 827214 bytes/sec ~ 827 kbytes/sec
21 # 49.6 Mb/min, 2.98 Gb/hour
22
23 #bitrate=10E6, quality=30: 7.737 Mb 58 sec ==> 136600 bytes/sec ~140
kbytes/sec
24 # 8.4 Mb/min, 504 Mb/hour
25
```

```
#bitrate=8E6, quality=30: 10.478 Mb 121 sec ==> 88588 bytes/sec ~90
kbytes/sec
# 5.4 Mb/min, 324 Mb/hour

#bitrate=8E6, quality=35: 4.097 Mb 65 sec ==> 64402 bytes/sec ~65
kbytes/sec
# 3.9 Mb/min, 234 Mb/hour


def do_video(Pi_camera, camera_semaphore, time_length):
picture_thread = threading.Thread(target=take_video,
args=(Pi_camera,
camera_semaphore, time_length))
picture_thread.start()


def take_video(camera, camera_semaphore, time_length):
t = time.time()
tstr = time.strftime('%Y-%m-%d_%H-%M-%S-%Z.h264')
fpath = os.path.join('videos', tstr)
found = False
if os.path.exists(fpath):
# file exists, try some variants
found = True # assume found until otherwise (which might not happen)
for i in range(0, 20):
fpath = os.path.join('images', time.strftime('%Y-%m-%d_%H-%M-%S-
%Z.h264') +
'-%d.h264'%i)
if not os.path.exists(fpath):
found = False
break
if found:
return

if not camera_semaphore.acquire(False):
return
try:
camera.start_recording(fpath)
camera.wait_recording(time_length)
camera.stop_recording(fpath)
# convert .h264 to mp4 with: MP4Box -fps 30 -add video.h264
video.mp4
except:
pass
camera_semaphore.release()


def do_picture(Pi_camera, camera_semaphore):
picture_thread = threading.Thread(target=take_picture,
args=(Pi_camera,
camera_semaphore))
picture_thread.start()


def take_picture(camera, camera_semaphore):
```

```
72 t = time.time()
73 tstr = time.strftime('%Y-%m-%d_%H-%M-%S-%Z.jpg')
74 fpath = os.path.join('images', tstr)
75 found = False
76 if os.path.exists(fpath):
77 # file exists, try some variants
78 found = True # assume found until otherwise (which might not happen)
79 for i in range(0, 20):
80 fpath = os.path.join('images', time.strftime('%Y-%m-%d_%H-%M-%S-%Z')
+
'-%d.jpg'%i)
81 if not os.path.exists(fpath):
82 found = False
83 break
84 if found:
85 return
86
87 if not camera_semaphore.acquire(False):
88 return
89 try:
90 camera.capture(fpath)
91 except:
92 pass
93 camera_semaphore.release()
94
95
96 def wait_to_start(server):
97 while True:
98 msg, address = server.recvfrom(1024)
99 if 'video_on' in msg:
100 print('Starting video')
101 return
102
103
104 def is_stop_recording(server):
105 (rd, wr, err) = select.select([server], [], [], 1)
106 if server in rd:
107 msg, address = server.recvfrom(1024)
108 if 'video_off' in msg:
109 print('Stopping video')
110 return True
111 return False
112
113
114 def is_camera_running():
115 try:
116 camera = picamera.PiCamera()
117 except:
118 return False
119 else:
120 camera.close()
121 return True
122
123
124 def main():
```

```
125 server = socket.socket(socket.AF_INET, socket.SOCK_DGRAM)
126 # server.setblocking(0)
127 server.bind(('localhost', CAMERA_PORT))
128
129 camera = picamera.PiCamera()
130 camera.resolution = (640, 480)
131 camera.framerate = 90
132
133 while True:
134 recording = False
135 wait_to_start(server)
136
137 recording = True
138 while recording:
139 tstr = time.strftime('%Y-%m-%d_%H-%M-%S-%Z.h264')
140 fpath = os.path.join(VIDEO_DST, tstr)
141 tstart = time.time()
142 camera.start_recording(fpath) # bitrate=BITRATE, quality=QUALITY)
143 while time.time() - tstart < VIDEO_SEGMENT_LENGTH_SECS:
144 camera.wait_recording(1)
145 if is_stop_recording(server):
146 recording = False
147 break
148 camera.stop_recording()
149
150
151 if __name__ == "__main__": # read from radio is not working
152 main()
153
```

E. PAYLOAD STARTUP

```
1 from __future__ import print_function
2 import os
3 import subprocess
4 import shlex
5 import time
6 import traceback
7
8 import camera
9
10 #systemd notes:
11 # /etc/systemd/system/HAB.services is used to make this program
start up after reboot
12 # sudo systemctrl enable HAB.service
13 # sudo systemctrl start HAB.service
14
15
16 def main():
17 pnames = ["/usr/bin/python camera.py", "/usr/bin/python radio.py"]
18
19 processes = []
20 for pname in pnames:
21 processes.append(subprocess.Popen(shlex.split(pname),
stdin=subprocess.PIPE))
```

```
22
23 # when starting the process wait a bit longer for it to start
24 time.sleep(3)
25 start = time.time()
26 while True:
27 for process in processes:
28 if process.poll() != None:
29 process = subprocess.Popen(shlex.split(pname),
stdin=subprocess.PIPE)
30 time.sleep(1)
31
32
33
########################################################################
########
34
########################################################################
########
35
########################################################################
########
36
37 if __name__ == "__main__":
38 while (True):
39 try:
40 main()
41 except:
42 s = traceback.format_exc()
43 fp = open("start_traceback.txt", "a")
44 fp.write(s+"\n")
45 fp.close()
```

F. PAYLOAD RADIO

```
1 #!/usr/bin/env python2
2 # -*- coding: utf-8 -*-
3 ##################################################
4 # GNU Radio Python Flow Graph
5 # Title: RDCS_Relay_Final_Headlessv3
6 # Generated: Wed Feb 6 15:38:12 2019
7 ##################################################
8
9 from gnuradio import analog
10 from gnuradio import eng_notation
11 from gnuradio import filter
12 from gnuradio import gr
13 from gnuradio import uhd
14 from gnuradio.eng_option import eng_option
15 from gnuradio.filter import firdes
16 from optparse import OptionParser
17 import time
18
19
20 class RDCS_Relay_Final_Headlessv3(gr.top_block):
21
```

```
22 def __init__(self):
23 gr.top_block.__init__(self, "RDCS_Relay_Final_Headlessv3")
24 
25 ##################################################
26 # Variables
27 ##################################################
28 self.tx_gain = tx_gain = 72
29 self.tx_freq = tx_freq = 435000000
30 self.squelch = squelch = -45
31 self.samp_rate = samp_rate = 88000
32 self.rx_gain = rx_gain = 30
33 self.rx_freq = rx_freq = 144600000
34 self.AGC_ref = AGC_ref = 0.24
35 
36 ##################################################
37 # Blocks
38 ##################################################
39 self.uhd_usrp_source_0 = uhd.usrp_source(
40 ",".join(("", "")),
41 uhd.stream_args(
42 cpu_format="fc32",
43 channels=range(1),
44 ),
45 )
46 self.uhd_usrp_source_0.set_samp_rate(samp_rate)
47 self.uhd_usrp_source_0.set_center_freq(rx_freq, 0)
48 self.uhd_usrp_source_0.set_gain(rx_gain, 0)
49 self.uhd_usrp_source_0.set_antenna('RX2', 0)
50 self.uhd_usrp_source_0.set_bandwidth(200000, 0)
51 self.uhd_usrp_sink_0 = uhd.usrp_sink(
52 ",".join(("", "")),
53 uhd.stream_args(
54 cpu_format="fc32",
55 channels=range(1),
56 ),
57 )
58 self.uhd_usrp_sink_0.set_samp_rate(samp_rate)
59 self.uhd_usrp_sink_0.set_center_freq(tx_freq, 0)
60 self.uhd_usrp_sink_0.set_gain(tx_gain, 0)
61 self.uhd_usrp_sink_0.set_antenna('TX/RX', 0)
62 self.uhd_usrp_sink_0.set_bandwidth(5000, 0)
63 self.low_pass_filter_0 = filter.fir_filter_ccf(1, firdes.low_pass(
64 1, samp_rate, 5000, 500, firdes.WIN_HAMMING, 6.76))
65 self.analog_pwr_squelch_xx_0 = analog.pwr_squelch_cc(squelch, 1e-4,
0, True)
66 self.analog_agc_xx_0 = analog.agc_cc(1e-4, AGC_ref, 1)
67 self.analog_agc_xx_0.set_max_gain(100e3)
68 
69 ##################################################
70 # Connections
71 ##################################################
72 self.connect((self.analog_agc_xx_0, 0), (self.uhd_usrp_sink_0, 0))
73 self.connect((self.analog_pwr_squelch_xx_0, 0),
(self.analog_agc_xx_0, 0))
```

```
74 self.connect((self.low_pass_filter_0, 0),
(self.analog_pwr_squelch_xx_0, 0))
75 self.connect((self.uhd_usrp_source_0, 0), (self.low_pass_filter_0,
0))
76
77 def get_tx_gain(self):
78 return self.tx_gain
79
80 def set_tx_gain(self, tx_gain):
81 self.tx_gain = tx_gain
82 self.uhd_usrp_sink_0.set_gain(self.tx_gain, 0)
83
84
85 def get_tx_freq(self):
86 return self.tx_freq
87
88 def set_tx_freq(self, tx_freq):
89 self.tx_freq = tx_freq
90 self.uhd_usrp_sink_0.set_center_freq(self.tx_freq, 0)
91
92 def get_squelch(self):
93 return self.squelch
94
95 def set_squelch(self, squelch):
96 self.squelch = squelch
97 self.analog_pwr_squelch_xx_0.set_threshold(self.squelch)
98
99 def get_samp_rate(self):
100 return self.samp_rate
101
102 def set_samp_rate(self, samp_rate):
103 self.samp_rate = samp_rate
104 self.uhd_usrp_source_0.set_samp_rate(self.samp_rate)
105 self.uhd_usrp_sink_0.set_samp_rate(self.samp_rate)
106 self.low_pass_filter_0.set_taps(firdes.low_pass(1, self.samp_rate,
5000, 500,
firdes.WIN_HAMMING, 6.76))
107
108 def get_rx_gain(self):
109 return self.rx_gain
110
111 def set_rx_gain(self, rx_gain):
112 self.rx_gain = rx_gain
113 self.uhd_usrp_source_0.set_gain(self.rx_gain, 0)
114
115
116 def get_rx_freq(self):
117 return self.rx_freq
118
119 def set_rx_freq(self, rx_freq):
120 self.rx_freq = rx_freq
121 self.uhd_usrp_source_0.set_center_freq(self.rx_freq, 0)
122
123 def get_AGC_ref(self):
124 return self.AGC_ref
```

```
125
126 def set_AGC_ref(self, AGC_ref):
127 self.AGC_ref = AGC_ref
128 self.analog_agc_xx_0.set_reference(self.AGC_ref)
129
130
131 def main(top_block_cls=RDCS_Relay_Final_Headlessv3, options=None):
132
133 tb = top_block_cls()
134 tb.start()
135 try:
136 raw_input('Press Enter to quit: ')
137 except EOFError:
138 pass
139 tb.stop()
140 tb.wait()
141
142
143 if __name__ == '__main__':
144 main()
    145
```

G. PAYLOAD CAMERA

```
1 from __future__ import print_function
2 import os
3 import time
4 import traceback
5
6 import picamera
7
8 VIDEO_DST = 'videos'
9
10 BITRATE = int(10E6)
11 QUALITY = int(30)
12
13 VIDEO_SEGMENT_LENGTH_SECS = 60*2 # in seconds
14
15
16 #Default: 37.16 Mb 46 sec ==> 827214 bytes/sec ~ 827 kbytes/sec
17 # 49.6 Mb/min, 2.98 Gb/hour
18
19 #bitrate=10E6, quality=30: 7.737 Mb 58 sec ==> 136600 bytes/sec ~140
kbytes/sec
20 # 8.4 Mb/min, 504 Mb/hour
21
22 #bitrate=8E6, quality=30: 10.478 Mb 121 sec ==> 88588 bytes/sec ~90
kbytes/sec
23 # 5.4 Mb/min, 324 Mb/hour
24
25 #bitrate=8E6, quality=35: 4.097 Mb 65 sec ==> 64402 bytes/sec ~65
kbytes/sec
26 # 3.9 Mb/min, 234 Mb/hour
27
```

```
28
29 def main():
30 if not os.path.isdir(VIDEO_DST):
31 os.mkdir(VIDEO_DST)
32
33 camera = picamera.PiCamera()
34 camera.resolution = (1920, 1080)
35 camera.framerate=30
36
37 while True:
38 tstr = time.strftime('%Y-%m-%d_%H-%M-%S-%Z.h264')
39 fpath = os.path.join(VIDEO_DST, tstr)
40 tstart = time.time()
41 camera.start_recording(fpath)
42 while time.time() - tstart < VIDEO_SEGMENT_LENGTH_SECS:
43 camera.wait_recording(1)
44 camera.stop_recording()
45
46
47 if __name__ == "__main__": # read from camera is not working
48 try:
49 main()
50 except:
51 s = traceback.format_exc()
52 fp = open("camera_traceback.txt", "a")
53 fp.write(s+"\n")
54 fp.close()
55
```

APPENDIX H. FINAL GNU RADIO FLOW GRAPH

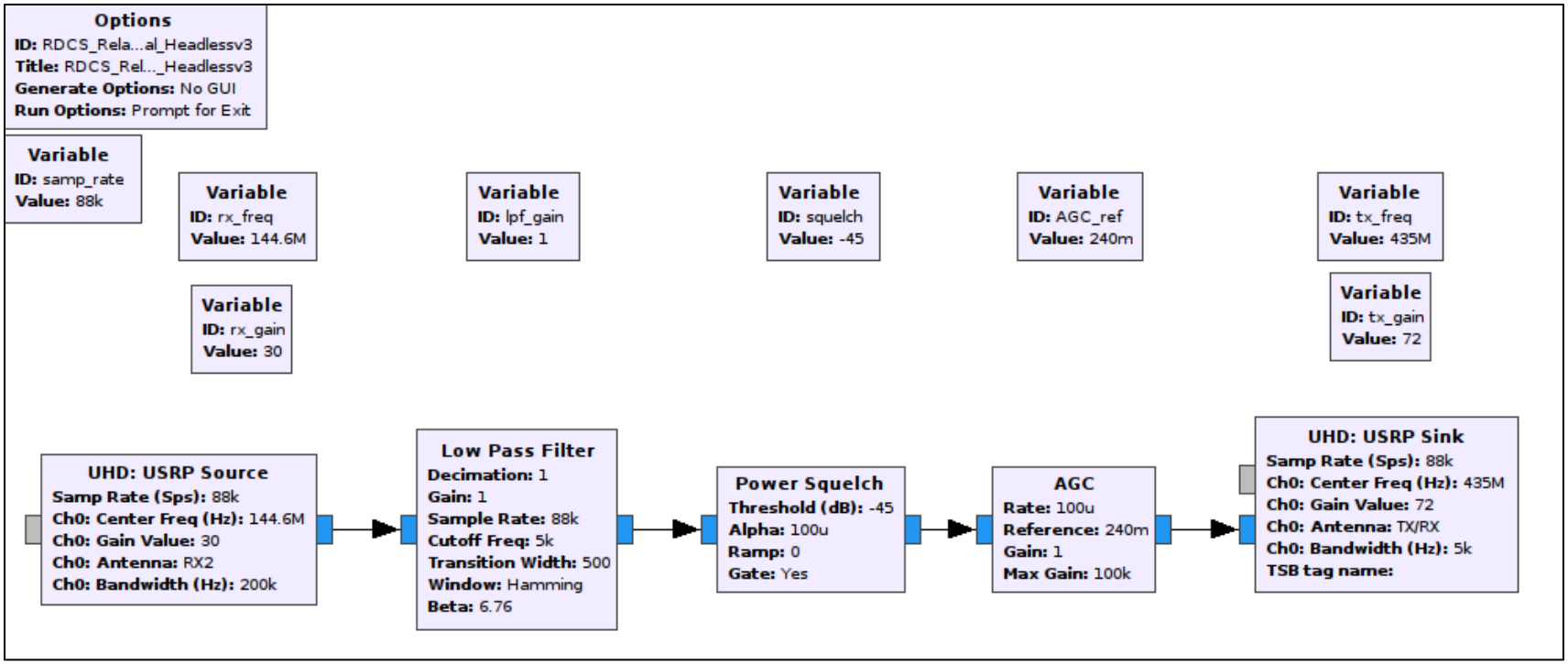

THIS PAGE INTENTIONALLY LEFT BLANK

APPENDIX I. RANDOM VIBRATION ANALYSIS CODE

The program is designed to read the xls file generated by the shaker table and analyze the data to determine random vibration response

Initial workspace

Program clears variables, the workspace, and formats compact

```
clear, clc, format compact;
```

Import Raw Data

```
[file,path] = uigetfile({'*.xls'},'Select Data File (Random Vibration)'); % Select Data
thrust_data = xlsread(file,1);      % Defining the data array (Thrust Axis)
x_data = xlsread(file,2);           % Defining the data array (X Axis)
y_data = xlsread(file,3);           % Defining the data array (Y Axis)
```

Assign Data from Excel Spreadsheet

```
% Frequency
freqs = thrust_data(:,1); % Define Random Vibe Frequencies
NASA_f = [20;2000]; % Sounding Rocket Qualification Profile

% Assign NASA Standards Data
NASA_ASD_thrust = [0.051 0.051]; % Sounding Rocket Qualification Profile
NASA_ASD_xy = [0.029 0.029]; % Sounding Rocket Qualification Profile

% Thrust Axis
thrust_control = thrust_data(:,3);
thrust_zenith = thrust_data(:,30);
thrust_payloadplus = thrust_data(:,33);
thrust_payloadminus = thrust_data(:,42);
thrust_nadir = thrust_data(:,57);

% X Axis
x_control = x_data(:,3);
x_zenith = x_data(:,24);
x_payloadplus = x_data(:,36);
x_payloadminus = x_data(:,45);
x_nadir = x_data(:,54);

% Y Axis
y_control = y_data(:,3);
y_zenith = y_data(:,27);
y_payloadplus = y_data(:,39);
```

```
y_payloadminus = y_data(:,48);
y_nadir = y_data(:,51);
```

Plot Standard Profile Against Control Data

```
% Thrust Axis
figure(1)
loglog(NASA_f,NASA_ASD_thrust,freqs,thrust_control,freqs,thrust_zenith,...
    freqs,thrust_payloadplus,freqs,thrust_payloadminus,freqs,thrust_nadir),
xlabel('Frequency [Hz]'), ylabel('ASD [G^2/Hz]'),
title('Thrust Axis Random Vibration Standards vs Control & Response'),
legend('NASA','Control', 'Zenith', 'Payload +Y', 'Payload -Y', 'Nadir')

% X Axis
figure(2)
loglog(NASA_f,NASA_ASD_xy,freqs,x_control,freqs,x_zenith,...
    freqs,x_payloadplus,freqs,x_payloadminus,freqs,x_nadir),
xlabel('Frequency [Hz]'), ylabel('ASD [G^2/Hz]'),
title('X Axis Random Vibration Standards vs Control & Response'),
legend('NASA','Control', 'Zenith', 'Payload +Y', 'Payload -Y', 'Nadir')

% Y Axis
figure(3)
loglog(NASA_f,NASA_ASD_xy,freqs,y_control,freqs,y_zenith,...
    freqs,y_payloadplus,freqs,y_payloadminus,freqs,y_nadir),
xlabel('Frequency [Hz]'), ylabel('ASD [G^2/Hz]'),
title('Y Axis Random Vibration Standards vs Control & Response'),
legend('NASA','Control', 'Zenith', 'Payload +Y', 'Payload -Y', 'Nadir')
```

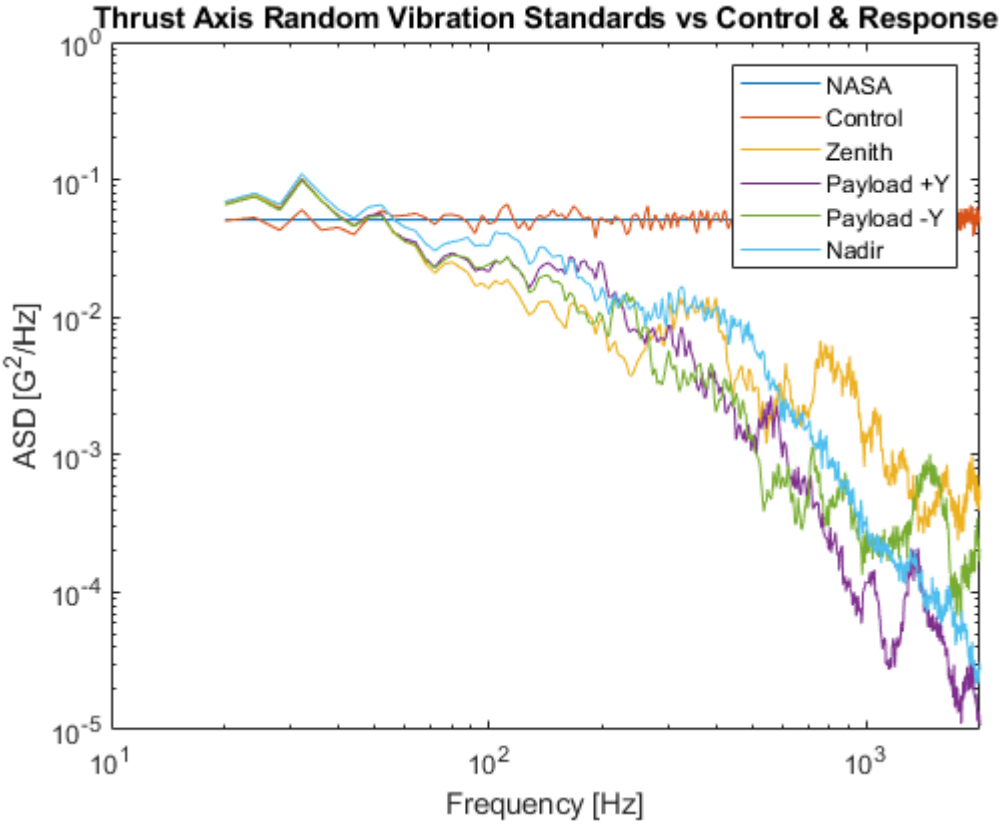
Thrust Axis Random Vibration Standards vs Control & Response
NASA
Control
Zenith
Payload +Y
Payload -Y
Nadir
ASD [G^2/Hz]
Frequency [Hz]

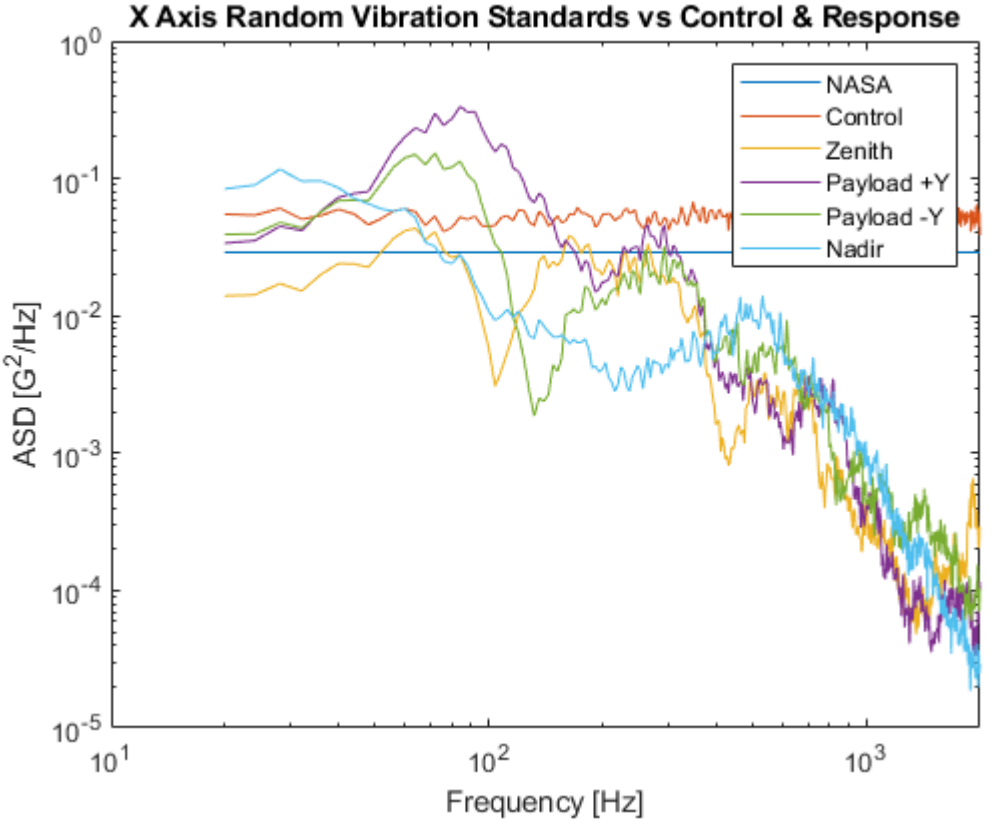
X Axis Random Vibration Standards vs Control & Response
NASA
Control
Zenith
Payload +Y
Payload -Y
Nadir
ASD [G^2/Hz]
Frequency [Hz]

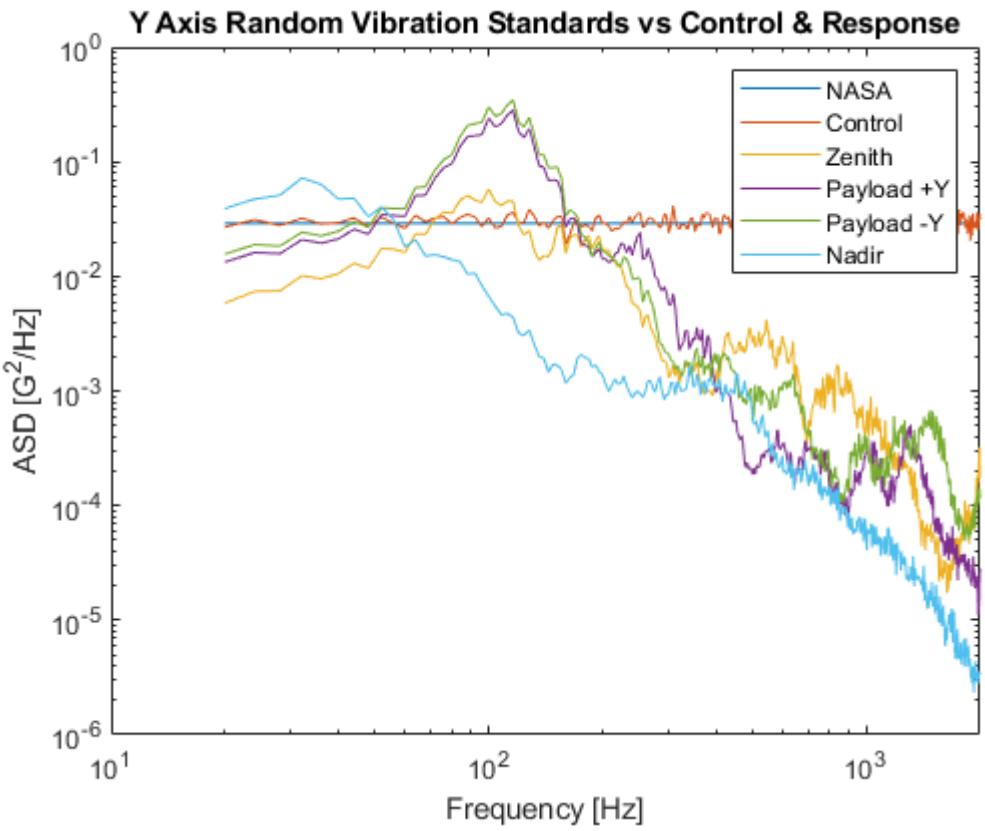

Calculate Max Error

```
% Thrust Axis
thrust_error = thrust_data(:,5);
thrust_error_max = max(thrust_error);
thrust_error_min = min(thrust_error);

if thrust_error_max > 3 | thrust_error_min < -3
    thrust_margin= 'N';
else
    thrust_margin = 'Y';
end

% X Axis
x_error = x_data(:,5);
x_error_max = max(x_error);
x_error_min = min(x_error);

if x_error_max > 3 | x_error_min < -3
    x_margin= 'N';
else
    x_margin = 'Y';
end

% Y Axis
```

```
y_error = y_data(:,5);
y_error_max = max(y_error);
y_error_min = min(y_error);

if y_error_max > 3 | y_error_min < -3
    y_margin= 'N';
else
    y_margin = 'Y';
end
```

Calculate Response GRMS

```
% Thrust Axis
thrust_control_Grms = sqrt(trapz(freqs,thrust_control));
thrust_zenith_Grms = sqrt(trapz(freqs,thrust_zenith));
thrust_payloadplus_Grms = sqrt(trapz(freqs,thrust_payloadplus));
thrust_payloadminus_Grms = sqrt(trapz(freqs,thrust_payloadminus));
thrust_nadir_Grms = sqrt(trapz(freqs,thrust_nadir));

% X Axis
x_control_Grms = sqrt(trapz(freqs,x_control));
x_zenith_Grms = sqrt(trapz(freqs,x_zenith));
x_payloadplus_Grms = sqrt(trapz(freqs,x_payloadplus));
x_payloadminus_Grms = sqrt(trapz(freqs,x_payloadminus));
x_nadir_Grms = sqrt(trapz(freqs,x_nadir));

% Y Axis
y_control_Grms = sqrt(trapz(freqs,y_control));
y_zenith_Grms = sqrt(trapz(freqs,y_zenith));
y_payloadplus_Grms = sqrt(trapz(freqs,y_payloadplus));
y_payloadminus_Grms = sqrt(trapz(freqs,y_payloadminus));
y_nadir_Grms = sqrt(trapz(freqs,y_nadir));
```

Calculate Amplification Factor

```
% Thrust Axis
thrust_zenith_AF_db = 10*log(thrust_zenith_Grms^2/thrust_control_Grms^2);
thrust_payloadplus_AF_db = 10*log(thrust_payloadplus_Grms^2/thrust_control_Grms^2);
thrust_payloadminus_AF_db = 10*log(thrust_payloadminus_Grms^2/thrust_control_Grms^2);
thrust_nadir_AF_db = 10*log(thrust_nadir_Grms^2/thrust_control_Grms^2);

% X Axis
x_zenith_AF_db = 10*log(x_zenith_Grms^2/x_control_Grms^2);
x_payloadplus_AF_db = 10*log(x_payloadplus_Grms^2/x_control_Grms^2);
x_payloadminus_AF_db = 10*log(x_payloadminus_Grms^2/x_control_Grms^2);
x_nadir_AF_db = 10*log(x_nadir_Grms^2/x_control_Grms^2);

% y Axis
y_zenith_AF_db = 10*log(y_zenith_Grms^2/y_control_Grms^2);
y_payloadplus_AF_db = 10*log(y_payloadplus_Grms^2/y_control_Grms^2);
```

```
y_payloadminus_AF_db = 10*log(y_payloadminus_Grms^2/y_control_Grms^2);
y_nadir_AF_db = 10*log(y_nadir_Grms^2/y_control_Grms^2);
```

Display Values

```
fprintf('                          RESULTS\n')
fprintf('Error (dB): \n')
fprintf('                         Thrust Axis    X Axis     Y Axis\n')
fprintf('  Maximum                      %3.3f     %3.3f      %3.3f\n',
thrust_error_max,x_error_max,y_error_max)
fprintf('  Minimum                     %3.3f    %3.3f     %3.3f\n',
thrust_error_min,x_error_min,y_error_min)
fprintf('  Within +/- 3dB Margin           ')
if thrust_margin == 'Y'
    fprintf('Y')
else
    fprintf('N')
end

if x_margin == 'Y'
    fprintf('         Y')
else
    fprintf('           N')
end

if y_margin == 'Y'
    fprintf('          Y')
else
    fprintf('          N')
end
fprintf('\n\n-------------------------------------------------------\n\n')
fprintf('Response (Grms):\n')
fprintf('             Thrust Axis     X Axis     Y Axis\n')
fprintf('  Control           %4.1f       %4.1f       %4.1f\
n',thrust_control_Grms,x_control_Grms,y_control_Grms)
fprintf('  Zenith            %4.1f       %4.1f       %4.1f\
n',thrust_zenith_Grms,x_zenith_Grms,y_zenith_Grms)
fprintf('  Payload +Y        %4.1f       %4.1f       %4.1f\
n',thrust_payloadplus_Grms,x_payloadplus_Grms,y_payloadplus_Grms)
fprintf('  Payload -Y        %4.1f       %4.1f       %4.1f\
n',thrust_payloadminus_Grms,x_payloadminus_Grms,y_payloadminus_Grms)
fprintf('  Nadir             %4.1f       %4.1f       %4.1f\
n',thrust_nadir_Grms,x_nadir_Grms,y_nadir_Grms)
fprintf('\n-------------------------------------------------------\n\n')
fprintf('Amplification Factors (dB)\n')
fprintf('              Thrust Axis     X Axis     Y Axis\n')
fprintf('  Zenith           %3.2f     %3.2f     %3.2f\n',thrust_zenith_AF_db,
x_zenith_AF_db,y_zenith_AF_db)
fprintf('  Payload +Y       %3.2f     %3.2f     %3.2f\
n',thrust_payloadplus_AF_db,x_payloadplus_AF_db,y_payloadplus_AF_db)
fprintf('  Payload -Y       %3.2f     %3.2f     %3.2f\
```

```
n',thrust_payloadminus_AF_db,x_payloadminus_AF_db,y_payloadminus_AF_db)
fprintf('  Nadir            %3.2f     %3.2f     %3.2f\
n',thrust_nadir_AF_db,x_nadir_AF_db,y_nadir_AF_db)
```

```
                        RESULTS
Error (dB):
                       Thrust Axis    X Axis     Y Axis
  Maximum                    1.244     1.353      1.544
  Minimum                   -1.613    -1.835     -1.838
  Within +/- 3dB Margin          Y         Y          Y

-----------------------------------------------------

Response (Grms):
             Thrust Axis     X Axis     Y Axis
  Control           10.1       10.1        7.6
  Zenith             3.0        2.9        2.5
  Payload +Y         2.8        5.1        4.2
  Payload -Y         2.7        3.8        4.5
  Nadir              3.3        3.0        1.8

-----------------------------------------------------

Amplification Factors (dB)
              Thrust Axis     X Axis     Y Axis
  Zenith           -24.14     -24.98     -22.12
  Payload +Y       -25.65     -13.57     -12.20
  Payload -Y       -26.53     -19.79     -10.52
  Nadir            -22.23     -24.21     -29.44
```

THIS PAGE INTENTIONALLY LEFT BLANK

APPENDIX J. FUNCTIONAL CHECK PROCEDURES

Equipment/Supplies

- 1 x RDCS
- 2 x Green Radios with antennas, including attenuators for tx and rx side
- 1 x Power Supply (or wall power)
- 1 x Laptop (Chase 1)
  - Configured for Cosmos to receive telemetry
    - MHX Radio plugged into Chase 1 and power source
  - Configured for wifi access to RDCS
- 1 x Hex key to power on RDCS

Ground Station Setup (One time requirement)	
Step	Completion
1. Setup Green Radios Outside Clean Room	
a) Radio A: Receive Radio Configuration	
-Attach 40 dB attenuator rigging to radio	
-Set rotary attenuator to 70 dB	
-Attach CB Antenna labeled “Radio A”	
-Turn on Radio A, set to Channel 4 (Rx Frequency 435.0 MHz)	
b) Radio B: Transmit Radio Configuration	
-Attach attenuators (110 dB of attenuation)	
-Attach CB Antenna labeled “Radio B”	
-Turn on Radio B, set to Channel 6 (Tx Frequency 144.6 MHz)	
-Ensure transmit power = low = 30 dBm	
2. Setup Ground station	
a) Chase 1	
-Plug in Chase 1 to power supply and place on desk	
-Log in as SSAG Admin	
-Open Cosmos	
-Select HAB, Standby for telemetry	
b) Turn on	
-Connect MHX to Chase 1. Ensure it is plugged into “data”	

-Connect MHX to power supply	
-Check lights on front of MHX to verify power. Shouldn't see RSSI lights yet	

RDCS				
Step	Pre Thrust Axis	Post Thrust Axis	Post Lateral X Axis	Post Lateral Y Axis
1. Power on RDCS with hex key				
a) BATT A: LED above switch with illuminate like C&DH				
b) BATT B: LED below switch will have steady light				
2. After ~1 minute, RDCS wifi should be visible on device (SSAGPI-001)				
a) Connect to SSAGPI-001 Wireless Network (RDCS Wifi)				
b) Terminus into RDCS command line on phone				
c) Verify startup script is running with command >>ps ax|grep python				
d) Verify radio script is running only once				

Telemetry				
Step	Pre Thrust Axis	Post Thrust Axis	Post Lateral X Axis	Post Lateral Y Axis
1. Verify telemetry received from RDCS				
a) BATT A Health and Status (I,V, Temp)				
b) BATT B Health and Status (I,V, Temp)				
c) GPS Status				

RF Performance				
Step	Pre Thrust Axis	Post Thrust Axis	Post Lateral X Axis	Post Lateral Y Axis
1. Verify RF performance				
a) Transmit on Radio B, 144.6 MHz				
b) Receive on Radio A, 435.0 MHz				
c) Verify "Loud and Clear"				

Camera and Video Performance				
Step	Pre Thrust Axis	Post Thrust Axis	Post Lateral X Axis	Post Lateral Y Axis
1. Verify Bus Camera and Video Performance				
a) Connect to HAB-BusOct18 wifi				
b) Login to HAB via Terminus				
c) Navigate to HAB/videos				
d) Use Terminus to verify videos were recorded at proper interval				
2. Verify Payload Camera and Video Performance				
a) Connect to SSAGPI-001 wifi				
b) Login to RDCS via terminus				
c) Navigate to /home/pi/payload/videos				
d) Use Terminus to verify videos were recorded at proper intervals				

Functional Check Matrix		
Component	Procedure	Step
Structure	Visual Inspection	Checklist
FingerTech Switches	Power On	RDCS 1
BATT A	Power On	RDCS 1.a
BATT B	Power On	RDCS 1.b
EPS	Power On	RDCS 1
C&DH	Telemetry	Telemetry 1
Raspberry Pi 3 (Payload)	Wifi Signal	RDCS 2
GPS	Telemetry	Telemetry 1
Battery Health (I,V)	Telemetry	Telemetry 1
Battery Temperature Switch	Telemetry	Telemetry 1
B205 Mini	Green Radio TX/RX	RF 3
GNURadio Script	Green Radio TX/RX	RF 4
LNA	Green Radio TX/RX	RF 4
Wideband Amplifier	Green Radio TX/RX	RF 4
Bus Camera (vertical)	Check Vidoes	Videos 1
Payload Camera (horizontal)	Check Vidoes	Videos 2
VHF Antenna	Visual Inspection/RX	RF 4
UHF Antenna	Visual Inspection/TX	RF 4
C&DH Antenna	Visual Inspection/Telemetry	Telemetry 1
Spot Tracker	Check App	SPOT 3

Settings and Configurations

1. **RDCS Raspberry Pi Payload Controller**
   Wifi Name: ssagpi-001
   Password: check sticker
   Terminus Settings:
   Host: 192.168.1.1
   Password: check sticker

2. **HAB Raspberry Pi Zero Bus Master Controller**
   Wifi Name: HAB-Bus-Oct18
   Password: check sticker
   Terminus Settings
   Host: 192.168.1.1
   Username: pi
   Password: check sticker

3. **Laptop Computer**
   User name: .\ssagadmin
   Password: check the sticker
   Double click COSMOS
   Then double click HAB

4. **Spot Trace Information**
   Website: https://login.findmespot.com/spot-main-web/myaccount/
   User name: NPS_SSAG
   Password: check documentation
   Serial: SSAGTrace1
   Tracking app: The SPOT App

APPENDIX K. PRE-LAUNCH CHECKLIST

L-72 hours, Wednesday, 20 February: Make Preparations

Task	POC	Initial When Complete, Date/Time
Conduct Flight Readiness Review	John, Dillon	
Distribute Recall Roster	John, Dillon	
Conduct HAB HUB analysis	John	
Locate and test power inverter in vehicle	Alex	
Review launch day procedures	John, Dillon	
Charge Green Radio Batteries	John	
Charge Jolly Logic Release Mechanism	John	
Charge Hand-Held Radios	Alex	
Replace SPOT Gen3 Batteries	Alex	
Attach tag to RDCS with contact information	John	
Charge BigRedBee Batteries	Dillon	
Charge TeleMega Batteries	Dillon	
Chage GoPros (3 x session, 3 x various)	Dillon	
Call John Newman to coordinate propellant delivery and facility occupation	Dillon	

L-48 hours, Thursday, 21 February: Pack

Task	POC	Initial When Complete, Date/Time
Pack everything		
Review launch day procedures	John, Dillon	
Conduct HAB HUB analysis	John	
Create group text	Dillon	

L-24 hours, Friday, 22 February, Travel

Team Member	**Transpo**	**4WD**	**Location**
Alex Savattone	POV	Yes	FAR
David Rigmaiden	POV	Yes	FAR
Dillon Pierce	RV	No	FAR
Giovanni Minelli	POV	No	FAR
John Pross	Rental	Yes	FAR
Levi Owen	POV	Yes	FAR
Noah Weitz	POV	Yes	FAR
Wenschel Lan			FAR
Greg Bischoff	POV	No	China Lake
Patrick Dionne	POV	No	FAR

L-24 hours, Friday, 22 February, Launch Setup

Task	POC	Initial When Complete, Date/Time
Call John Newman to coordinate propellant delivery and facility occupation	Dillon	
Coordinate with RocketLab personnel for launch setup delivery / launch time	Dillon	
Setup Launch Rails	Dillon	
Conduct RDCS Functional Test	John	
Review launch day procedures and assigned roles		
Conduct HAB HUB analysis to determine launch time	John	
Text Greg Bischoff Launch time	John	
Help unload vehicles		
Setup ground station table		
Setup base station antenna	David	
Ensure SPOT Gen3 trackers in chase vehicles		
Setup launch equipment	Dillon	
Construct Rocket Motor	Dillon	
Verify Flight Computer Configurations ☐ Verify primary TeleMega (S/N 4268) o Drogue Deploy: Apogee o Apogee Lockout: 10 sec o Main Deploy: 450m o Tx Freq.: 434.550 MHz o Callsign: K6NPS o Telemetry Rate: 38400 baud ☐ Verify backup TeleMega (S/N 4290) o Drogue Deploy: Apogee + 3 sec o Apogee Lockout: 10 sec o Main Deploy: 400m o Tx Freq.: Not Enabled ☐ Verify EasyMini (S/N 4595) o Mode: Redundant Apogee o Apogee Delay: Apogee + 10 sec o Apogee Lockout: 15 sec ☐ Verify TeleDongle (S/N 2885) o Freq: 434.55 MHz o Telemetry Rate: 38400 baud ☐ Verify BigRedBee o Freq: 433.92 MHz o Tx Interval: 5 sec	Dillon	

○ Callsign: K6NPS -5 ○ Verify packet Tx and Rx with radio		
Build Deployment Charges ☐ Check resistance of each canister ☐ Make nosecone black powder charge - label ○ Full canister ☐ Make main black powder charges - label ○ 4 g – primary ○ 5 g – backup ☐ Construct CubeSat ejection systems ○ Completely remove the plastic protective sheath from over the initiator head ○ Cut the plastic protective sheath to about 3/8th inch and re-install on the initiator ○ Use the cotton tipped applicator with silicon lube to wipe a residue of lube to the inside cavity of the charge cup ○ Install and pull initiator to within an inch or so of the charge cup ○ Mix a small amount of 5 min epoxy. Dab a small amount of this epoxy completely around the bottom of the initiator protective sheath ○ Assemble and let cure for at least 10 minutes ○ Measure out .2cc of black powder with measuring scoop ○ Pour powder into the prepared charge cup ○ Apply a Pyro charge cover disk or use a piece of 3M blue masking tape over the charge cup to seal in the propellant ○ Carefully place the Charge Cup into the Pyro Housing ○ Carefully place the spring onto the Puncture Piston	Dillon	

○ Insert the Puncture Piston into the Pyro Housing ○ Attach Pyro Housing to the Mounting Cap ○ Repeat process for backup system ○ Screw 45g CO_2 cartridge into primary ejection system ○ Screw 75g CO_2 cartridge into backup ejection system		
☐ Assemble the rocket main parachute ○ Place Nomex parachute protector on Kevlar shock chord ○ Place SPOT3 tracker on Kevlar shock chord ○ Connect chute to shock chord with quick link ○ Fold the parachute ○ Place parachute in parachute protector and wrap ○ Connect lower airframe to main section airframe ○ Secure lower airframe with 4 x 6–32 retention screws ○ Connect shock chord to motor ring ○ Slide main parachute into main body tube ○ Leave electronics bay quick link out for later connection	Dillon	
☐ Assemble the rocket nosecone parachute ○ Place Nomex parachute protector on Kevlar shock chord ○ Place SPOTTrace tracker on Kevlar shock chord in retention bag ○ Connect chute to shock chord with quick link ○ Fold the parachute ○ Place parachute in parachute protector and wrap ○ Set aside for later connection	Dillon	

☐ Assemble the electronics bay sled o Place LiPo batteries in mounts o Mount backup and primary flight computers o Ensure switches are open o Connect primary flight computer to switch o Connect backup flight computer to switch o Connect batteries o Close switches o Check functionality of both flight computers o Open switches	Dillon	

REPORT COMPLETED TASKS TO LIST MANAGER: Dr. Wenschel Lan

Team 1: NPS Rocket	Team 2: RDCS Recovery	Team 3: Base Operations
Dillon	John: Radios, Cosmos	Wenschel: SPOTter
Levi	Alex: Driver	Noah: Radios, Cosmos
David: Driver	Gio, Navigator	

Time	Task	Initial when complete w/ time
L-120	Insert motor into rocket ☐ Liberally grease casing ☐ Ensure screwed in tight	Dillon
L-110	Assemble electronics bay ☐ Ensure switches are open ☐ Connect main parachute BP charges to terminals ☐ Thread CO_2 leads through bulkhead ☐ Slide electronics sled onto threaded rods ☐ Ensure appropriate height of sled ☐ Connect BP charges to appropriate flight computer ☐ Ensure continuity of charges ☐ Place GoPro in mount – Tape for tight fit ☐ Turn on GoPro ☐ Connect CubeSat ejection systems to appropriate flight computer ☐ Place forward and rear bulkhead on coupler ☐ Ensure wingnuts and nuts are tight	Dillon
L-95	Connect electronics bay to main parachute ☐ Slide SPOT3 onto Kevlar cord ☐ Turn on SPOT3 ☐ Secure quick link to aft end of rocket ☐ Place ejection charges on top of main parachute ☐ Liberally grease lower portion of electronics bay ☐ Slide e-bay into main airframe ☐ Place 4 x 4–40 shear pins in electronics bay connection	Dillon
L-90	Assemble the rocket drogue parachute ☐ Place Nomex parachute protector on Kevlar shock chord ☐ Connect chute to shock chord with quick link ☐ Fold the parachute ☐ Place parachute in parachute protector and wrap	Dillon

	☐ Secure upper airframe to electronics bay with 4 x 6–32 retention screws ☐ Connect shock chord to electronics bay ☐ Slide drogue parachute into upper airframe tube	
L-90	Get final HAB HUB prediction. Confirm Launch time ☐ Text Greg Bischoff launch time	John
L-75	All Team meeting	Team 1, 2, 3
L-75	Turn on Go-Pro for launch time-lapse	Alex
L-60	Set up tables, unload equipment	Team 1, 2, 3
L-45	Prep Chase Vehicles with chow and water	Team 1, 2
L-30	Set up ground stations x2 ☐ Connect Chase laptops to power ☐ Connect MHX radios to Laptops ☐ Setup MHX car antenna	Alex
L-30	Prepare RDCS for Encapsulation ☐ Remove Spot Panel ☐ Remove Spot Tracker from stowage position ☐ Turn on Spot Tracker and wait for satellite acquisition ☐ Replace Spot Tracker	John
L-30	Prepare Nosecone for launch ☐ Connect ¼" threaded rod to end of nosecone ☐ Place retention nut at appropriate height ☐ Connect BP charge to Easy Mini through the rear bulkhead ☐ Connect BigRedBee to battery ☐ Connect EasyMini to battery ☐ Connect RPi to battery ☐ Slide sled and rear bulk plate into nosecone ☐ Secure assembly with eyebolt ☐ Ensure functionality of all sensors ☐ Connect nosecone parachute assembly to eyebolt ☐ Turn on SPOTTrace ☐ Slide nosecone parachute on top of ejection charge	Dillon
L-15	Power up Ground Stations ☐ Turn on laptop ☐ Run COSMOS "HAB" icon ☐ Open applicable windows o Command and Telemetry Server o Command Sender o Telemetry Viewer	Alex
L-15	Power up Green Radios ☐ Ensure attenuators on green radios per functions checklist	John

	☐ Turn on Green Radios	
L-10	Encapsulate RDCS at the hut ☐ Liberally grease aluminum transition ☐ Hold Aluminum Transition piece: Gio ☐ Fold RDCS Parachute: Dillon ☐ Maneuver Nose Cone: John ☐ Ensure Antennas and Parachute remain clear: Alex ☐ Ensure rocket CG location: 4” in front of CP	Dillon, Team 2
L-5	Secure Payload Fairing to rocket ☐ Walk to launch pad ☐ Lift Nose Cone: Alex ☐ Turn on RDCS: John ☐ Verify RDCS Operation over WiFi: John ☐ Secure Nose Cone with shear pins: Dillon ☐ Assist Dillon with Rocket: Gio ☐ Secure Payload Fairing to Rocket: Dillon o 4 x 6–32 screws ☐ Go vertical with rocket ☐ Verify nosecone sensors are still operational ☐ Start Go-Pro recordings o 2 x Go-Pros rocket o 2 x Go-Pro Launch pad ☐ Execute Main.py on rocket RPi – background the script o Ensure valid data returns over SSH ☐ Turn on primary flight computer o Verify voltage:_____ o Verify flight mode:_____ o Verify continuity:_____ ☐ Turn on backup flight computer o Verify voltage:_____ o Verify flight mode:_____ o Verify continuity:_____ ☐ Slide ignitor all the way into rocket motor ☐ Place ignitor securing cap on nozzle ☐ Discharge alligator clips from launch pad ☐ Verify no charge on alligator clips with meter o Voltage:_____	Dillon, Team 2

	☐ Connect alligator clips to ignitor ☐ Verify continuity of ignitor ☐ Walk to launch positions	
L-1	Go/No go for launch ☐ Place key in control box ☐ Turn control box on ☐ Confirm NPS rocket Go for launch: Dillon ☐ Confirm RDCS Go for launch: John ☐ Arm the control box ☐ Visually confirm airspace and surrounding area clear ☐ Conduct 10 second countdown	John, Dillon
L	Launch ☐ Time: _____ ☐ Lat/Long: _____	Wenschel
L+1	Watch COSMOS and track RDCS progress	Team 2, Team 3
L+1	Track rocket via BigRedBee APRS transmission ☐ Location:	Alex
L+2	Attempt to establish connection with TeleMega via ground station ☐ Location:	Dillon
L+3	Conduct RDCS radio test	John, Noah
L+15	Breakdown Chase 1 Ground Station for mobile ☐ Disconnect Chase 1 Laptop and MHX ☐ Connect MHX to car antenna ☐ Connect laptop and MHX to inverter ☐ Power on MHX	Alex
TBD	Conduct radio relay attempts with green or hand held radios ☐ Record Successful relay attempts below	Team 2, Team 3
TBD	Verify RDCS Drift profile	Team 3

TBD	NPS Rocket Recovery, Team 1 Depart ☐ Take Shovel ☐ Take Hand-held GPS ☐ 1 x IC-T22A ☐ Water ☐ Chow ☐ Time: _____ ☐ Estimated Destination Lat/Lon: _____	Team 1
TBD	RDCS Recovery, Team 2 Depart ☐ Take SPOT Gen3 ☐ Turn on SPOT Gen3 and ensure tracking ☐ Take Shovel ☐ Take trashbag ☐ Take hand-held GPS ☐ 2 x Green Radios ☐ Water ☐ Chow ☐ Time: _____ ☐ Estimated Destination Lat/Long: _____	Team 2
TBD	NPS Rocket Recovery, Team 1, Finds Rocket Body ☐ Time: _____ ☐ From a distance, verify all ejection charges have ignited ☐ Disarm primary and backup flight computers	
TBD	NPS Rocket Recovery, Team 2, Finds Nose Cone ☐ Time: _____ ☐ From a distance, verify ejection charge has ignited ☐ Connect to RPi NPS_Rocket network o Password: raspberry ☐ Terminate all python scripts	
TBD	NPS Rocket Recovery, Team 1, Begins return to FAR ☐ Time: _____	
TBD	NPS Rocket Recovery, Team 1, Arrives FAR ☐ Time: _____	
TBD	RDCS Recovery, Team 2, Finds RDCS ☐ Time: _____	
TBD	RDCS Recovery, Team 2, Begins return to FAR ☐ Time: _____	

TBD	RDCS Recovery, Team 2, Arrives FAR Time: _____	
TBD	Begin break down / clean up	All available
TBD	Debrief	
TBD	Return to NPS if able to arrive NLT 2200	

Successful Relay Attempts				
Time	Radios	TX Radio Location	RX Radio Location	RDCS Location
0758	Green → Green	FAR	FAR	FAR

Team 1 Check-in Matrix			
Time	Method	Location	Notes
Launch	Face-to-Face	FAR	Depart Direction: Personnel: Time: Estimated Travel Time:
L + 1			
L + 2			
L + 3			
L + 4			
L + 5			
L + 6			
L + 7			
L + 8			

Additional Notes:

Team 2 Check-in Matrix			
Time	Method	Location	Notes
Launch	Face-to-Face	FAR	Depart Direction: Personnel: Time: Estimated Travel Time:
L + 1			
L + 2			
L + 3			
L + 4			
L + 5			
L + 6			
L + 7			
L + 8			

Additional Notes:

PACKING LIST

RDCS and Ground Station

- ☐ Chase 1 Ground Station pelican cases (includes the following items)
  - Laptop with power cord/inverters
  - Converter (USB to COM port)
  - Cable (COM port to radio)
  - Slave radio
  - Antenna
- ☐ Chase 2 (Base Ops) Ground Station pelican cases (includes the following items)
  - Laptop with power cord/inverters
  - Converter (USB to COM port)
  - Cable (COM port to radio)
  - Slave radio
  - Antenna
- ☐ RDCS Items
  - RDCS, integrated with
    - Parachutes (two)
      - Automated release mechanism
- ☐ 2 x Green Radios
- ☐ 2 x Green Radio Batteries
- ☐ 3 x Hand-held radios
  - Semi – Duplex : Base Operations
  - Full – Duplex: Greg Bischoff at China Lake
  - Rocket Team: NPS Rocket Recovery Team
- ☐ 3 x Hand-held radio chargers
- ☐ 3 x SPOT Gen3
- ☐ 2 x SPOT Trace
- ☐ 2 x Hand-held GPS
- ☐ Camera/video recorder
- ☐ Binoculars
- ☐ Duct tape
- ☐ 2 x Extra battery pack
- ☐ 48 x AAA alkaline
- ☐ 24 x AA alkaline
- ☐ Sharpies
- ☐ Table (one)
- ☐ Phillips screw driver
- ☐ Hex screw driver to power on RDCS
- ☐ Go-Pro for launch time lapse
- ☐ 5 gallon water
- ☐ Base Station Antenna Element
- ☐ Base Station Hitch mount
- ☐ Yeti
- ☐ Extension Cord

Rocket

Nosecone

- ☐ Nosecone
- ☐ ¼” x 15” threaded aluminum rod
- ☐ ¼” washer
- ☐ Nosecone sled
    - BigRedBee Tracker
        - BigRedBee LiPo Battery
        - 3 x 4/40 mounting screws
    - Li-Ion Battery Pack
    - Raspberry Pi 3 A+
        - SD Card
    - RocketBoard
        - 4 x standoffs
        - 4 x mounting screws
    - EasyMini
        - 9v battery
        - 4 x 4/40 mounting screws
        - Pratt ejection canister
- ☐ Rear Adapter Plate
- ☐ ¼” steel eyebolt
- ☐ 3’ Kevlar shock chord
- ☐ 48” Fruity Chute Parachute
    - Parachute protector
- ☐ 2 x quick links
- ☐ SPOTTrace
    - Retention Bag
- ☐ GoPro session

Upper Airframe

- ☐ 2 x 4–40 Nylon shear pins
- ☐ Aluminum Transition
- ☐ 4 x 6–32 shortened aluminum retention screws
- ☐ Drogue Parachute (24” Fruity Chute)
    - Parachute protector
- ☐ 2 x quick links
- ☐ 30’ Kevlar Shock Chord
    - 2 x quick links
    - Shock Chord protector
- ☐ 14” carbon fiber section

Electronics Bay

- Forward closure
- 2 x wing nuts
- Fiberglass Coupler
- Electronics Bay Sled
- 2 x FingerTech switches
    - 4 x 2–56 mounting screws
- 2 x TeleMega Flight Computers
    - 8 x 4–40 mounting screws
    - 2 x 900mAh LiPo batteries
- Rear Closure
    - 2 x washers
    - 2 x bolts
- 3 x zip ties for mounting
- 2 x RAPTOR Ejection Systems
    - 45g CO_2 Cartridge
    - 75g CO_2 Cartridge
    - Pyro charge cover disks
    - Pyro housing
    - Puncture piston
    - Return Spring
    - Charge cups
    - Replacement O-rings
    - Powder measure vials
- Ejection Canisters (4 long and 4 standard length)
- Black Powder
- MJG igniters

Main Body Tube

- Main Parachute (Fruity Chute 84”)
    - Parachute Protector
- 2 x quick links
- 30’ Kevlar Shock Chord
- 4 x 6–32 aluminum retention screws
- 4 x 4–40 shear pins
- SPOT3
- 8” carbon fiber section
- 57” carbon fiber section
- 2 x 3D printed aft spacing tool

Motor

- CTI P98 – 6gXL Motor Casing
- Forward Closure
- Rear Closure
- 2 x propellant liner
- 2 x nozzles
- Spacer
- Spanner Wrench

Documentation

- BigRedBee Manual
- TeleMega Manual
- EasyMini Manual
- Rocket Binder
- *RocketBoard* Binder

Flight Box

- Wire Stripper
- Extra Wire
- Wire Cutter
- Head lamp
    - Extra batteries
- Tweezers
- Large and small mixing sticks
- JB Weld 5-minute epoxy
- Aluminum Foil
- Sandpaper
- Nitrile Gloves
- Extra Shear Pins
- Extra retention screws
- Spare Batteries
- Screwdrivers
    - Hex
    - Standard
    - Phillips
    - Larger hex for switches
- Pencil
- Notepad
- Painter's tape
- Tube marking angle
- X-acto knife

- Multi-meter
- Shop towels
- Baby wipes
- 2 x GoPro session with charging cables
- Kenwood Radio
- Yagi Antenna
    - Large-to-small coax adapter
    - TeleDongle
- Super Lube
- High-vacuum grease
- Crescent wrench
- Dixie Cups
- Black Powder
- Extra igniters
- Dog Barf (Fire retardant stuffing)
- Personal laptop
    - Charger

THIS PAGE INTENTIONALLY LEFT BLANK

APPENDIX L. ROUND-EARTH GEOMETRY COMPARISON

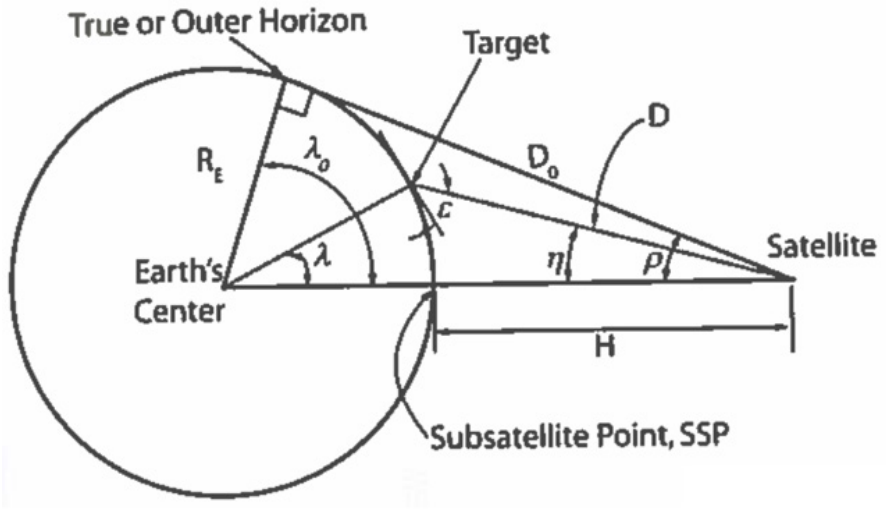

Figure L.1 Round-Earth Geometry. Source [82].

$$\sin\rho = \frac{\mathrm{R_e}}{(\mathrm{R_e} + H)} \qquad \text{Equation L.1}$$

$$\sin\eta_{\max} = \sin\rho\cos\varepsilon_{\min} \qquad \text{Equation L.2}$$

$$\lambda_{\max} = 90° - \varepsilon_{\min} - \eta_{\max} \qquad \text{Equation L.3}$$

$$D_{\max} = R_E \frac{\sin\lambda_{\max}}{\sin\eta_{\max}} \qquad \text{Equation L.4}$$

	$\mathbf{D_{Uplink}}$ $\varepsilon_{\min} = 10°$	$\mathbf{D_{Downlink}}$ $\varepsilon_{\min} = 5°$
Flat (km)	346	688
Round (km)	305	482
Difference (%)	13.3	42.7

Table L.1 Flat-and Round-Earth Geometry Comparison

Equations L.1, L.2, L.3, and L.4 were used to calculate the signal path distance, D, for both flat- and round-earth geometry [82]. These values are presented and compared

in Table L.1. The differences in D between flat-and round-earth geometry for both the uplink and downlink paths can be reduced if less conservative look angles $(\varepsilon_{\min})$ are assumed for calculations based on a round-earth assumption.

LIST OF REFERENCES

[1] R. Launius, "Sputnik and the origins of the space age," NASA, Oct. 10, 2007. [Online]. Available: https://history.nasa.gov/sputnik/sputorig.html

[2] C. Covault, "Desert Storm reinforces military space direction," *Aviat. Week & Space Techno.,* pp 42, Apr. 8, 1991.

[3] *Joint Operations*, JP 3-0, Joint Chiefs of Staff, Washington, DC, 2018. [Online]. Available: https://www.jcs.mil/Portals/36/Documents/Doctrine/pubs/jp3_0ch1.pdf

[4] *Marine Corps Operating Concept,* United States Marine Corps, Washington, DC, USA, 2016. [Online]. Available: https://www.mcwl.marines.mil/Portals/34/Images/MarineCorpsOperatingConceptSept2016.pdf

[5] *Marine Corps Strategy for Assured Command and Control*, United States Marine Corps, Washington, DC, USA, 2017. [Online]. Available: https://www.hqmc.marines.mil/Portals/61/Marine_Corps_Strategy_for_Assured_Command_and_Control_March_2017.pdf?ver=2017-05-30-160731-940

[6] C. Cynamon, "Military satellite communications," Air Force Space Command, 2010. [Online]. Available: https://afcea-la.org/sites/afcea-la.org/files/AFCEA%20Brief%20Feb2010.pdf

[7] E. Bryan, K. Kemmerly, and P. Konyha, *Air University Space Primer*, Maxwell Air Force Base, AL, USA, Air University Press, 2009, ch. 14, pp 183.

[8] M. Goldstein, "Telecommunications: Competition, capacity, and costs in the fixed satellite services industry," Washington, DC, USA, GAO Report No. GAO-11-777, 2011.

[9] C. Chaplain, "Defense satellite communications: DoD needs additional information to improve procurements," Washington, DC, USA, GAO Report No. GAO-15-459, 2015.

[10] T. Harrison, K. Johnson, and T. Roberts, "Space threat assessment 2018," Cen. for Str. Int. Stu. Washington, DC, USA, 2018. [Online]. Available: https://aerospace.csis.org/wp-content/uploads/2018/04/Harrison_SpaceThreatAssessment_FULL_WEB.pdf#page=12

[11] S. Freedberg, "US Jammed Own Satellites 261 Times in 2015; What if Enemy Did?," *Breaking Defense*, Dec. 2, 2015. [Online]. Available: https://breakingdefense.com/2015/12/us-jammed-own-satellites-261-times-in-2015-what-if-an-enemy-tried/

[12] Program Executive Office (Space Systems), “Mobile User Objective System selected acquisition report,” San Diego, CA, USA, 2016. [Online]. Available: http://www.esd.whs.mil/Portals/54/Documents/FOID/Reading%20Room/Selected_Acquisition_Reports/16-F-0402_DOC_72_MUOS_DEC_2015_SAR.pdf

[13] Air Force Space and Missile Systems Center, “Wideband Global SATCOM selected acquisition report,” El Segundo, CA, USA, 2016. [Online]. Available: http://www.dtic.mil/dtic/tr/fulltext/u2/1019569.pdf

[14] Air Force Space and Missile Systems Center, “Advanced Extremely High Frequency selected acquisition report,” El Segundo, CA, USA, 2016. [Online]. Available: http://www.dtic.mil/dtic/tr/fulltext/u2/1019569.pdf

[15] Space Exploration Technologies Corporation, “Launch manifest,” 2018. [Online]. Available: https://www.spacex.com

[16] National Security Space Office, “Plan for operationally responsive space,” Washington, DC, USA, 2007. [Online]. Available: http://www.airforcemag.com/SiteCollectionDocuments/Reports/2007/August/Day21/DoD_ORS%20plan0417.pdf

[17] D. Werner, “What’s next for Air Force weather satellites?,” *SpaceNews,* Jan. 9, 2019. [Online]. Available: https://spacenews.com/air-force-weather-ams-2019/

[18] *Radio Regulations,* Intl. Telecom. Union, Geneva, SUI, 2016. [Online]. Available: https://www.itu.int/en/publications/ITU-R/pages/publications.aspx?parent=R-REG-RR-2016&media=electronic

[19] *Techniques for Satellite Communications,* Department of the Army, Washington, DC, USA, 2017. [Online]. Available: https://fas.org/irp/doddir/army/atp6-02-54.pdf

[20] Lockheed Martin Corporation, “AEHF,” 2018. [Online]. Available: https://www.lockheedmartin.com/en-us/products/aehf.html

[21] Defense Science Board, “Task force on military satellite communication and tactical networking executive summary,” Washington, DC, USA, 2017. [Online]. Available: https://www.acq.osd.mil/dsb/reports/2010s/DSB-MilSatCom-FINALExecutiveSummary_UNCLASSIFIED.pdf

[22] E. Gündüzhan and K. D. Brown, “Narrowband satellite communications: Challenges and emerging solutions,” *Johns Hopkins APL Technical Digest*, vol. 33, no. 1, 2015. [Online]. Available: http://techdigest.jhuapl.edu/views/33_1/PDF/33_01-Gunduzhan.pdf

[23] Defense Advanced Research Projects, "Broad agency announcement blackjack," Arlington, VA, USA, Rep. HR001118S0032, 2018. [Online]. Available: https://www.darpa.mil/attachments/HR001118S0032-Amendment-01.pdf

[24] P. C. Swintek, "Critical vulnerabilities in the space domain: Using nanosatellites as an alternative to traditional satellite architectures," M.S. thesis, Dept. of Defense Analysis, NPS, Monterey, CA, USA, 2018. [Online]. Available: https://calhoun.nps.edu/handle/10945/59600

[25] Harris, "Harris Falcon III® RF-7850A-MR multi-channel airborne networking radio." [Online]. Available: https://www.harris.com/solution/harris-falcon-iii-rf-7850a-mr-multi-channel-airborne-networking-radio

[26] Naval Air Systems Command, "F/A-18 A-D Hornet." [Online]. Available: http://www.navair.navy.mil/index.cfm?fuseaction=home.displayPlatform&key=32F08227-0DE1-437F-93AB-C7241517AA8D

[27] Space Data Corporation, "SkySat™." [Online]. Available: https://www.spacedata.net/government/skysat/

[28] T. Childers, "Marines expand communication range with Combat SkySat," *15th MEU News*, March 30, 2012. [Online]. Available: https://www.15thmeu.marines.mil/News/News-Article-Display/Article/545376/marines-expand-communication-range-with-combat-skysat/

[29] R. Garner, "Scientific balloons FAQ," National Aeronautics and Space Administration, August 3, 2017. [Online]. Available: https://www.nasa.gov/scientificballoons/faqs

[30] Google Earth, "Google Earth." [Online]. Available: https://www.google.com/earth/. [Accessed 24 October 2018].

[31] Federal Aviation Administration, "Title 14 – Aeronautics and space," *Code of Federal Regulations,* vol. 2, sec. 101, 2018. [Online]. Available: https://www.govinfo.gov/content/pkg/CFR-2018-title14-vol2/xml/CFR-2018-title14-vol2-part101.xml#seqnum101.7.

[32] D. T. Pierce, "Development of a rocket test platform capable of delivering standard dimension payloads to near-space altitudes," unpublished.

[33] Digital Dutch, "1976 standard atmosphere calculator," Accessed Sep. 25, 2018. [Online]. Available: https://www.digitaldutch.com/atmoscalc/index.htm.

[34] National Weather Service, "The jet stream," Access Apr. 6, 2019. [Online]. Available: https://www.weather.gov/jetstream/jet.

[35] The National Association for Amateur Radio, “Band plan,” Accessed Mar. 20, 2019. [Online]. Available: http://www.arrl.org/band-plan

[36] Harris Corporation, “Harris III AN/PRC-117G(V)1(C),” Harris Corporation, [Online]. Available: https://www.harris.com/sites/default/files/downloads/solutions/an-prc-117g-multiband-networking-manpack-radio-datasheet.pdf. [Accessed Sep. 15, 2018].

[37] Harris Corporation, “Harris Falcon III AN/PRC-152A,” Harris Corporation, [Online]. Available: https://www.harris.com/sites/default/files/downloads/solutions/harris-falcon-iii-an-prc-152a-wideband-networking-handheld-radio.pdf. [Accessed Sep. 15, 2018]

[38] Nagoya Antenna, “CB/VHF/UHF HAM radio handheld antenna NA-701,” Nagoya Antenna, [Online]. Available: https://www.nagoya.com.tw/comm/upfile/p_160325_07185.pdf. [Accessed Sep. 20, 2018].

[39] Harris Corporation, “Harris RF-3150-AT152,” Harris Corporation, [Online]. Available: https://www.harris.com/sites/default/files/rf-3150-at152_tcm26-9092.pdf [Accessed Sep. 21, 2018].

[40] Harris Corporation, “Harris RF-3165-AT122,” Harris Corporation, [Online]. Available: https://www.harris.com/sites/default/files/rf-3165-at122_tcm26-9097.pdf. [Accessed Sep. 21, 2018].

[41] Department of Defense, “Contracts for Dec. 15, 2017,” Accessed Oct. 1, 2019. [Online]. Available: https://dod.defense.gov/News/Contracts/Contract-View/Article/1398382/.

[42] Trivec-Avant Corporation, “AV2099-4 Rev A antenna system,” M. Berberet, email, Oct. 2018.

[43] Trivec-Avant Corporation, “AV2099,” Accessed Oct. 1, 2019. [Online]. Available: https://trivec.com/shipboard/av2099/.

[44] B. L. Lovdahl, “Software-defined radio payload design for CubeSat and X-band communications,” M.S. thesis, Dept. of Mech. and Aero Eng., NPS, Monterey, CA, USA, 2018. [Online]. Available: https://calhoun.nps.edu/handle/10945/61218.

[45] Raspberry Pi, “Raspberry Pi 2 model B.” [Online]. Available: https://www.raspberrypi.org/products/raspberry-pi-2-model-b/. [Accessed Sep. 3 2018].

[46] Raspberry Pi, “Raspberry Pi 3 model A+,” Raspberry Pi, [Online]. Available: https://www.raspberrypi.org/app/uploads/2018/11/Raspberry_Pi_3A_product_brief.pdf. [Accessed Sep. 4 2018].

[47] Raspberry Pi, “Raspberry Pi 3 model B+,” Raspberry Pi, [Online]. Available: https://static.raspberrypi.org/files/product-briefs/Raspberry-Pi-Model-Bplus-Product-Brief.pdf. [Accessed Sep. 4 2018].

[48] Raspberry Pi, “Camera module V2.” [Online]. Available: https://www.raspberrypi.org/products/camera-module-v2/. [Accessed Apr. 4 2019].

[49] Institute of Electrical and Electronic Engineers, “Standard definitions and concepts for dynamic spectrum access: Terminology relating to emerging wireless networks, system functionality, and spectrum management,” New York, NY, USA, IEEE Std 1900.1-2008, 2008.

[50] Ettus Research, “USRP B200mini series,” Ettus Research, [Online]. Available: https://www.ettus.com/wp-content/uploads/2019/01/USRP_B200mini_Data_Sheet.pdf. [Accessed Sep. 9, 2018].

[51] Analog Devices, “Adalm-Pluto SDR active learning module,” Analog Devices, [Online]. Available: https://www.analog.com/media/en/news-marketting-collateral/product-highlight/ADALM-PLUTO-Product-Highlight.pdf. [Accessed Sep. 10, 2018].

[52] Mini-Circuits, “SBLP-156+,” Mini-Circuits, [Online]. Available: https://www.minicircuits.com/pdfs/SBLP-156+.pdf. [Accessed Sep. 12, 2018].

[53] G. Gordon and W. Morgan, *Principles of Satellite Communications*, New York, NY, USA, John Wiley and Sons, Inc., 1993.

[54] Electronics Notes, “Half-wave dipole antenna / Aerial,” Accessed Sep 20. 2018, [Online]. Available:https://www.electronics-notes.com/articles/antennas-propagation/dipole-antenna/half-wave-dipole.php

[55] Mini-Circuits, “ZX60-P103LN+,” Mini-Circuits, [Online]. Available: https://www.minicircuits.com/pdfs/ZX60-P103LN+.pdf. [Accessed Sept. 15, 2018].

[56] Mini-Circuits, “ZX60-P103LN+,” Mini-Circuits, [Online]. Available: https://www.minicircuits.com/pdfs/ZX60-V82+.pdf. [Accessed Sept. 16, 2018].

[57] Space Systems Academic Group, *High-Altitude Balloon (HAB) Bus Interface Control Document Rev. 1*, Monterey, CA, USA, Naval Postgraduate School, 2018.

[58] Byonics, “GPS receivers.” [Online]. Available: https://www.byonics.com/gps. [Accessed Apr. 8 2019].

[59] Grainger, “Stainless steel lock nuts.” [Online]. Available: https://www.grainger.com/category/fasteners/nuts/lock-nuts?attrs=Basic+Material%7CStainless+Steel&filters=attrs. [Accessed Apr. 10 2019].

[60] FingerTech Robotics, “FingerTech mini power switch.” [Online]. Available: https://www.fingertechrobotics.com/proddetail.php?prod=ft-mini-switch. [Accessed Oct.10 2018].

[61] Electronics Notes, “Quarter-wave vertical antenna,” Accessed Oct. 1 2018, [Online]. Available: https://www.electronics-notes.com/articles/antennas-propagation/vertical-antennas/quarter-wave-vertical.php.

[62] Raspberry Pi, “Raspberry Pi hardware.” [Online]. Available: https://www.raspberrypi.org/documentation/hardware/raspberrypi/README.md [Accessed Apr. 9 2019].

[63] Microhard, “Nano n920X2,” Microhard, [Online]. Available: http://www.microhardcorp.com/brochures/n920X2.Brochure.Rev.1.0.pdf. [Accessed Apr. 9 2019].

[64] Boyd Corporation, “SOLIMIDE HT-340 data sheet,” Boyd Corporation, [Online]. Available: https://www.boydcorp.com/datasheets/SOLIMIDE-HT-340-Data-Sheet.pdf. [Accessed Dec. 4 2018].

[65] DuPont, “Kapton HN polymide film,” DuPont, [Online]. Available: http://www.dupont.com/content/dam/dupont/products-and-services/membranes-and-films/polyimde-films/documents/DEC-Kapton-HN-datasheet.pdf. [Accessed Dec. 4 2018].

[66] SPOT, “Spot Trace.” [Online]. Available: https://www.findmespot.eu/en/index.php?cid=130&pk_campaign=trace&pk_kwd=website. [Accessed Apr. 8 2019].

[67] The Rocketman, “High altitude balloon parachutes.” [Online]. https://the-rocketman.com/recovery-html/. [Accessed Oct. 18 2018].

[68] Jolly Logic, “Chute release.” [Online]. Available: https://www.jollylogic.com/products/chuterelease/. [Accessed Apr. 8 2019].

[69] Overlook Horizon, “Rocketman parachutes.” [Online]. Available: https://www.overlookhorizon.com/product/rocketman-parachutes/. [Accessed Apr. 8 2019].

[70] R. Larson, L. Boswell, T. Kanold, and L. Stiff, *Geometry*, [Online]. Available: https://www.stcs.org/view/11849.pdf. [Accessed Apr. 2, 2018]

[71] T. Benson, “Velocity during recovery,” National Aeronautics and Space Administration [Online]. Available: https://www.grc.nasa.gov/www/k-12/VirtualAero/BottleRocket/airplane/rktvrecv.html. [Accessed Oct. 25 2019].

[72] R. C. Olsen, “Introduction to the space environment,” unpublished.

[73] J. J. Sellers, *Understanding Space: An Introduction to Astronautics.* New York, NY, USA: McGraw-Hill, 2004

[74] Harris Corporation, “Harris Falcon III RF-7800H-MP,” Harris Corporation, [Online]. Available: https://www.harris.com/sites/default/files/downloads/solutions/rf-7800h-mp-wideband-hf-vhf-tactical-radio-system-datasheet.pdf. [Accessed Sep. 16, 2018].

[75] Analog Devices, “RF agile transceiver,” Analog Devices, [Online]. Available: https://www.analog.com/media/en/technical-documentation/data-sheets/AD9364.pdf. [Accessed Dec. 4 2018].

[76] Mini-Circuits, “SLP-200,” Mini-Circuits, [Online]. Available: https://www.minicircuits.com/pdfs/SLP-200+.pdf. [Accessed Jan. 5, 2019].

[77] Air Force Space Command, “Test requirements for launch, upper-stage, and space vehicles,” El Segundo, CA, USA. 2014, [Online]. Available: file://special/jwpross$/Downloads/SMC-S-016_05SEP2014%20(1).pdf.

[78] J. Lang, J. Kozak, K. Baker, J. Pross, B. Smereskey, D. Pierce, A. Rizzo, and T. Starks, “SS4861 winter 2019 final report,” Space Systems Academic Group, NPS, Monterey, CA, 2019.

[79] National Aeronautics and Space Administration, “NASA sounding rocket user handbook,” Wallops Island, VA, USA. 2015, [Online]. Available: https://sites.wff.nasa.gov/code810/files/SRHB.pdf.

[80] Google Maps, “Google Maps.” [Online]. Available: https://www.google.com/maps. [Accessed 1 Mar. 2019].

[81] habhub, “habhub.” [Online]. Available: http://habhub.org/. [Accessed 15 Feb. 2019].

[82] J. R. Wertz, D. F. Everett, and J.J. Puschell, *Space Mission Engineering: The New SMAD*, pp 182, Portland, OR: Microcosm Press, 2011.

THIS PAGE INTENTIONALLY LEFT BLANK

INITIAL DISTRIBUTION LIST

1. Defense Technical Information Center
   Ft. Belvoir, Virginia

2. Dudley Knox Library
   Naval Postgraduate School
   Monterey, California